論文 / 著書情報
Article / Book Information

題目(和文)	
Title(English)	Electric Field-Driven Electrosynthesis of Conducting Polymers and Modification of Electrode Surfaces Based on Bipolar Electrochemistry
著者(和文)	ZHOUYaqian
Author(English)	Yaqian Zhou
出典(和文)	学位:博士（工学）, 学位授与機関:東京工業大学, 報告番号:甲第12121号, 授与年月日:2021年9月24日, 学位の種別:課程博士, 審査員:稲木 信介,冨田 育義,山口 猛央,宍戸 厚,吉沢 道人
Citation(English)	Degree:Doctor (Engineering), Conferring organization: Tokyo Institute of Technology, Report number:甲第12121号, Conferred date:2021/9/24, Degree Type:Course doctor, Examiner:,,,,
学位種別(和文)	博士論文
Type(English)	Doctoral Thesis

Electric Field-Driven Electrosynthesis of Conducting Polymers and Modification of Electrode Surfaces Based on Bipolar Electrochemistry

Yaqian ZHOU

2021

Department of Chemical Science and Engineering

School of Materials and Chemical Technology

Tokyo Institute of Technology

Contents

Chapter 1

General Introduction

1. Fundamentals of Bipolar Electrochemistry

The concept of bipolar electrochemistry has been proposed for many years and derived brilliant achievements in the long course of history. Beginning in the 1960s, Fleischmann and co-workers described fluidized bed electrodes, where a voltage applied on driving electrodes is capable of proceeding electrochemical reactions at discrete conducting particulate surface, improving the efficiency of electrosynthesis.[1–3] In the past two decades, bipolar electrochemistry as a relatively old technology, ushered in a renaissance due to its attractive features. Nowadays, it has become a well-established technique to initiate a series of interesting and novel research branches in the fields from materials science to analytical chemistry, attributing to its superior nature advantages, such as the wireless reaction manner, the gradient potential distribution, multiple reaction sites, the low concentration of electrolyte and the electrophoresis effect.[4–7] At the beginning of this thesis, the author introduces the basic principles, electrolytic apparatuses, advantages and versatile applications of “Bipolar Electrochemistry”.

1-1 Principles

In this section, the author highlights the features of bipolar electrochemistry by comparing it with a conventional electrolytic system and then discusses the basic theories of bipolar electrochemistry.

1-1-1 Bipolar electrochemical system

A conventional electrochemical setup simply consists of a pair of electrodes named

an anode and a cathode in an electrolytic solution. Voltage difference from an external power source is mainly applied on electrode surfaces. On anodic and cathodic surfaces, homogeneous potentials formed to induce electrooxidation at the anodic surface and electroreduction at the cathodic surface, respectively. In this system, a large amount of supporting electrolyte is required to neutralize excess electric charges near to electrode surface (Figure 1a).

A bipolar electrochemistry setup, one pair of electrodes connected with an external power source is known as driving electrodes, and a conductive material that has no external electrical connection, is located inside the electrolytic solution as a bipolar electrode (BPE). Driving electrodes generate a uniform electric field across the bulk electrolyte solution, generating the poles of the BPE oriented in the opposite polarities of the driving electrodes (Figure 1b).[8] If the potential difference between the both ends of the BPE is high enough, faradaic electrochemical reactions can occur at the anodic and cathodic poles of the BPE together to maintain the electroneutrality within the BPE. The interfacial potential difference between the BPE and the solution is highest at the terminals of the electrode, so faradaic processes are observed there firstly.[9]

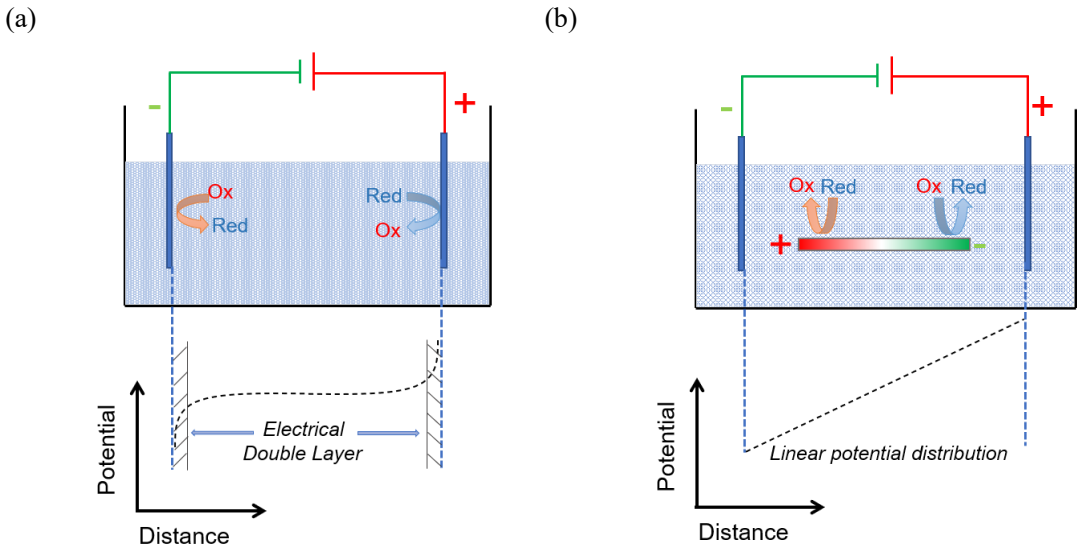

Figure 1. Schematic representation of (a) a conventional electrochemical setup and (b) a bipolar electrochemical setup.[10]

1-1-2 Potential distribution on the BPE

The voltage applied on the driving electrodes resulted in an electric field across the electrolytic solution that causes the BPE float to an equilibrium potential. Since the BPE is a conductor, it has an equipotential surface, but the interfacial potential difference between the BPE and the solution changes along its length because of the presence of an electric field in the electrolytic solution. The generated anodic and cathodic overpotentials can drive electrochemical reactions on the BPE. The total overpotential between both sides of the BPE (ΔV_{BPE}) can be roughly estimated using Equation (1)[11]:

$$\Delta V_{BPE} = \frac{d_{BPE}\, E}{d_E} \qquad (1)$$

where E is the applied voltage between the driving electrodes with the separating distance of d_E, d_{BPE} is the length of the BPE (Figure 2). The value of ΔV_{BPE} is a critical parameter to analyze electrochemical processes at BPEs. However, it does not take into consideration of the fact that the part of energy is consumed on the surface of the driving electrodes. Thus, it is necessary to estimate the exact ΔV_{BPE} by introducing the electric field transmission efficiency (θ) as the correction term. The value of E can be extracted by multimeter. Thus, it is possible to confirm a function Equation (2) between θ and $d_{BPE}E/d_E$. [12] By using this correction factor, exact ΔV_{BPE} can be estimated as follows.

$$\Delta V_{BPE} = \theta \frac{d_{BPE}\, E}{d_E} \qquad (2)$$

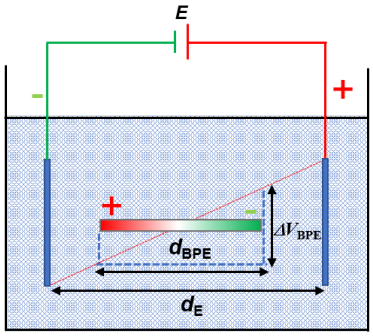

Figure 2. Schematic representation of a BPE under an external electric field (side view).[10]

1-2 Common Electrolytic setups for Bipolar Electrolysis

To satisfied diverse demands in practical applications, researchers flexibly designed various electrolytic setups based on the basic principles of bipolar electrochemistry. These electrolytic apparatuses have been widely employed in current research. The better we perceive them, the more flexible we can employ them in our own work.

1-2-1 Open and close BPEs

The system of bipolar electrochemistry exists two possible current paths including electronic and ionic. The majorities of works focus on the use of *open BPEs*, in which current can pass through both the ionic channel of electrolyte and the electronic channel of the BPE (Figure 3a). Oppositely, several interesting works described the use of *close BPEs*. In a closed BPE system, the anode and cathode of the BPE in the electrolytic solution are physically separated from one another. And, the only current path between the two half of cells is through the BPE (Figure 3b). [4]

(a) (b)

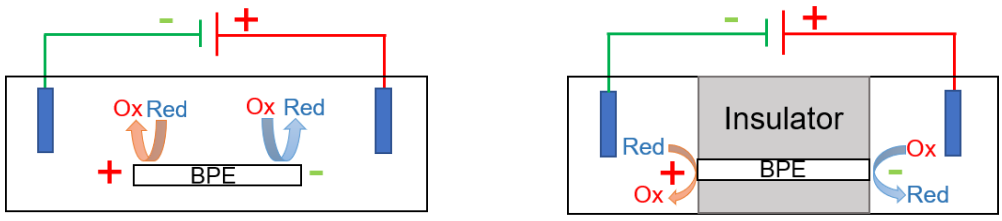

Figure 3. Schematic representation of (a) open BPEs and (b) closed BPEs.[4]

1-2-2 Continuous and split BPEs

Most BPEs are continuous, meaning that the electrode is made of a single conductor like that shown in figure 4a. This type belongs to *continuous BPEs*. However, a BPE formed by connecting two or more separate electrodes is called *split BPEs*, and they are particularly employed when the current need to be measured in situ due to *split BPEs* can be connected to an ammeter (Figure 4b). *Continuous BPEs* and *split BPEs* generate local

electric fields with similar characteristics.[4]

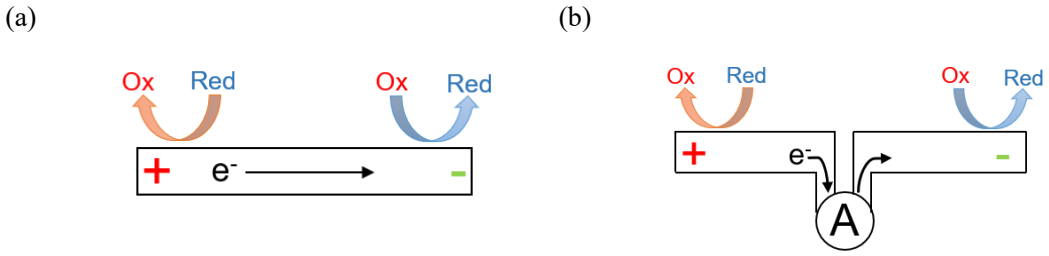

Figure 4. Schematic representation of (a) continuous BPEs and (b) split BPEs.[4]

1-2-3 Paralleled apparatus, U-type apparatus and cylindrical apparatus

A typical potential distribution in bipolar electrochemical system is linear (Figure 5a). With the development of bipolar electrochemistry, Inagi and co-workers designed several new-style electrolytic setups, which made it possible to control a potential distribution on a BPE. In a U-type electrolytic cell with an insulating wall, BPE faces to the driving electrodes and a shielding wall inserted between anode and cathode of driving electrodes. Measurement of an IR drop and potential profiles around the shielding wall revealed a sigmoidal potential distribution profile on the BPE (Figure 5b). In contrast to the sigmoidal slope in the U-type apparatus, a mountain-like slope formed when a shielding cylinder covers the BPE surface and spatially separated the anode and cathode of driving electrodes. A circular anodic area appeared underneath the region covered by the cylinder, together with a surrounding cathodic area with an interface gradient (Figure 5c).[13]

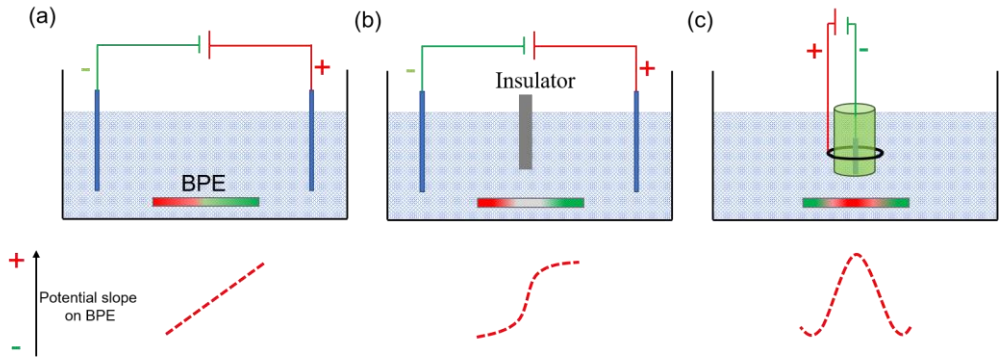

Figure 5. Schematic representation of the BPE apparatuses and potential distributions of (a) paralleled apparatus, (b) U-type apparatus and (c) cylindrical apparatus.[13]

1-3 Advantages

Bipolar electrochemistry as a relatively old technology that regains considerable renewed interest because of their interesting features.[7] According to mentioned principle and fundamental electrolytic setups, it is perspicuous to conclude outstanding advantages of bipolar electrochemistry in this section.

1-3-1 Wireless nature

The BPE placed in the electrolytic solution is controlled by a pair of driving electrodes and a power supply, which endows it a wireless contact manner. This nature makes the BPE no limitation in shape and size, which offers a straightforward method to create anisotropic materials on the BPE from nanoscale to macroscale.[14–19] Besides, multiple BPEs function equally in one external electric field, which allow simultaneous control over thousands or millions of electrodes.[20] This provides access to many pioneering experiments, including mass production of modified objects and high-throughput screening of materials.

1-3-2 Gradient potential distribution

Another beneficial and attractive feature of the BPE is multiple polarities and the ability to generate a potential gradient on the BPE surface, derived from the linear IR drop in the bulk solution. By adjusting the applied voltage on a pair of driving electrodes and electrolytic apparatuses as mentioned in 1-2-3, the slope of IR drop can be easily manipulated. The formed potential gradient here can act as an in situ generated template for gradient surface modifications on BPE surfaces. Therefore, this methodology is attractive to fabricate gradient materials facilely.[21]

1-3-4 Low concentration of electrolyte

A large amount of electrolyte is intrinsically necessary to generate electrical double

layers in the conventional electrochemical system. However, the bipolar electrochemical system only requires a small amount of electrolyte to form an electric field across the bulk solution. This advantage contributes to the situation that need avoid employing a large amount of electrolyte during the electrolytic process, which is consistent with the concept of green chemistry.

1-3-3 Electrophoresis effect

Bipolar electrochemical conditions generate a spatial electric field across the whole electrolytic solution, triggering the electrophoresis of ionic species in the bulk solution. Electrophoresis improves the mass transfer of ionic species towards a specific direction, thus electrolysis assisted with simultaneous electrophoresis effect produces a synergetic effect in bipolar electrochemical system, which is a powerful approach to obtain various functional materials.[22–24]

2. Application

Based on principles and advantages of bipolar electrochemistry, it can be widely applied from materials science to analytical chemistry and beyond, opening new branches for electrochemistry family. This section summaries the representative practical applications of the technology on various fields of advanced materials, electroanalysis, motion generation and electrosynthesis.

2-1 Material science

Attributing to the wireless nature of the BPE, the electrophoretic effect and the highly controllable potential distribution, bipolar electrochemistry has been widely used for wire formation, generation of gradient material, asymmetric modification of objects and site-selective pattern as well as electrochemical exfoliation.

2-1-1 Wire formation

Bipolar electrolysis assisted with electrophoresis is a powerful approach to grow one-dimensional materials in a wireless manner. Bipolar electrochemical condition offers an electric field across the electrolytic solution, which is beneficial for the electrophoresis of ions in a specific direction. Thus, these two concepts chime in easily. An early notable achievement was reported by Bradley and co-workers, who reported that anodic dissolution and cathodic electroplating of Cu led to the dendritic deposition of Cu metal paralleling to the direction of the external electric field under the direct current (DC)-bipolar conditions. The Cu particles were eventually electrically connected to each other (Figure 6a).[25–28] Developing this experiment, they realized electrical contacts for the creation of rectifying devices using homogeneously Si semiconductor plate sandwiched by two Cu rings.[29] Besides, Kuhn and coworkers achieved ring-like patterns on objects at different scales, which attributed to electrophoretic migration of anionic salts under DC-bipolar electrochemistry (Figure 6b).[30]

Recently, Inagi and co-workers carried out pioneering works on growing polymer wires between isolated Au wires acting as BPEs. When electropolymerization of 3,4-ethylenedioxythiophene and its derivatives were conducted by alternating current (AC)-bipolar electrolysis, it demonstrated the unusual electropolymerization behavior, leading to one-dimensional propagation from both terminals of Au wires. The conductive networks were achieved from terminals of several Au wires and its interconnection grew in accordance with the direction of the external electric field. The electrophoresis of charged oligomers in bulk solution is crucial to the formation of PEDOT microfiber structures (Figure 6c).[31] Synthesis of linear PEDOT fibers by using a micro-space to surround BPEs[32] and fabrication of PEDOT hybrid fibers[33] were performed based on this methodology as well. It is worth expecting that wire formation using bipolar electrochemistry would produce commercial applications in the near future.

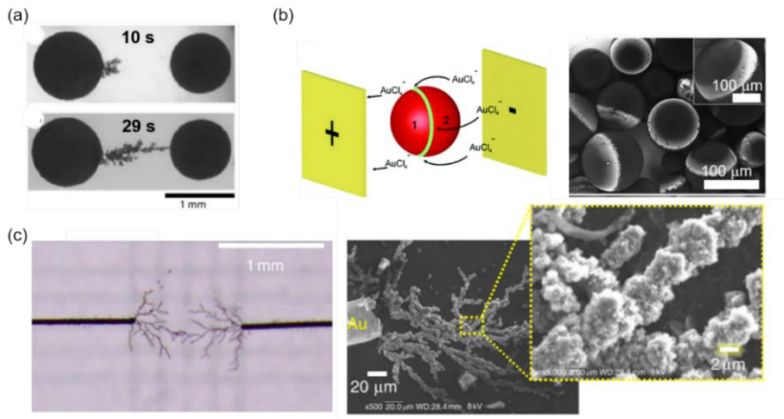

Figure 6. (a) Formation of Cu wires between two isolated Cu particles using bipolar electrochemistry. Cu deposits formed after 10 s and 29 s under an applied electric field of 30.3 V/cm.[25] (b) Conceptual illustration of electrodeposition of metal onto bipolar GC-bead electrodes using $AuCl_4^-$ anions and SEM image of GC-beads modified with Au rings.[30] (c) Optical microscope image of PEDOT fibers bridging the 1 mm gap between Au wires (ΔV_{BPE} = 8.3 V, 90 s) and SEM images of the PEDOT fibers.[31]

2-1-2 Generation of gradient material

Potential gradient, as one beneficial feature of bipolar electrochemistry, has attracted extensive attention, which can be regarded as an in situ generated controllable template for gradient electrode surface modification. Moreover, its simplicity for distributing the potential combined with wireless nature of the BPE, makes it become an attractive technique in preparation of various gradient materials.

A pioneering work was developed by Björefors and co-workers, where an alkanethiol-modified gold electrode was employed as the BPE. At the cathodic surface of the BPE, the reductive cleavage of Au-thiol bond proceeded to leave various degrees of thiol group in different positions, which successfully created a functional molecular gradient.[34] Similar work was demonstrated by Bouffier and co-workers for modulation of wetting properties on the BPE surface.[35] Inagi group showed electrochemical oxidation of pillar[6]arene by bipolar electrochemistry, endowing different morphologies of deposits depending on the positions on the BPE. And, the tendency of shape and size of the pillar[6]arene hexagonal cylindrical structures at each position kept a similar

manner to the cases of corresponding potentiation oxidation (Figure 7a).[36] Besides, Zigah et al. allowed simultaneously oxidative and reductive electrografting of two different organic films at each end of a glassy carbon substrate, using 4-(2-aminoethyl) benzenediazonium (Figure 7b).[37] Daasbjerg et al. reported unusual patterns by reductively grafting aryl diazonium, iodonium, and sulfonium salts onto gold surfaces due to these salts require different reduction potentials to facilitate the gradient grafting.[38]

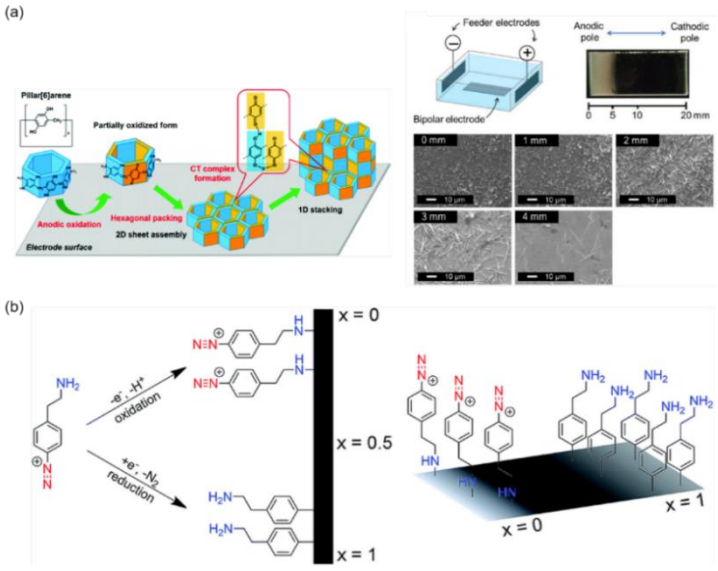

Figure 7. (a) Anodic oxidation of pillar[6]arene generates its partially oxidized form and hexagonal packing lead to 2D sheet assembly via charge transfer (CT) interaction, followed by 1D stacking to give cylindrical structures on the electrode surface. Schematic representation of a setup for bipolar electrolysis, photograph of the indium-tin oxide (ITO) BPE after electrolysis and SEM images of the pillar[6]arene CT structures on the BPE, measured at each position from the anodic pole.[36] (b) Simultaneous grafting of two different organic films on glassy carbon using bipolar electrochemistry with 4-(2-aminoethyl) benzenediazonium.[37]

Inagi and co-workers also extend the one-step preparation of gradient material by bipolar electrochemistry to polymer field. Electrochemical reaction and doping across the conducting polymer films proceeded, which afford these films with gradient functionality (Figure 8a).[39,40] Besides, the simultaneous paired electrochemical polymer reactions on the anode and cathode of the conducting polymer film was realized.[41] Later, they showed electrochemical surface modification on the BPEs in a gradient manner. Using the electro-click chemistry, an azide-functionalized conducting polymer film was modified with a

terminal alkyne by the electrogenerated Cu(I) catalyst on the BPE. The catalyst Cu(I) was generated at the cathodic part of the bipolar electrode having a concentration gradient, which affected the density of the introduced perfluoroalkyl group. When water droplet stands on each position of the modified film, contact angle showed a gradually decreased tendency as well.[42] Fabrication of both gradient and patterned polymer brushes were also achieved by electrochemically mediated atom transfer radical polymerization (eATRP) incorporating a bipolar electrochemical method. Due to the generated gradient profile on the BPE, $[Cu^{I}]/[Cu^{II}]$ ratio varied slightly along the BPE surface. The attendant variations generally affected the polymerization rate at various positions. Setting the sandwiched structure of the BPE and the initiator-modified glass substrate, three-dimensional polymer brush was fabricated with the controllable thickness, the modified area and the steepness by varying the electrolytic conditions (Figure 8b).[43] Further, this gradient polymer brush acts as a template for layer-by-layer (LBL) deposition of a cationic and an anionic polymer, which produced polyelectrolyte multilayer.[44]

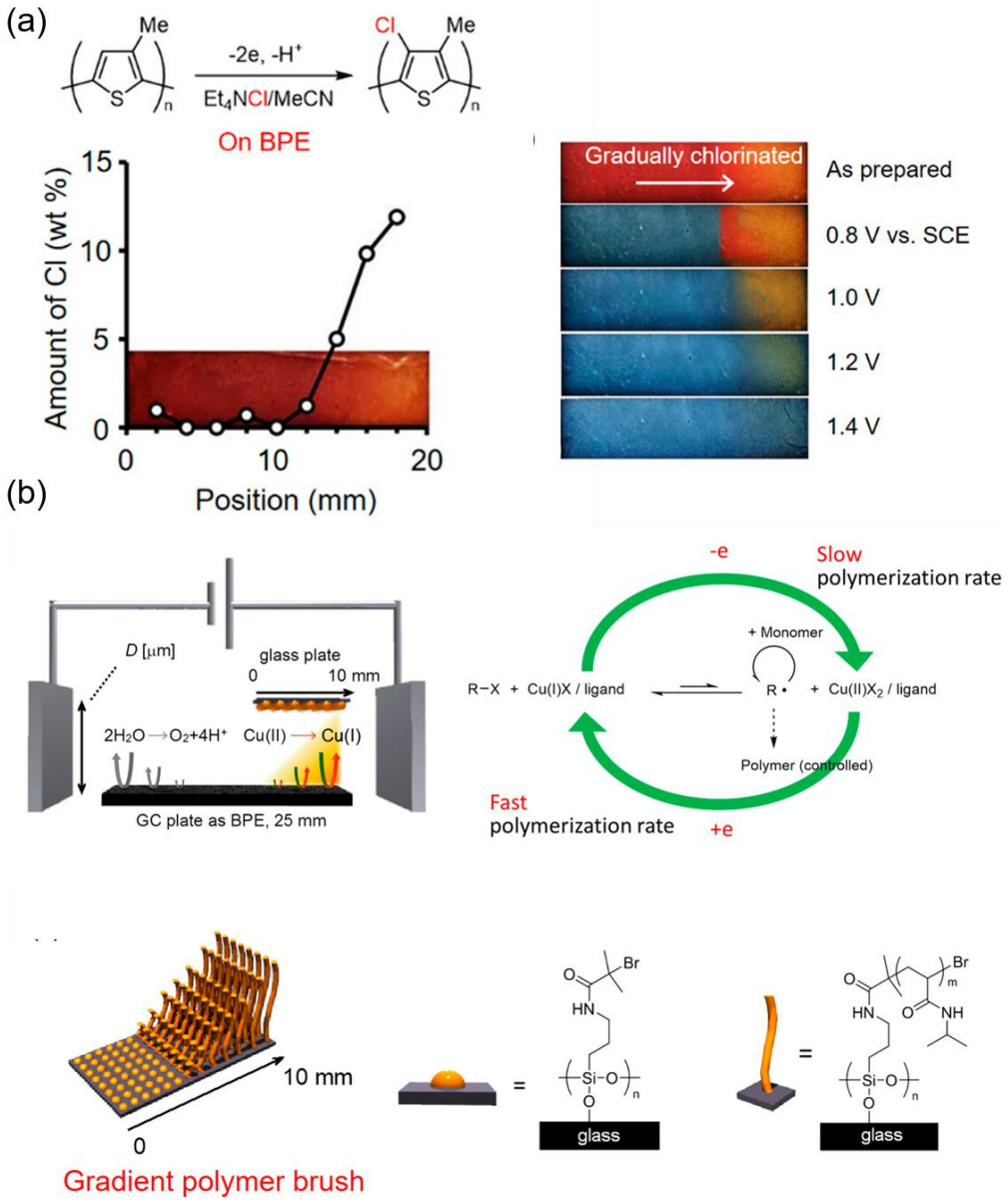

Figure 8. (a) Photograph of the gradually chlorinated P3MT film on the BPE. The profile showing the amount of chlorine atoms across the film is changed. Photographs of the gradually chlorinated P3MT film in the course of anodic doping at different potentials.[39] (b) Illustration of the setup for surface-initiated eATRP using bipolar electrochemistry. General scheme for eATRP of the NIPAM monomer using a Cu catalyst. Representation of a gradient poly(NIPAM) brush propagated from the initiator-modified glass substrate.[43]

The method has also been widely developed to fabricate gradient compositions or morphologies of inorganic materials.[45–54] Shannon and co-workers demonstrated the electrochemical reduction of Cd^{2+} and $S_2O_4^{2-}$ using bipolar electrodeposition, which

generated one-dimensional chemical composition gradients of CdS along the Au surface, depending on the interfacial potential difference at each position (Figure 9a).[45] Schmuki and coworkers manufactured well-defined TiO_2 nanotube size-gradient films using the bipolar electrochemistry approach, whose size distribution within the gradients can be controlled by altering the current or the length of the bipolar titanium sheet. These obtained gradient electrodes possess integrated energy and power density gradients (Figure 9b).[46] Kiani and coworkers reported gradient electrodeposition of copper on the surface of the BPE, which showed distinguished morphologies at different positions of the BPE. The morphology of nanodendrites in the vicinity of nanoparticles presented from the cathodic pole to the midpoint of the BPE. Modification of this BPE surface with 1-dodecanethiol offered the self-movement of the water droplet (Figure 9c).[47] He and coworkers deposited Ni-Cu-Fe gradient alloys on nickel substrates by bipolar electrochemistry and it showed distinct structures at each position of the BPE. When testing as an electrocatalyst for oxygen evolution reaction (OER), the OER activity was generally affected by the surface roughness (Figure 9d).[48]

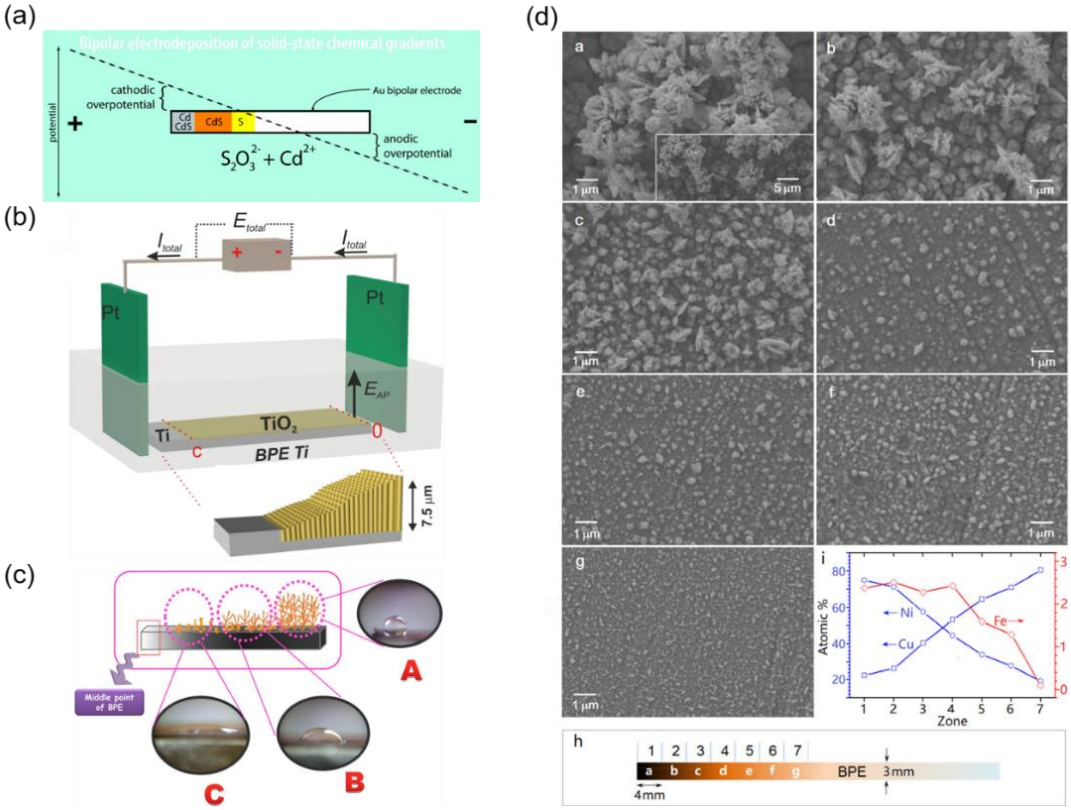

Figure 9. (a) Compositional gradient of Cd, CdS and S via electrochemical deposition of an inorganic salt on the BPE.[45] (b) Schematic description of the experimental set-up and a magnification of the BPE with TiO_2 nanotube size gradients.[46] (c) Schematic representation for the self-movement of a water droplet at the gradient-nanostructured Cu on the BPE.[47] (d) FESEM images of the deposits in the seven sampling zones shown in panel (from 1 to 7) and atomic percentages of Ni, Cu and Fe in the seven zones from EDS point analyses. The Ni-Cu-Fe gradient alloy was deposited on the BPE at a driving voltage of 11 V for 360 s.[48]

2-1-3 Asymmetric modification of objects and site-selective pattern

Bipolar electrochemistry has placed emphasis on its symmetry-breaking nature for material synthesis.[55] Bradley and co-workers pioneeringly employed the method to achieve site-selective deposition of palladium as the catalyst onto graphite, carbon nanotubes and carbon nanofiber.[56–58] The similar dissymmetric decorations on carbon material were also reported using metal (Figure 10a,b)[16,59–65] organic compound[19] and conducting polymer (Figure 10c).[17,63,66,67] Moreover, conducting organic single crystals of $(TMTTF)_2PF_6$ and $(TMTSF)_2PF_6$ have been used as the BPE for the site-selective

electrodeposition of copper, producing a new metal-organic Janus structure.[18] Site-selective bipolar electrodeposition of various metal layers on freestanding $MoSe_2$ macroparticles and microparticles has been developed, which showed superior efficiency towards hydrogen evolution reaction.[68] So far, bipolar electrochemistry has been proven to be a very versatile and powerful approach for site-selective and wireless electrodeposition on objects.

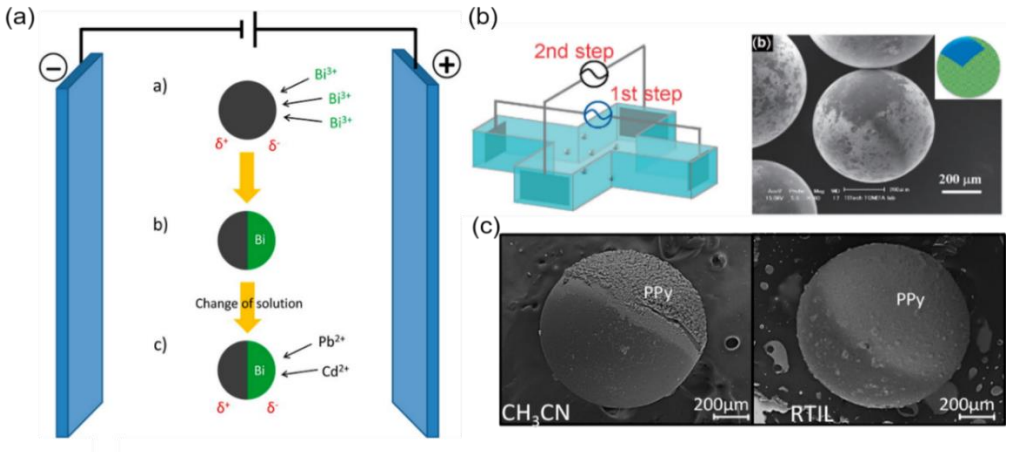

Figure 10. (a) Schematic illustration of the bipolar electrodeposition of a bismuth film on a glassy carbon bead. Cadmium and lead further deposited on the bismuth film modified glassy carbon bead.[64] (b) Illustration of cross-AC-bipolar electrochemical setup for tetra-functionalization of GC particles and SEM image of tetra-functionalized GC particles with Au.[65] (c) Glassy carbon beads obtained by bipolar electrochemistry in a solution containing 1 mM benzoquinone and 50 mM pyrrole (left) in acetonitrile with 33 mM $TBAPF_6$ and (right) in (1-butyl-3-methylimidazolium bis(trifluoromethylsulfonyl)imide. The electric field in both cases was 60 V/cm.[17]

However, this concept has been limited to deposition of electroactive precursors for a long time. This limitation impedes direct modification using other non-electroactive species. To address this problem, Kuhn and co-workers have extended this concept to materials that cannot be obtained from electroactive precursors, named indirect bipolar electrodeposition (IBED). The approach did not involve a direct electron transfer between the BPE and the deposit precursor, but rather considered local pH changes around the conducting BPE. Such a pH change in the vicinity of the polarized BPE leads to controlled polymerization or precipitation of an insulating deposit. This method has been

demonstrated on various non-electroactive precursors including silica, silicone, titanate, crystalline titanium dioxide and organic insulating polymers (Figure 11a).[69] Once metal ions located on the surface of metallic substrates as BPEs were wirelessly generated, these reactive metal ions combined with ligand species in solution can form extended metal-organic framework structures. When zinc or copper used as the BPE, it acts as not only the BPE, but also an original metal source, generating Zn–imidazolate network [Zn(2-MeIm)$_2$] (2-MeIm=2-methylimidazole) and [$Cu_3(BTC)_2(H_2O)_3$] (BTC=1,3,5-benzentricarboxylate) (Figure 11b).[70] Recently, Shiku and co-workers designed site-selective electrodeposition of Ca-alginate hydrogels at target areas of BPEs. Water electrolysis gave acidification at the anodic pole, resulting in the release of Ca^{2+} from $CaCO_3$ particles. Finally, Ca-alginate hydrogels locally fabricated at target BPEs or in target areas of BPEs by placing the position of the driving electrodes (Figure 11c).[71]

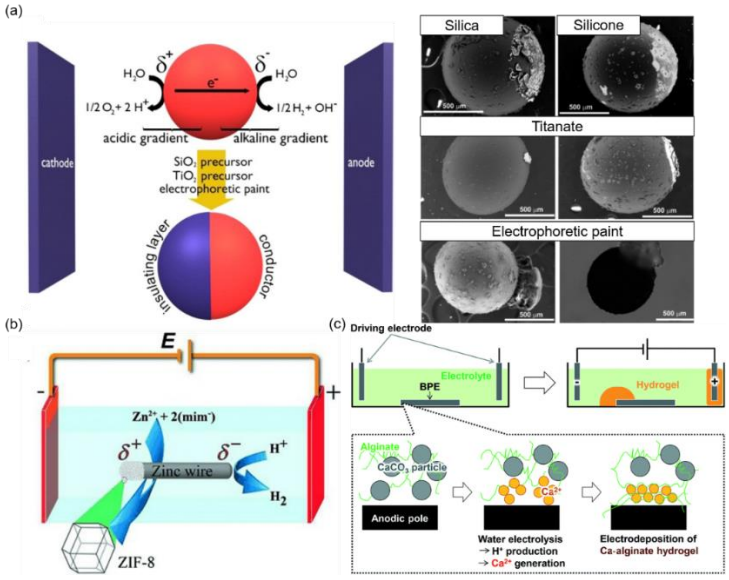

Figure 11. (a) Modification of sub-millimeter-sized glassy carbon beads with different materials by indirect bipolar electrodeposition (IBED) and corresponding SEM pictures.[69] (b) Mechanism of the formation of ZIF-8. Crystal growth on the anodically polarized side of a zinc wire is triggered by IBED.[70] (c) Schematic illustration of fabrication of Ca-alginate hydrogels based on anodic acidification using a BPE. A BPE is immersed in an electrolytic solution containing sodium alginate and $CaCO_3$ particles, and driving electrodes are inserted into the solution. A bias is applied between the driving electrodes to produce H^+ by water electrolysis at the anodic pole in the BPE, resulting in the release of Ca^{2+} from $CaCO_3$ particles. Then, Ca-alginate hydrogels form at the anodic pole.[71]

The modification by the bipolar electrochemistry is not limited to fabricate asymmetrical material, it also makes site-selective patterns possible. For this purpose, a spot-bipolar configuration was applied to achieve a local spot of electric potential on BPEs. Potential difference is generated between inner and outer area on BPEs, which can drive redox reactions. Based on this concept, copper-circles array was deposited on a copper substrate at localized positions (Figure 12a).[72] Besides, local deposition of poly(3-methylthiophene) (PMT) was carried out by anodic polymerization of 3-methylthiophene (MT) on the ITO substrate in the similar spot patterning system.[73] When conducting polymer films consisting of PMT and poly(3,4-ethylenedioxythiophene) (PEDOT) were used as the BPE, local potential distribution make it possible for spot modification of conducting polymer films by doping and chlorination. By extending the approach, a drawing application and array-type patterning in a site-controlled manner were presented (Figure 12b).[74]

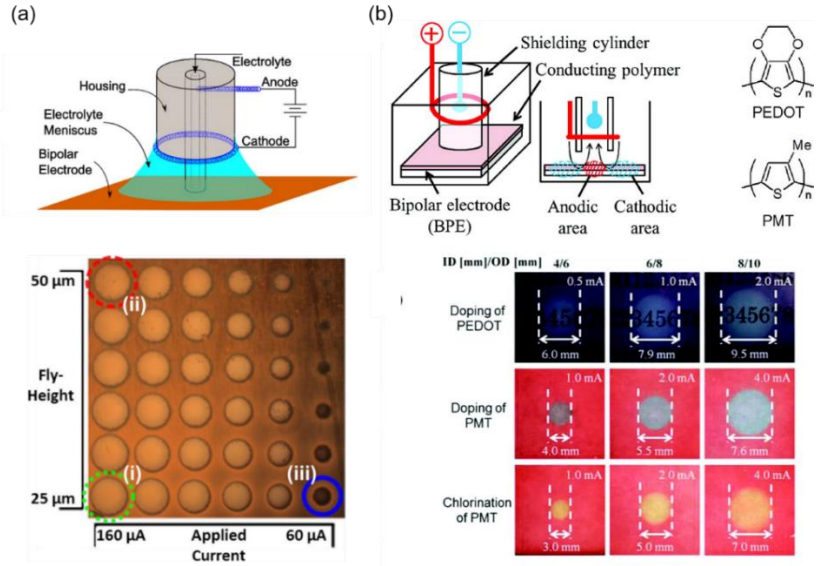

Figure 12. (a) Perspective view schematic of the scanning bipolar cell (SBC) and its important components and optical micrograph of an array of copper deposits on a copper substrate plated at a range of applied current and nozzle fly-heights. Stylus profilometry scans were performed to determine the heights of the three circled deposits: (i) = 0.35 µm, (ii) = 0.24 µm, and (iii) = 0.07 µm.[72] (b) Schematic illustrations of the setup used for bipolar patterning and the chemical structures of PEDOT and PMT. Pictures of the conducting polymer films showing doped PEDOT, PMT, and chlorinated PMT.[74]

2-1-4 Electrochemical exfoliation

Layered and 2D materials are at the forefront of materials science for several sensing and biosensing applications, whose chemical and physical properties could change with a decreasing number of layers.[75] Among various methods to exfoliate a layer, bipolar electrochemical method offers a low cost, high speed and comparatively straightforward approach. In the solution-based electrochemical exfoliation with BPEs, bulk objects in the form of suspensions as BPEs were electrochemically polarized between two driving electrodes even in the absence of a direct ohmic contact, resulting in exfoliation. Relying on this concept, Pumera and co-workers have already prepared WS_2 nanoparticles[76] and nanosheets(Figure 13a),[77] layered metal chalcogenides Sb_2S_3 and Bi_2S_3,[78] $MoSe_2$ nanolabels[79] and black phosphorus nanoparticle[80]. Shaijumon and co-workers employ this bipolar electrochemical technique to exfoliate pristine $Co(OH)_2$-bulk into thinner and smaller sheets, enhancing its electrocatalytic activity towards oxygen evolution reaction (Figure 13b).[81] Wang and co-workers demonstrated a controllable process for simultaneously exfoliating a graphite source as the BPE and depositing both high-quality oxidized graphene and reduced graphene oxide layers on driving electrodes (Figure 13c).[82]

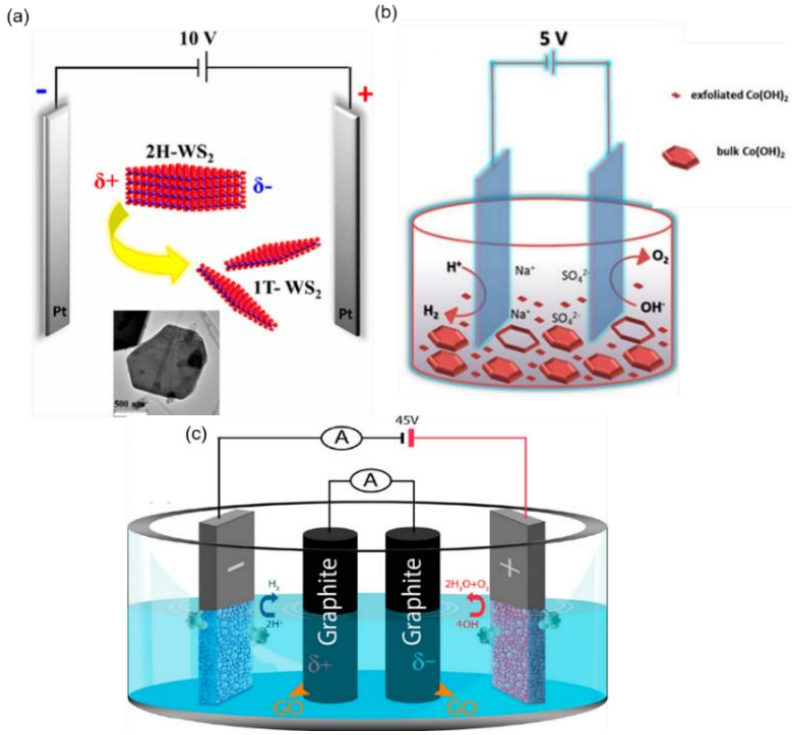

Figure 13. (a) Schematization of the solution-based electrochemical exfoliation method.[77] (b) Schematic of bipolar electrochemical preparation of $Co(OH)_2$ nanostructures.[81] (c) Schematic of the bipolar electrochemical setup of simultaneously exfoliating a graphite source and depositing both graphene oxide and reduced graphene oxide layers on driving electrodes.[82]

2-2 Electroanalysis

The BPE exhibits two distinct poles having the opposite polarizations, allowing to separate the localization of the sensing pole versus the reporting pole. Besides, arrays of BPEs with various sizes and shapes can be addressed simultaneously to accomplish high throughput analytical purpose. These advantages make bipolar electrochemistry become popular in electroanalysis.

2-2-1 Electrocatalyst Screening

An efficient large-scale array of electrocatalyst-screening platform has been developed to estimate oxygen reduction reaction (ORR) or hydrogen evolution reaction (HER). ORR electrocatalyst candidates of Pt, Au and ITO were deposited onto the cathodic poles of the BPEs, while the anodic poles were composed of parallel Ag microband electrodes.

The ORR proceeded at cathodic pole and Ag dissolution happened at anodic pole of BPE. Because the electrochemical activity of the two poles is directly coupled via the BPE, the extent of Ag electrodissolution is directly related to the ORR activity. Higher electrocatalytic activity of electrocatalyst candidate for ORR reaction, more Ag microbands dissolved. Comparing the final numbers of dissolved Ag microbands for the various electrocatalysts, it is easier to readout the activity of each electrocatalyst candidate (Figure 14a).[83] Successful evaluation of three Pd−M (M = Au, Co, W) bimetallic electrocatalysts was performed as well.[84] Besides, this method was also applicable to construct a parallel electrocatalyst screening platform for the HER. Several bimetallic and trimetallic systems involving in Co, Fe, Ni, Mo, and W were modified on cathode of BPEs. The HER occurring at the BPE cathodes was electrically coupled to the electrodissolution of an array of Cr microbands presented at the BPE anodes. Ni_8−Mo_2 modified BPE dissolved the most Cr microbands, which are identified to be the most active for the HER in a neutral electrolyte solution (Figure 14b).[85] Besides, when Prussian blue is electrodeposited on one side of the BPE as the signal reporter, the other side is for the loading of various catalysts. Due to the quantitative relation between the redox reactions occurring at both sides of the BPE, the discoloration speeds of Prussian blue to Prussian white are related to the amount of the catalytic activity of the catalyst, which provides a fast and facile imaging analysis of several electrocatalysts for ethanol and methanol oxidation.[86]

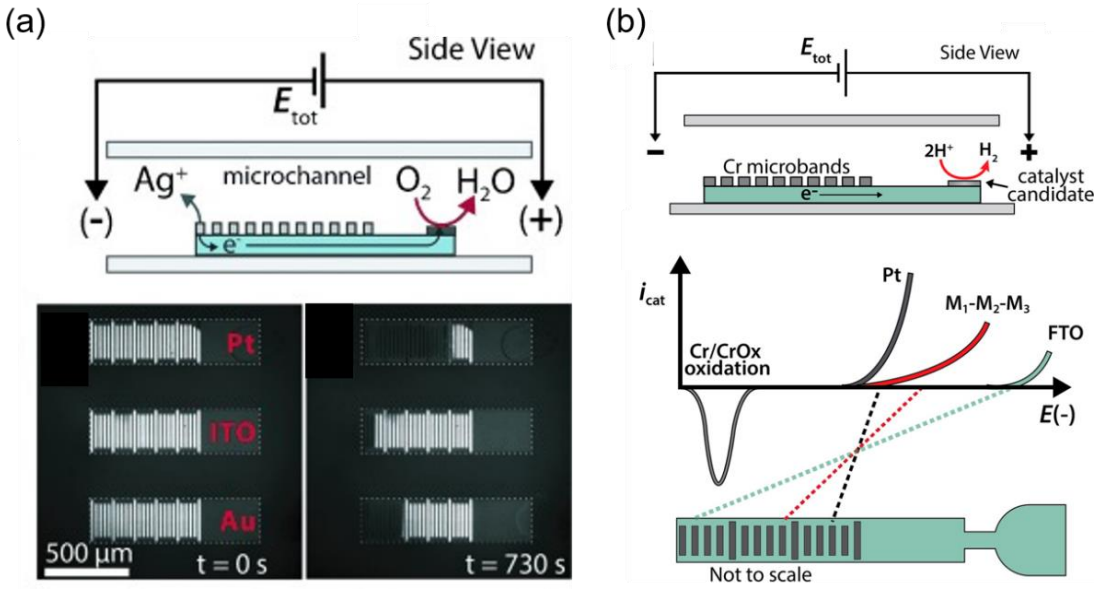

Figure 14. (a) Side view of one BPE shows the electrochemical processes at the anodic and cathodic poles. Optical micrograph of an array of three BPEs modified with the indicated catalyst candidates prior to the application of E_{tot}. The ITO support has been outlined using the gray dashed lines. Optical micrograph of the same BPE array after application of E_{tot}. The change in the number of Ag microbands reveals the relative activity of each catalyst candidate.[83] (b) Schematic representation of the BPE screening experiment and the relationship between the voltages needed to drive both Cr electrooxidation and the HER at several materials.[85]

2-2-2 Detection using electrochemical nanoprobes

The solid-state nanopore has been widely used for single-molecule detection over the past two decades. A wireless nanopore electrode (WNE) offers a novel and general accessible detection mechanism for the detection of single small molecules and ions, without the requirement of sealing traditional metal wires inside a nanoelectrode. Long and co-workers reported a silver (Ag)-coated WNE, oxidation of Ag happened at anodic pole of WNE, while H_2 was generated at cathodic pole when sufficient voltage was applied. H_2 at the orifice of the nanopore enhanced the spike of ionic current. Therefore, H_2 and silver ions can be detected by observing the ionic current signatures (Figure 15).[87] Furthermore, since the reduction potential for Hg^{2+} is higher than H^+, the reduction of Hg^{2+} could replace the H^+ as a prior reaction occurring at the cathodic pole of WNE. Thus, frequency of the spike signals was decreased after addition of Hg^{2+}. By calculating the

relationship before and after addition of Hg^{2+}, detection of Hg^{2+} from 100 pM to 100 nM was performed by monitoring the decrease of the spike signal frequency. Also, they employed catechol modified gold coating to achieve highly selective and sensitive probing of NADH concentrations as low as 1 pM. In addition, it enables the real-time nanopore monitoring of the respiration chain in living cells and the evaluation of the influence of anticancer drugs in an MCF-7 cell.[88] Other groups also demonstrated related researches using carbon coating,[89] platinum particle,[90] silver nanoparticles[91] and molybdenum sulfide quantum dots as WNE[92] in replace of silver coating for single-molecule detection.

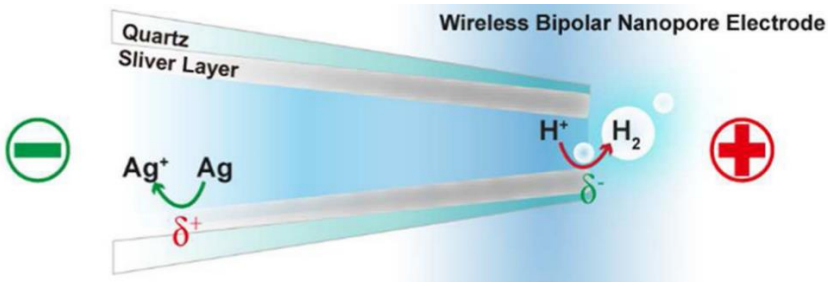

Figure 15. Illustration of H_2 and Ag^+ sensing by a WNE at the single-molecule level. Since the silver layer of a WNE could be polarized under the electric field, the generation of H_2 and Ag^+ occurs at the two extremities of the silver layer, respectively. The applied potential is provided by a pair of Ag/AgCl electrodes. The working electrode is inserted in the WNE, and the other electrode at the outside solution of WNE is defined as the virtual ground in the opposite side of the nanopore. The bulk area out of the orifice and the area inside the WNE are defined as the trans side and cis sides, respectively.[87]

2-2-3 Reporting by electrochemical actuation

Due to charge compensation by anionic counter ions during the redox reactions of conducting polymers, oxidation causes swelling and reduction leads to shrinkage, which results in the electrochemomechanical deformation (ECMD). To break the request of a direct physical connection to a power supply for triggering electrochemical reactions, it is interesting to develop this concept in bipolar electrochemistry. Kuhn and co-workers prepared a free-standing polypyrrole film with an intrinsic morphological asymmetry of

their two faces. When this polypyrrole film as the BPE immersed in an electrolyte solution, it showed a directional bending and motion because shrinking and swelling of counter ions on the polypyrrole film with intrinsic bilayer morphologies.[93] Then, they employed the wireless electromechanical actuation as a straightforward approach to read chemical information due to the wireless mechanical deformation of freestanding polymer film correlating in a quantitative way with the concentration of different molecules such as hydrogen peroxide, hydroquinone, and glucose (Figure 16).[94] This easy optical readout technique opened interesting perspectives on sensing and elaboration of self-regulating biomimetic systems.

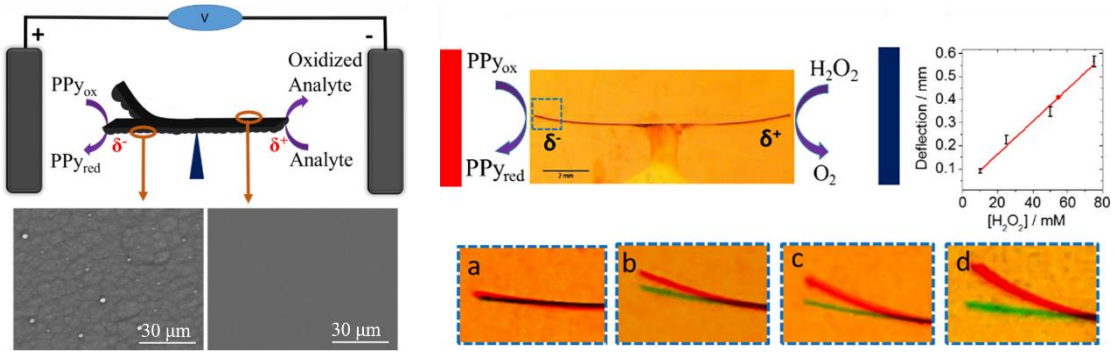

Figure 16. Schematic illustration of the bipolar electrochemical cell used for electromechanical readout. The free-standing polypyrrole (PPy) film is placed between two feeder electrodes. δ^+ and δ^- indicate the polarization potential at the two extremities. Scanning electron microscopic images of the two faces of the PPy film are shown below. Bipolar electromechanical setup to measure H_2O_2 concentration in 0.1 M phosphate-buffered saline (PBS). Blue and red borders denote the negative and positive feeder electrodes, respectively. Zoom-in at the negatively polarized PPy extremity in the presence of (a) 10, (b) 25, (c) 50, and (d) 75 mM H_2O_2. The green-colored PPy strip indicates its initial position, and red the position after 60 s. Calibration curve for different H_2O_2 concentrations. The electric field between the feeder electrodes is 1.6 V/cm for all measurements.[94]

2-2-4 Electrochemiluminescent and Electrochromic Sensing

Combining bipolar electrochemistry with electrochemiluminescence (ECL), analytical target species generate reaction at the sensing pole, while luminophores produce reaction at the reporting pole. The current passed through the two poles of the BPE be equal, therefore, luminescent intensity can perform the concentration of analytical

target species well. The coupling between BPE and ECL was firstly reported by Manz et al. in the early 2000s. When they used $Ru(phen)_3^{2+}$ or $Ru(bpy)_3^{2+}$ with tri-*n*-propylamine (TPrA) as co-reactant in a U shape floating electrode placed across a microfluidic channel, ECL was successfully generated to detect three natural amino acids of L-valine, L-aspartic acid, and L-alanine.[8] Starting from this contribution, other aspects, often more complex, have been investigated. Due to a potential gradient along the BPE, emission of ECL-active luminophores with differing oxidation potentials can happen simultaneously on the same BPE, producing spatially resolved multicolor BPE.[95] Three dimensional ECL(3D ECL) relying on simultaneous emission at thousands of conductive carbon microbeads occurred. Moreover, dual-color 3D ECL is also possible in the same reactor.[96] Crooks et al. built a system including a microelectrochemical array composed of 1000 individual BPEs, which was controlled by a simple power supply and two driving electrodes. ECL was generated simultaneously at each anode end of BPE (Figure 17a).[20] In addition, two dimensional BPE (2D-BPE) configuration consisting of a planar electrode situated at the intersection of two orthogonal microfluidic channels was designed. The 2D-BPE geometry caused electrochemical reactions can be localized at particular locations. Therefore, ECL emission was possible to localize on different sections of the 2D-BPE.[97] Nowadays, this technique has also been widely developed towards bioanalysis. Crooks's group demonstrated wireless electrochemical DNA microarray sensor (Figure 17b).[98] Chen's group reported a series of works about highly sensitive ECL biosensor on the basis of a closed bipolar electrode (BPE) apparatus for the analysis of biomolecule.[99–102]

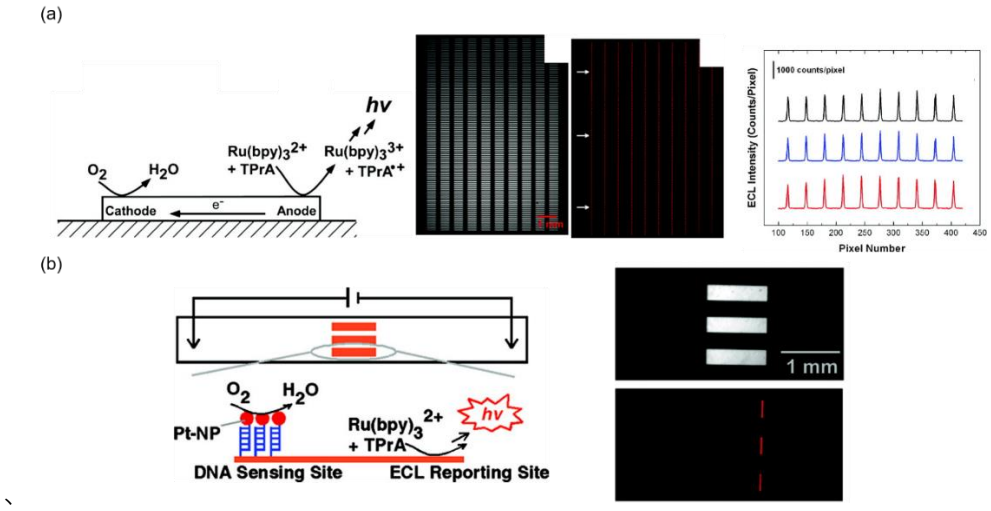

Figure 17. (a) ECL principle represented in a microarray. Optical micrograph of the bipolar electrode array and ECL intensity emitted at E_{tot} = 85.0 V. ECL intensity profile obtained from the three rows.[20] (b) ECL principle on the decorated BPE was demonstrated. Optical micrograph of the BPE configuration was recorded and false-color luminescence micrographs showed the ECL emission at E_{tot} = 16.0 V when complementary target DNA functionalized with Pt-NPs is hybridized to probe DNA on the electrode surface.[98]

ECL employed on the reporting pole requires sophisticated equipment and optical alignment for data collection. In this case, electrochromic material based on the color change is a straightforward approach to capture the converted analyte signal, in replace of electroluminescent material. Prussian blue (PB) spot electrodeposited on the ITO thin film electrode as the electrochromic indicator to detect glucose and hydrogen peroxide (H_2O_2) has been reported. When sensor part preloaded with dried GOx and $Fe(CN)_6^{3-}$, the catalytic oxidation of glucose by GOx resulted in conversion of $Fe(CN)_6^{3-}$ to $Fe(CN)_6^{4-}$. Then, $Fe(CN)_6^{4-}$ is oxidized back to $Fe(CN)_6^{3-}$, while reduction of PB to colorless Prussian white (PW) occurred at a reporting section simultaneously. The H_2O_2 sensor operation is similar, except the oxidation of $Fe(CN)_6^{4-}$ was catalyzed in the presence of H_2O_2. The resulting $Fe(CN)_6^{3-}$ was then reduced, while PW is oxidized to PB.[103] Owing to the quantitative relationship between the two reactions occurring at both sides of the BPE, the amount of deposited PB was used as an indicator for reporting target protein concentration of carcinoembryonic antigen (CEA). The presence of CEA induced the

steric hindrance, decreasing the electron transfer of redox molecule probe ($[Fe(CN)_6]^{3-/4-}$), which influenced the amount of PB deposited at the cathode of BPE (Figure 18).[104] Using other redox indicators, such as methyl viologen (MV), which turns from a colorless oxidized state to a dark purple reduced state, was reported as well.[105,106]

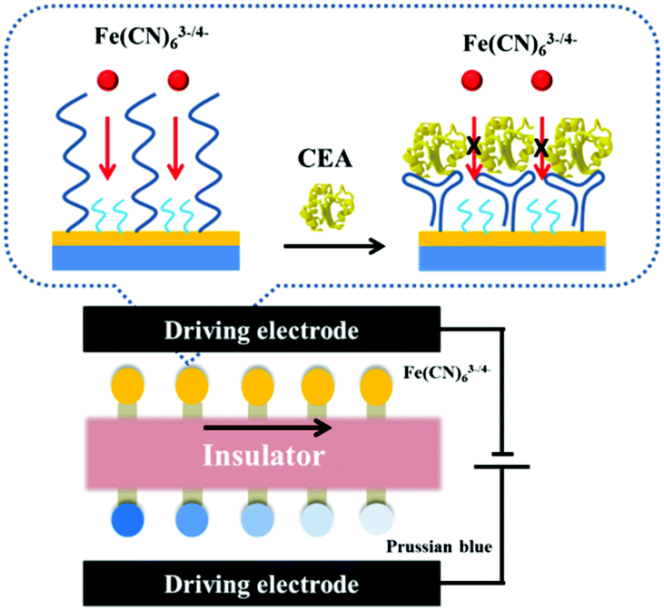

Figure 18. Schematic illustration of closed bipolar electrochromic strategy for high-throughput analysis of CEA. First, the single-strand DNA aptamer of CEA was attached on BPE anodes to capture CEA due to strong and specific binding affinity. When CEA was bound on the electrode surface, the electron transfer of redox molecule probe ($[Fe(CN)_6]^{3-/4-}$) was inhibited due to steric hindrance. On the basis of the quantitative relation between the two reactions occurring at both ends of the BPE, the current passing the closed BPE cathode was accordingly decreased, which influenced the amount of PB deposited at the BPE cathode pole and can be recognized by the naked eye. [104]

2-3 Motion generation

In bipolar electrochemistry, an external electric field can easily break or lower the symmetry of millimeter-sized and micrometer-sized conducting objects and thus as a straightforward approach to generate directed motion under different mechanisms. Moreover, the motion is possible to be combined with other functionalities, such as light emission.

2-3-1 Deposition/dissolution

Kuhn and Loget demonstrated a self-regeneration process for the directed linear motion of metallic objects. The principle of this approach is the simultaneous dissolution of a BPE at its anodic pole and subsequent deposition of the same metal at the cathodic pole under an externally applied electric field. Base on this concept, a zinc (Zn) BPE filament in a capillary generated motion in an effective speed of ca. 60 μm/s because Zn was electrochemically dissolved at the anodic pole and redeposited at the cathodic pole, inducing propelling objects in one direction (Figure 19).[107]

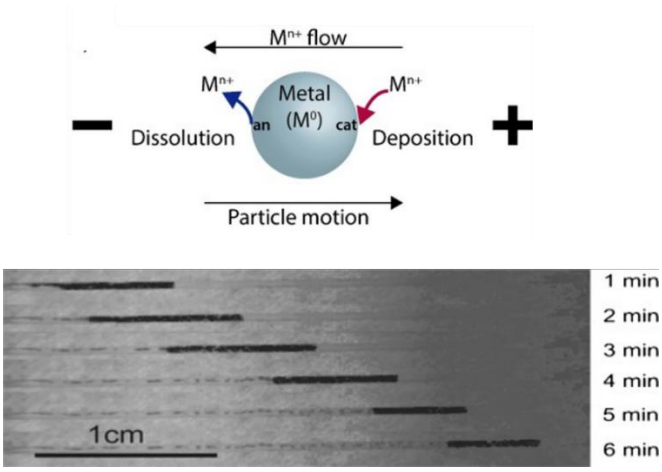

Figure 19. Dynamic bipolar self-regeneration principle and optical micrographs as a function of time illustrating the concept of self-regeneration. A Zn wire was formed at an electrode by electrodeposition of Zn^{2+} inside a glass capillary. The Zn wire was freed by removing the electrode from the solution. E_{tot} = 125 V was applied between driving electrodes at the ends of the capillary. This resulted in oxidation of Zn at the BPE anode and deposition at its cathode. This process results in apparent movement of the Zn wire.[107]

2-3-2 Asymmetric bubble production

In addition to self-regeneration, bubble propulsion generated by bipolar electrochemistry can also trigger BPE movement in an electric field. An external electric field-polarized conducting object (BPE) induces two spatially separated electrochemical reactions, involving in directionally controlled gas bubbles evolution, which will trigger the motion of the object. Water splitting can be carried out at both extremities of the BPE.

To keep identical electron production and consumption at both sides, the produced hydrogen (H_2) volume at cathodic side is twice the produced oxygen (O_2) volume at anodic side. This asymmetric bubble production is responsible for a linear motion. Furthermore, the bubble formation took place only at the cathodic side of the object in an aqueous hydroquinone (HQ) solution, leading to a higher speed. The described motion is not only efficient for inducing linear translation of objects, but also can be adapted to rotational motion in a horizontal plane or a vertical plane when rotors were used as BPEs (Figure 20).[108] Later, this contribution was extended to the levitation of objects in glass capillaries, demonstrating the possibility of cargo-lifting with the help of such bubble driven motors.[109]

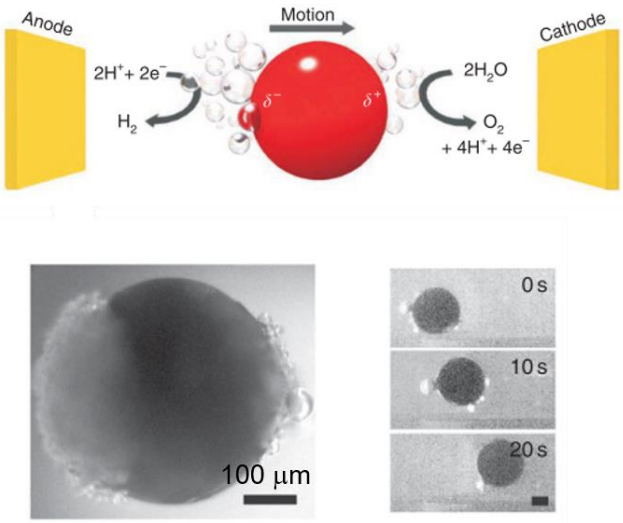

Figure 20. Linear motion of spherical objects. Scheme of the water splitting by bipolar electrochemistry. Optical micrograph of a stainless steel 1 mm spherical metal particle exposed to a 1.6 kV m^{-1} electric field in aqueous solution with 24 mM H_2SO_4. The left part of the bead is the cathodic pole where H_2 bubbles are produced, and the right part is the anodic pole where O_2 bubbles are produced. scale bar, 250 µm. (c) Translational motion generated with a 285-µm glassy carbon sphere in a PDMS microchannel exposed to a 5.3 kV m^{-1} electric field in aqueous 7 mM H_2SO_4.[108]

Miniaturized structures of the BPE in bipolar electrochemistry that can move in a controlled way and integrate various functionalities are interesting due to the potential applications from sensors to autonomous micromotors. In this context, generation of motion has been combined with electronic functionalities such as emission of light.

Synergetic action of bipolar electrochemistry in terms of simultaneous bubble production and ECL generation has been achieved.[110] Furthermore, electric current that flows inside a BPE not only was achieved for motion control, but also for power electronic devices, such as LEDs. Here, electron flow across the BPE from the oxidation-side to reduction-side. This local current can power an electronic device of LED, accompanied by bubble-induced propulsion of BPE, leading to a new class of electronic swimmers (e-swimmers).[111]

2-3-3 Ion exchange on conducting polymer

Recently, a complementary approach was reported to induce the motion of an object. On the basis of symmetry breaking on the polypyrrole film, directed crawling motion of it in a wireless way was achieved. Here, conducting polypyrrole films having different surfaces as the BPE were prepared for bipolar electrochemistry. The unequal incorporation of counterions into the polypyrrole film surfaces occurred when bipolar reduction and oxidation proceed on the BPE, resulting the different degrees of swelling and shrinking of the polypyrrole film. Under a periodic electric field, deformations of the polypyrrole film produced a directed crawling motion (Figure 21).[112] Besides, a system of a miniaturized light emitting diode in a polypyrrole matrix was established to achieve simultaneous wireless actuation and light emission.[113] These works create possibilities for wireless polymer-based (micro)robotics in the near future.

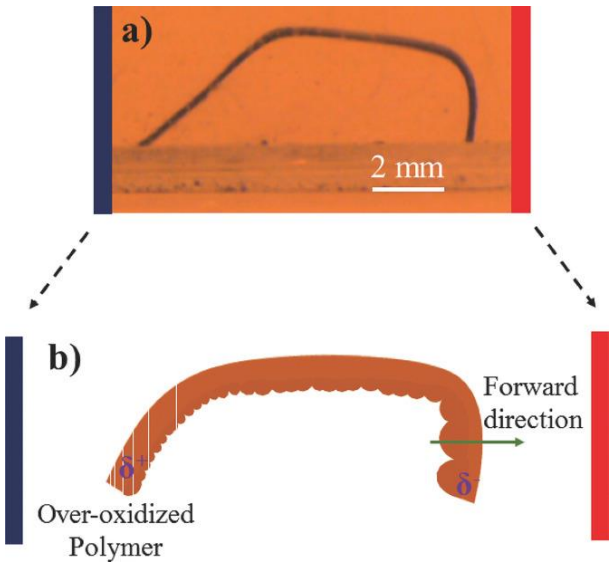

Figure 21. (a) Asymmetric shape of the polypyrrole strip under potential switching. (b) Schematic illustration of the asymmetric shape of the two ends of the polymer that responsible for the crawling in a specific direction in the presence of 0.5 m $LiClO_4$ and at 20 V. Red: positive feeder electrode; blue: negative feeder electrode. δ^+ and δ^- indicate polarization of polypyrrole film with respect to the solution.

3. Survey of this Thesis

Bipolar electrochemistry, as a unique technique, has received special attentions on materials science. BPEs work in the electrolyte solution without any direct electrical connection to a power source, endowing them wireless, high throughput and free-sized properties. Gradient potential distributions on the BPE surface can be regarded as an in situ generated controllable template for personalized surface modifications. Besides, the gradient potential across the bulk solution triggers simultaneous electrophoresis effect during the electrolysis, which contributes to the directed migration of charged species. These advantages doom broad application potentials of bipolar electrochemistry. The research purpose of this thesis is to provide new ideas on unresolved issues in current research using bipolar electrochemistry and excavate more application possibilities of bipolar electrochemistry.

Electropolymerization is a common approach for conducting polymers (CPs)

preparation. It usually gives CP films covered on the electrode surface. However, the anisotropic morphology of CPs is of great importance to practical applications benefiting from the excellent electron transfer efficiency. In Chapter 2, the author achieved direct electropolymerization of perpendicular CP fiber arrays on the electrode surface using a cylindrical electrochemical apparatus, due to the electrophoresis effect of charged oligomers under bipolar electrochemical conditions. Plausible growth mechanism that several micrometer-sized islands initially formed during an induction period and the subsequent growth followed a S-K mode was proposed. Furthermore, the author demonstrated a thorough investigations of influence factors, including electrolytic setups, electrolytic parameters, electrodes substrates and so on. The applied voltage and the gap between the cylinder and the BPE decided the successful growth of CP fiber arrays. The diameter of the cylinder, the solvent and the supporting electrolyte affected morphologies of the CP fiber. In addition, the CP fiber array can grow not only on flat ITO surface, but also on other substrates, even for the glassy carbon beads-decorated electrode surface. This facile method is expected to have a wide applicability on preparation of perpendicular CP fiber arrays for practical applications.

Inspired by the exploitation of electrophoresis effect in bipolar electrochemical system in Chapter 2. In Chapter 3, the author aims to take advantage of the electrophoretic migration of charged monomers into a template under bipolar electrolysis, to fabricate robust CP nanowires. Electrodeposition of electroactive monomers is one of popular methods to prepare CP nanomaterials because of its simplicity and controllability. In general, a hard commercial template is commonly employed to modify the electrode surface to regulate the size and the shape of nanostructures. However, the nanopores of the template have a high aspect ratio, highly limited the diffusion of monomers into the narrow space; therefore, the electropolymerized CPs tend to perform a hollow tubular structure with a low mechanical strength. To solve the problem, electrodeposition of monomers was carried out using the bipolar electrochemical system. The migration of charged monomers into the template was effectively improved due to the electrophoresis

effect in the bulk solution, resulting in densely packed CP depositions after the template removal. Ruthenium-containing cationic monomer was used for reductive electropolymerization firstly. Actuated by an external electric field, positively charged monomer effectively migrated to the cathode of the BPE, producing ruthenium-containing free-standing polymer nanowires. Anionic 3-thiophenetrifluoraborate monomer was employed for oxidative polymerization. Negatively charged 3-thiophenetrifluoraborate monomer was forced to move towards the BPE anode, which also gave the robust polymer nanowires. These obtained polymer nanowires possess a good mechanical property to keep 1D perpendicular structures, even after removing the templates. This work proved the inherently high synergy of electrolysis and electrophoresis in the bipolar electrochemical system.

Under the electric field-driven, bipolar electrochemistry can not only induce electrophoresis of charged species for fabricating CP materials, but also generate inhomogeneous potential distribution on the BPE for surface modifications. The preparation of organic thin films on electrode surface is significant due to their attractive potential applications in various fields. In Chapter 4, the author established a bipolar electrolytic micelle disruption (BEMD) method to prepare gradient and patterned films, because a wirelessly controllable potential distribution can be formed on the BPE surface under bipolar electrochemical conditions, acting as the in-situ template. In the BEMD approach, a reported electrolytic micelle disruption method was well integrated with bipolar electrolytic technology for personalized film preparations. A U-shaped bipolar electrolytic setup generated a sigmoidal potential distribution on the BPE, while a cylindrical bipolar electrolytic setup provides a site-selective potential feature on the BPE. When the micelles composed of electroactive surfactants moved to the BPE surface, the structure of micelles was disrupted selectively on the BPE with the oxidation of surfactants. In this process, various organic compounds incorporated into micelles were released on the localized area of the BPE, following the potential distribution. Finally, a variety of gradient and patterned organic thin films formed on the BPE surface. These

organic compounds as film-forming materials can be a monomer, an organic dye and luminescent molecules. Such a general BEMD approach opens a long-term perspective for electrode surface modifications with organic films.

4. References

[1] J. R. Backhurst, J. M. Coulson, F. Goodridge, R. E. Plimley, M. Fleischmann, *Journal of The Electrochemical Society*, **1969**, *116*, 1600-1607.

[2] M. Fleischmann, J. Ghoroghchian, D. Rolison, S. Pons. *The Journal of Physical Chemistry*, **1986,** *90*, 6392–6400.

[3] M. Fleischmann, J. W. Oldfield. *Journal of Electroanalytical Chemistry* and *Interfacial Electrochemistry*, **1971**, *29*, 211–230.

[4] S. E. Fosdick, K. N. Knust, K. Scida, R. M. Crooks, *Angewandte Chemie International Edition*, **2013**, *52*, 10438–10456.

[5] G. Loget, D. Zigah, L. Bouffier, N. Sojic, A. Kuhn, *Accounts of Chemical Research*, **2013**, *46*, 2513–2523.

[6] N. Shida, Y. Zhou, S. Inagi, *Accounts of Chemical Research,* **2019**, *52*, 2598–2608.

[7] A. Kuhn, R. M. Crooks, S. Inagi, *ChemElectroChem*, **2016**, *3*, 351–352.

[8] A. Arora, J. C. T. Eijkel, W. E. Morf, A. Manz, *Analytical Chemistry*, **2001**, *73*, 3282–3288.

[9] G. Loget, A. Kuhn, *Analytical and Bioanalytical Chemistry*, **2011**, *400*, 1691–1704.

[10] N. Shida, S. Inagi, *Chemical Communications*, **2020**, *56*, 14327–14336.

[11] R. M. Crooks, *ChemElectroChem*, **2016**, *3*, 357–359.

[12] G. Loget, J. Roche, A. Kuhn, *Advanced Materials*, **2012**, *24*, 5111–5116.

[13] E. Villani, S. Inagi, *Analytical Chemistry*, **2018,** *90, 6390–6396.*

[14] M. Li, S. Liu, Y. Jiang, W. Wang, *Analytical Chemistry* ,**2021**, *93*, 8152–8160.

[15] M. Ongaro, J. Roche, A. Kuhn, P. Ugo, *ChemElectroChem*, **2014**, *1*, 2048–2051.

[16] M. Ongaro, A. Gambirasi, M. Favaro, A. Kuhn, P. Ugo, *Electrochimica Acta*, **2014**, *116*, 421–428.

[17] S. Kong, O. Fontaine, J. Jérô Me Roche, L. Bouffier, A. Kuhn, D. Zigah, *Langmuir*, **2014**, *30*, 2973–2976.

[18] I. Malytska, C. Cécile, M. Méziè, M. Kielar, L. Hirsch, G. Wantz, N. Avarvari, A.

Kuhn, L. Bouffier, *The Journal of Physical Chemistry C*, **2017**, *121*, 12921–12927.

[19] L. Koefoed, E. B. Pedersen, L. Thyssen, J. Vinther, T. Kristiansen, S. U. Pedersen, K. Daasbjerg, *Langmuir*, **2016**, *32*, 6289–6296.

[20] K. F. Chow, F. Mavré, J. A. Crooks, B. Y. Chang, R. M. Crooks, *Journal of the American Chemical Society*, **2009**, *131*, 8364–8365.

[21] S. Inagi, *Polymer Journal*, **2016**, *48*, 39–44.

[22] Z. Chen, E. Villani, S. Inagi, *Current Opinion in Electrochemistry*, **2021,** *28*, 100702.

[23] T. Watanabe, M. Ohira, Y. Koizumi, H. Nishiyama, I. Tomita, S. Inagi, *ACS Macro Letters*, **2018**, *7*, 551–555.

[24] Y. Koizumi, H. Nishiyama, I. Tomita, S. Inagi, *Chemical Communications*, **2018**, *54*, 10475–10478.

[25] J. C. Bradley, H. M. Chen, J. Crawford, J. Eckert, K. Ernazarova, T. Kurzeja, M. Lin, M. McGee, W. Nadler, S. G. Stephens, *Nature*, **1997,** *389*, 268–271.

[26] S. Hamlen, *Offshore Engineer*, **1997**, *42*, 38–39.

[27] J. C. Bradley, J. Crawford, K. Ernazarova, M. McGee, S. G. Stephens, *Advanced Materials*, **1997**, *9*, 1168–1171.

[28] J. C. Bradley, J. Crawford, M. McGee, S. G. Stephens, *Journal of The Electrochemical Society*, **1998**, *145*, L45–L47.

[29] J. C. Bradley, Z. Ma, S. G. Stephens, *Advanced Materials*, **1999**, *11*, 374–378.

[30] J. Roche, G. Loget, D. Zigah, Z. Fattah, B. Goudeau, S. Arbault, L. Bouffier, A. Kuhn, *Chemical Science*, **2014**, *5*, 1961–1966.

[31] Y. Koizumi, N. Shida, M. Ohira, H. Nishiyama, I. Tomita, S. Inagi, *Nature Communications*, **2016**, *7*, 10404.

[32] M. Ohira, Y. Koizumi, H. Nishiyama, I. Tomita, S. Inagi, *Polymer Journal*, **2017**, *49*, 163–167.

[33] Y. Koizumi, M. Ohira, T. Watanabe, H. Nishiyama, I. Tomita, S. Inagi, *Langmuir*, **2018**, *34*, 7598–7603.

[34] C. Ulrich, O. Andersson, L. Nyholm, F. Björefors, *Angewandte Chemie - International Edition*, **2008**, *47*, 3034–3036.

[35] L. Bouffier, S. Reculusa, V. Ravaine, A. Kuhn, *ChemPhysChem*, **2017**, *18*, 2637–2642.

[36] C. Tsuneishi, Y. Koizumi, R. Sueto, H. Nishiyama, K. Yasuhara, T. A. Yamagishi, T. Ogoshi, I. Tomita, S. Inagi, *Chemical Communications*, **2017,** *53*, 7454–7456.

[37] L. Koefoed, K. Shimizu, S. U. Pedersen, K. Daasbjerg, A. Kuhn, D. Zigah, *RSC Advances*, **2016,** *6*, 3882–3887**.**

[38] L. Koefoed, S. Us. Pedersen, K. Daasbjerg, *ChemElectroChem*, **2016**, *3*, 495–501.

[39] S. Inagi, Y. Ishiguro, M. Atobe, T. Fuchigami, *Angewandte Chemie International Edition*, **2010**, *49*, 10136–10139.

[40] Y. Ishiguro, S. Inagi, T. Fuchigami, *Langmuir*, **2011**, *27*, 7158–7162.

[41] S. Inagi, H. Nagai, I. Tomita, T. Fuchigami, *Angewandte Chemie International Edition*, **2013**, *52*, 6616–6619.

[42] N. Shida, Y. Ishiguro, M. Atobe, T. Fuchigami, S. Inagi, *ACS Macro Letters*, **2012**, *1*, 656–659.

[43] N. Shida, Y. Koizumi, H. Nishiyama, I. Tomita, S. Inagi, *Angewandte Chemie International Edition*, **2015**, *54*, 3922–3926.

[44] N. Shida, H. Nishiyama, I. Tomita, S. Inagi, *Chemistry Letters*, **2019**, *48*, 1174–1177.

[45] S. Ramakrishnan, C. Shannon, *Langmuir*, **2010**, *26*, 4602–4606.

[46] W. Wei, F. Björefors, L. Nyholm, *Electrochimica Acta*, **2015**, *176*, 1393–1402.

[47] N. Dorri, P. Shahbazi, A. Kiani, *Langmuir*, **2014**, *30*, 1376–1382.

[48] J. J. Liu, X. F. Yang, F. Li, Z. Yang, J. Xie, Y. Li, J. B. He, *ChemElectroChem*, **2019**, *6*, 5237–5241.

[49] R. Beugré, A. Dorval, L. L. Lavallée, M. Jafari, J. C. Byers, *Electrochimica Acta*, **2019**, *319*, 331–338.

[50] M. E. Najafabadi, H. Bagheri, *Microchimica Acta*, **2018,** *185*, 80.

[51] Y. Li, Y. Dong, Y. Yang, P. Yu, Y. Zhang, J. Hu, T. Li, X. Zhang, X. Liu, Q. Xu, Q. Huang, and C. Lin, *ACS Biomaterials Science & Engineering*, **2018,** *5*, 425–431.

[52] G. Loget, S. So, R. Hahn, P. Schmuki, *Journal of Materials Chemistry A*, **2014**, *2*, 17740–17745.

[53] F. Xu, H. Wang, X. Di He, N. Deng, F. Li, B. Li, J. H. Xie, S. K. Han, J. B. He, *Journal of Electroanalytical Chemistry*, **2018**, *823*, 213–220.

[54] L. Jamilpanah, S. Azizmohseni, S. A. Hosseini, M. Hasheminejad, N. Vesali, A. Iraji Zad, M. Pourfath, S. M. Mohseni, *physica status solidi (RRL) – Rapid Research Letters*, **2018**, *12*, 1800418.

[55] G. Loget, A. Kuhn, *Journal of Materials Chemistry*, **2012**, *22*, 15457–15474.

[56] J. C. Bradley, Z. Ma, *Angewandte Chemie International Edition*, **1999**, *38*, 1663–1666.

[57] M. Niamlaem, O. Phuakkong, P. Garrigue, B. Goudeau, V. Ravaine, A. Kuhn, C. Warakulwit, D. Zigah. *ACS Applied Materials & Interfaces*, **2020,** *12*, 23378–23387.

[58] J. C. Bradley, S. Babu, P. Ndungu, *Fullerenes, Nanotubes, and Carbon Nonstructures*, **2005**, *13*, 227–237.

[59] G. Loget, G. Larcade, V. Lapeyre, P. Garrigue, C. Warakulwit, J. Limtrakul, M. H. Delville, V. Ravaine, A. Kuhn, *Electrochimica Acta*, **2010**, *55*, 8116–8120.

[60] C. Warakulwit, T. Nguyen, J. Majimel, M.H. Ne Delville, V. Lapeyre, P. Garrigue, V. Ravaine, J. Limtrakul, A. Kuhn, *Nano Letters*, **2008,** *8*, 500–504.

[61] Z. Fattah, G. Loget, V. Lapeyre, P. Garrigue, C. Warakulwit, J. Limtrakul, L. Bouffier, A. Kuhn, *Electrochimica Acta*, **2011**, *56*, 10562–10566.

[62] L. Zuccaro, A. Kuhn, M. Konuma, H. K. Yu, K. Kern, K. Balasubramanian, *ChemElectroChem*, **2016**, *3*, 372–377.

[63] G. Logeta, G. Larcadea, V. Lapeyrea, P. Garriguea, C. Warakulwitb, J. Limtrakulb, M. H. Delvillec, V. Ravainea, A. Kuhn. *Electrochimica Acta*, **2010,** *55*, 8116–8120**.**

[64] H. Sopha, J. J. Roche, I. S.˘ Vancara, A. Kuhn, *Analytical Chemistry,* **2014,** *86*, 10515–10519.

[65] Y. Koizumi, N. Shida, I. Tomita, S. Inagi, *Chemistry Letters,* **2014**, *43*, 1245–1247.

[66] S. Babu, P. Ndungu, J. C. Bradley, M. P. Rossi, Y. Gogotsi, *Microfluid Nanofluid*, **2005,** *1*, 284–288.

[67] O. Phuakkong, M. Sentic, H. Li, C. Warakulwit, J. Limtrakul, N. Sojic, A. Kuhn, V. Valérie Ravaine, D. Zigah, *Langmuir,* **2016**, *32*, 12995–13002.

[68] I. Malytska, T. Doneux, M. Bougouma, A. Kuhn, L. Bouffier, *Journal of Physical Chemistry C*, **2019**, *123*, 5647–5652.

[69] G. Loget, J. J. Roche, E. Gianessi, L. Bouffier, A. Kuhn, *Journal of the American Chemical Society*, **2012**, *134*, 20033–20036

[70] S. Yadnum, J. Roche, E. Lebraud, P. Négrier, P. Garrigue, D. Bradshaw, C. Warakulwit, J. Limtrakul, A. Kuhn, *Angewandte Chemie International Edition* **2014**, *53*, 4001–4005.

[71] K. Ino, T. Matsumoto, N. Taira, T. Kumagai, Y. Nashimoto, H. Shiku, *Lab on a Chip*, **2018,** *18*, 2425–2432.

[72] T. M. Braun, D. T. Schwartz, *Journal of The Electrochemical Society,* **2015**, *162*, D180–D185.

[73] T. Kuwahara, K. Sato, M. Kondo, M. Shimomura, *Synthetic Metals,* **2014**, *198*, 274–276.

[74] Y. Ishiguro, S. Inagi, T. Fuchigami, *Journal of the American Chemical Society,* **2012,** *134,* 4034-4036.

[75] Z. Sofer, D. Bouša, J. Luxa, V. Mazanek and M. Pumera. *Chemical Communications,* **2016,** *52,* 1563–1566.

[76] C. C. Mayorga-Martinez, B. Khezri, A. Y. S. Eng, Z. Sofer, P. Ulbrich, M. Pumera, *Advanced Functional Materials,* **2016**, *26*, 4094–4098.

[77] S. X. Leong, C. C. Mayorga-Martinez, X. Chia, J. Luxa, Z. Sofer, M. Pumera, *ACS Applied Materials and Interfaces,* **2017**, *9*, 26350–26356.

[78] S. M. Tan, C. C. Mayorga-Martinez, Z. Sofer, M. Pumera, *Chemistry - A European Journal*, **2020**, *26*, 6479–6483.

[79] R. J. Toh, C. C. Mayorga-Martinez, Z. Sofer, M. Pumera, *Analytical Chemistry*, **2016**, *88*, 12204–12209.

[80] C. C. Mayorga-Martinez, N. M. Latiff, A. Y. S. Eng, Z. Sofer, M. Pumera, *Analytical Chemistry*, **2016**, *88*, 10074–10079.

[81] N. P. Dileep, T. V. Vineesh, P. V Sarma, M. V Chalil, C. S. Prasad, M. M. Shaijumon, *ACS Applied Energy Materials*, **2020**, *3*, 1461–1467.

[82] I. Khakpour, A. R. Baboukani, A. Allagui, C. Wang, *ACS Applied Energy Materials*, **2019**, *2*, 4813–4820.

[83] S. E. Fosdick, R. M. Crooks, *Journal of the American Chemical Society*, **2012,** *134*, 863–866.

[84] S. E. Fosdick, S. P. Berglund, C. B. Mullins, R. M. Crooks, *Analytical Chemistry*, **2013,** *85*, 2493–2499.

[85] S. E. Fosdick, S. P. Berglund, C. B. Mullins, R. M. Crooks, *ACS Catalysis*, **2014,** *4*, 1332–1339.

[86] X. Zhang, C. Shang, W. Gu, Y. Xia, J. Li, E. Wang, *ChemElectroChem*, **2016**, *3*, 383–386.

[87] R. Gao, Y.L. Ying, Y.X. Hu, Y.J. Li, Y.T. Long, *Analytical Chemistry*, **2017**, *89*, 7382–7387.

[88] Y.L. Ying, Y.X. Hu, R. Gao, R. J. Yu, Z. Gu, L. P. Lee, Y.T. Long, *Journal of the American Chemical Society*, **2018,** *140*, 5385–5392.

[89] K. Hu, Y. Wang, H. Cai, M. V Mirkin, Y. Gao, G. Friedman, Y. Gogotsi, *Analytical Chemistry*, **2014,** *86*, 8897–8901.

[90] Y. Fan, R. Hao, C. Han, B. Zhang, *Analytical Chemistry*, **2018**, *90*, 13837–13841.

[91] C. Han, R. Hao, Y. Fan, M. A. Edwards, H. Gao, B. Zhang, *Langmuir*, **2019,** *35*, 7180–7190.

[92] S. M. Lu, Y. J. Li, J. F. Zhang, Y. Wang, Y. L. Ying, Y. T. Long, *Analytical*

Chemistry, **2019,** *91*, 10361–10365.

[93] B. Gupta, B. Goudeau, A. Kuhn, *Angewandte Chemie International Edition*, **2017**, *56*, 14183–14186.

[94] L. Zhang, B. Gupta, B. Goudeau, N. Mano, A. Kuhn, *Journal of the American Chemical Society*, **2018,** *140*, 15501–15506.

[95] H. Li, L. Bouffier, S. Arbault, A. Kuhn, C. F. Hogan, N. Sojic, *Electrochemistry Communications*, **2017**, *77*, 10–13.

[96] A. dePoulpiquet, B. Diez-Buitrago, M. Milutinovic, B. Goudeau, L. Bouffier, S. Arbault, A. Kuhn, N. Sojic, *ChemElectroChem*, **2016**, *3*, 404–409.

[97] S. E. Fosdick, J. A. Crooks, B.-Y. Chang, R. M. Crooks, *Journal of the American Chemical Society*, **2010,** *132*, 9226–9227.

[98] K. F. Chow, F. Mavré, R. M. Crooks, *Journal of the American Chemical Society*, **2008**, *130*, 7544–7545.

[99] H. W. Shi, W. Zhao, Z. Liu, X. C. Liu, M. S. Wu, J. J. Xu, H. Y. Chen, *Talanta*, **2016**, *154*, 169–174.

[100] M.-S. Wu, Z. Liu, H.-W. Shi, H.-Y. Chen, J.-J. Xu, *Analytical Chemistry*, **2015**, *87*, 530–537.

[101] M. S. Wu, Z. Liu, J. J. Xu, H. Y. Chen, *ChemElectroChem*, **2016**, *3*, 429–435.

[102] Y. Z. Wang, W. Zhao, P. P. Dai, H. J. Lu, J. J. Xu, J. Pan, H. Y. Chen, *Biosensors and Bioelectronics*, **2016**, *86*, 683–689.

[103] H. Liu, R. M. Crooks, *Analytical Chemistry*, **2012,** *84*, 2528–2532.

[104] Q. Zhai, X. Zhang, Y. Xia, J. Li, E. Wang, *Analyst*, **2016**, *141*, 3985–3988.

[105] W. Xu, K. Fu, C. Ma, P. W. Bohn, *Analyst*, **2016**, *141*, 6018–6024.

[106] W. Xu, K. Fu, P. W. Bohn, *ACS Sensors*, **2017,** *2*, 1020–1026.

[107] G. Loget, A. Kuhn, *Journal of the American Chemical Society*, **2010**, *132*, 15918–15919.

[108] G. Loget, A. Kuhn, *Nature Communications*, **2011**, *2*, 535.

[109] G. Loget, A. Kuhn, *Lab on a Chip*, **2012,** *12*, 1967–1971.

[110] M. Sentic, G. Loget, D. Manojlovic, A. Kuhn, N. Sojic, *Angewandte Chemie International Edition*, **2012**, *51*, 11284–11288.

[111] J. Roche, S. Carrara, J. Sanchez, J. Lannelongue, G. Loget, L. Bouffier, A. Kuhn, *Scientific Reports*, **2014,** *4*, 6705.

[112] B. Gupta, B. Goudeau, P. Garrigue, A. Kuhn, *Advanced Functional Materials*, **2018**, *28*, 1705825.

[113] B. Gupta, M. C. Afonso, L. Zhang, C. Ayela, P. Garrigue, B. Goudeau, A. Kuhn, *ChemPhysChem*, **2019,** *20*, 941–945.

Chapter 2

Template-free Vertical Growth of Poly(3,4-ethylenedioxythiophene) Fiber Arrays by Alternating Current-Bipolar Electrolysis

Abstract: Here, fabrication of a conducting polymer (CP) fiber array without template by bipolar electrochemistry was proposed. Alternating current-bipolar electrolysis using a cylindrical insulator is capable of the perpendicular growth of a uniform poly(3,4-ethylenedioxythiophene) (PEDOT) array from various electrode surfaces. A thorough investigation on the influence of electrolytic parameters revealed that the gap between the cylinder and the bipolar electrode, and the applied voltage are crucial for the growth of a PEDOT array, which was explained by the simulated results of COMSOL Multiphysics. Other parameters such as supporting electrolyte, solvent and diameter of the cylinder affected the morphologies of the fibers. In a word, the methodology offers an efficient and facile way to fabricate CP fiber arrays.

Introduction

Conducting polymers (CPs) play an important role in the field of organic devices.[1,2] The electrochemical synthesis is a common technique for obtaining CPs, which usually endows CP films with a particulate or granular morphology on the electrode surface. On the other hand, CP fibers with the high aspect ratio and the anisotropic morphology, are also of great interest due to their unique properties, such as an efficient anisotropic carrier mobility. Electrode surfaces are often modified with a template before electropolymerization, which is regarded as one of the most promising strategies to obtain CP fiber arrays.[3–5] However, the attachment and removal of templates require redundant working processes, and the use of a template may obstruct other required surface modifications on the electrodes. Therefore, a facile way to prepare CP fiber arrays without a template is a very valuable research issue.

To address this issue, electric field-guided growth is deemed to be efficient to grow CPs in a specific direction, generating CP fibers. In past studies, individual Pt electrode nodes were successfully connected when electrodes were physically linked to an external voltage source, in which three-dimensional poly(3-methylthiophene) networks were formed between several Pt nodes.[6] Besides, two-dimensional growth of polypyrrole having a neuron-like pattern was presented using a needle-to-circle electrodes system.[7] Recently, Inagi and co-workers have pioneered the growth of poly(3,4-ethylenedioxythiophene) (PEDOT) fibers by using the external electric field as a guide. In that bipolar electrochemical system, Au wires that were used as bipolar electrodes (BPEs) and dendritic PEDOT fibers grew from the ends of Au wires by electropolymerization of 3,4-ethylenedioxythiophene (EDOT) under an alternating current (AC) condition.[8,9] Besides, hexachloroplatinate ($[PtCl_6]^{2-}$) and poly(styrenesulfonate) (PSS) were successfully incorporated into electrogenerated PEDOT as dopants to offer hybrid fibers including PEDOT−Pt hybrid fibers and PEDOT−PSS hybrid fibers using the same approach.[10] In addition, a PEDOT thin film grown from terminals of the Au wire was patterned on various nonconductive

substrates.[11] These studies lead the author to challenge the template-free fabrication of CP fiber arrays towards more efficient material preparations and practical applications in electronic devices.

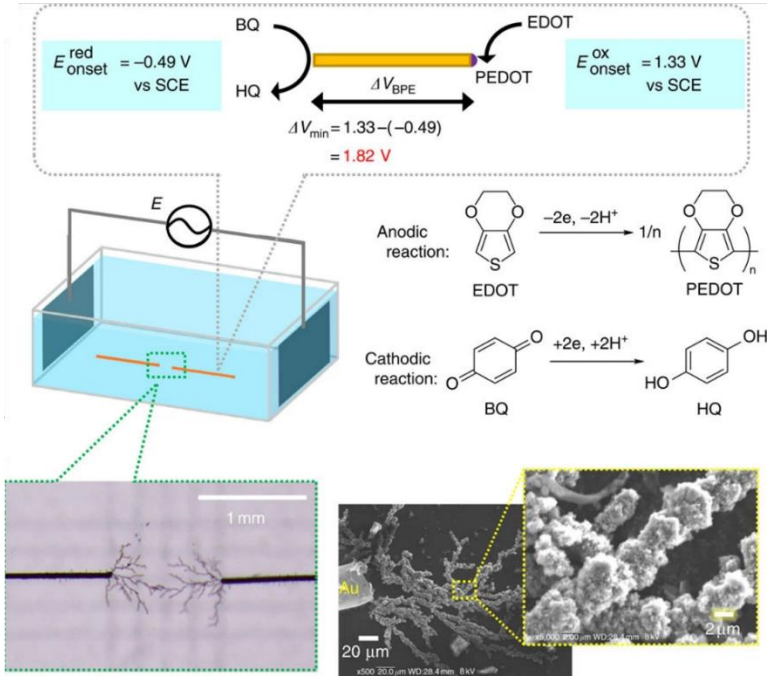

Figure 1. AC-bipolar electropolymerization of EDOT.[8]

Result and Discussion

Preparation of Perpendicular PEDOT Fiber Array by AC-bipolar Electropolymerization

Figure. 2a shows the apparatus for bipolar electropolymeization of EDOT. An electrolytic solution of acetonitrile (MeCN) with 1 mM tetrabutylammonium perchlorate (Bu_4NClO_4), 5 mM 1,4-benzoquinone (BQ) and 50 mM EDOT was employed for the bipolar electrolysis. When applying an iterative potential on the BPE, the circular anodic or cathodic area formed alternately underneath the area covered by the cylinder, with a surrounding cathodic or anodic area having a gradient interface, which depends on the direction of the electric field (Figure 2c). The formed potential difference on the BPE surface (ΔV_{BPE}) promotes redox reactions on the BPE surface. Here, the oxidation of

EDOT occurs in the anodic region, while the reduction of BQ proceeds in the cathodic area simultaneously (Figure. 2b). The redox reactions undergo smoothly when ΔV_{BPE} exceeds 1.82 V in theoretically. The required minimum potential difference was estimated from the onset potentials of a pair of redox reactions reported from linear sweep voltammetry measurements.[8] In experiments, an iterative potential of 100 V was imposed between a pair of driving electrodes and the cylinder was positioned 1 mm from the BPE surface (d = 1 mm). During the electropolymerization, a perpendicular PEDOT fiber array grew on the circular area in 30 min, but only a ring-like very thin film was observed in the surrounding area of the BPE surface (Figure. 2d)

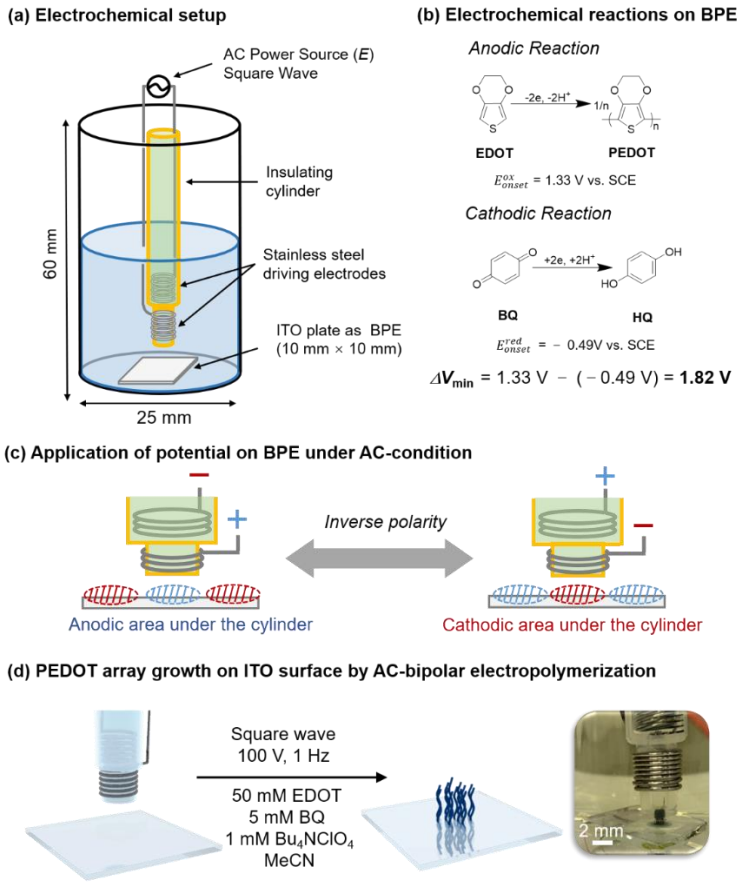

Figure 2. (a) Schematic illustration of AC-bipolar electrolytic setup. (b) Simultaneous electrochemical reactions on the BPE under AC-bipolar electrolysis. EDOT experiences oxidative polymerization on the anodic surface of the BPE and BQ undergo sacrificial reduction on the cathodic surface of the BPE. (c) Under AC-condition, switched potential distribution on the BPE surface. (d) A vertical PEDOT fiber array on the BPE was presented by the graphical representation and the photograph.[12]

Figure. 3 demonstrates the time course of the height of PEDOT fiber arrays and corresponding photographs under the application of 100 V. The lengths of fibers were measured based on SEM images for short fibers (Figure 22 in Experimental Section), or optical images for fibers over 1 mm. The lengths of fibers are about 80 μm, 330 μm, 1000 μm and 2000 μm in 5 min, 15 min, 30 min and 45 min, respectively. Fiber formation was not observed within 5 min, which corresponded to an induction period (Figure 3a). 15 min later, a short fiber array grew on the BPE surface (Figure 3b), which continued to grow under application of the 100 V iterative potential (Figure 3c). The growth rate of fibers increased constantly with prolonged time, especially when the growing fiber terminals reached the bottom of the cylinder (Figure 3d).

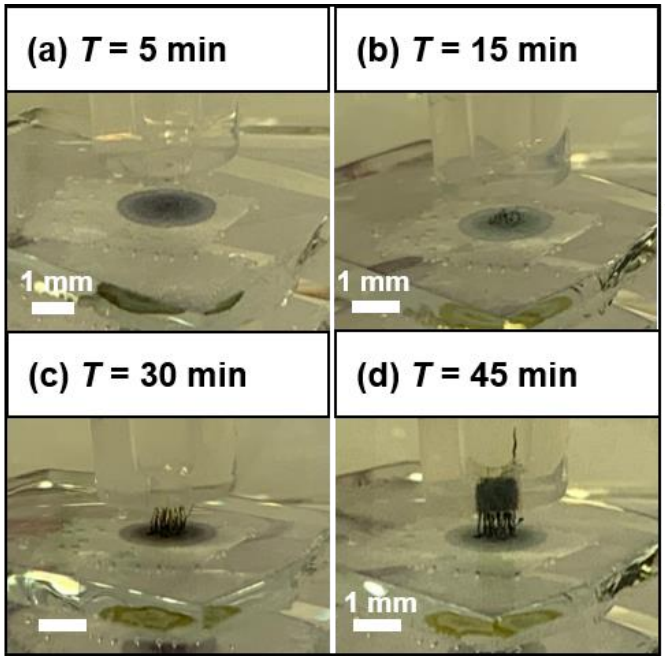

Figure 3. Photographs of time course for the growth of a perpendicular PEDOT fiber array under 100 V applied voltage: (a) 5 min, (b) 15 min, (c) 30 min and (d) 45 min.[12]

Proposed Mechanism for the Formation of PEDOT Fiber Array

At the first stage of fiber array growth, a thin PEDOT film was observed, which should belong to the induction period. Hence, the careful investigation of this film was conducted. Macrostructures of the film were characterized by SEM and laser microscope measurements, while microstructures were analyzed by AFM. SEM images demonstrated

several micrometer-scale particles formed on the surface (Figure 4a,b). Laser microscopy clearly performed those several particles as well (Figure 4c,d). AFM image on the area around islands performed distinguishing morphologies compared to the pristine ITO, reflecting the presence of PEDOT film around the islands (Figure 4e,f). These features suggested that the initial PEDOT film formation followed the Stranski-Krastanov (S-K) mode that three-dimensional islands form following the formation of a two-dimensional layer. Reported works have clearly suggested that potentiostatic electrodeposition of PEDOT film on the electrode surface using the MeCN solution performs a S-K mode film growth.[13]

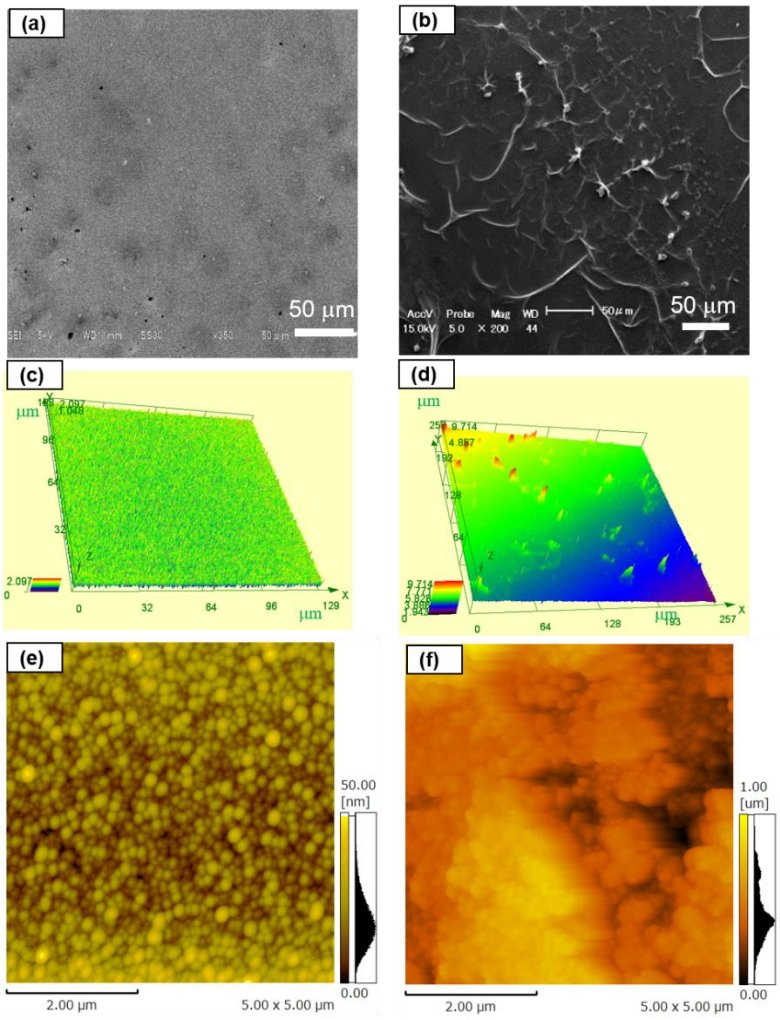

Figure 4. SEM images, 3D laser microscope images and AFM images of the pristine ITO surface (a, c, e) and the formed PEDOT film (b, d, f).[12]

Therefore, a mechanism for PEDOT fiber arrays formation was proposed (Figure 5). Firstly, the voltage applied on driving electrodes offers a sufficient ΔV_{BPE} on the BPE (Stage 1). Then, anodic oxidation of EDOT proceeds, generating a PEDOT film on the BPE. The film growth follows a S-K mode to produce several micrometer-sized particles (*i.e.* islands). This process performs an induction period of the fiber array formation (Stage 2). The formation of these particles is significant to the further fiber growth. Once these particles appeared, they act as nodes for initiating PEDOT fiber polymerization due to the highest potential on the top of these particles (Stage 3).

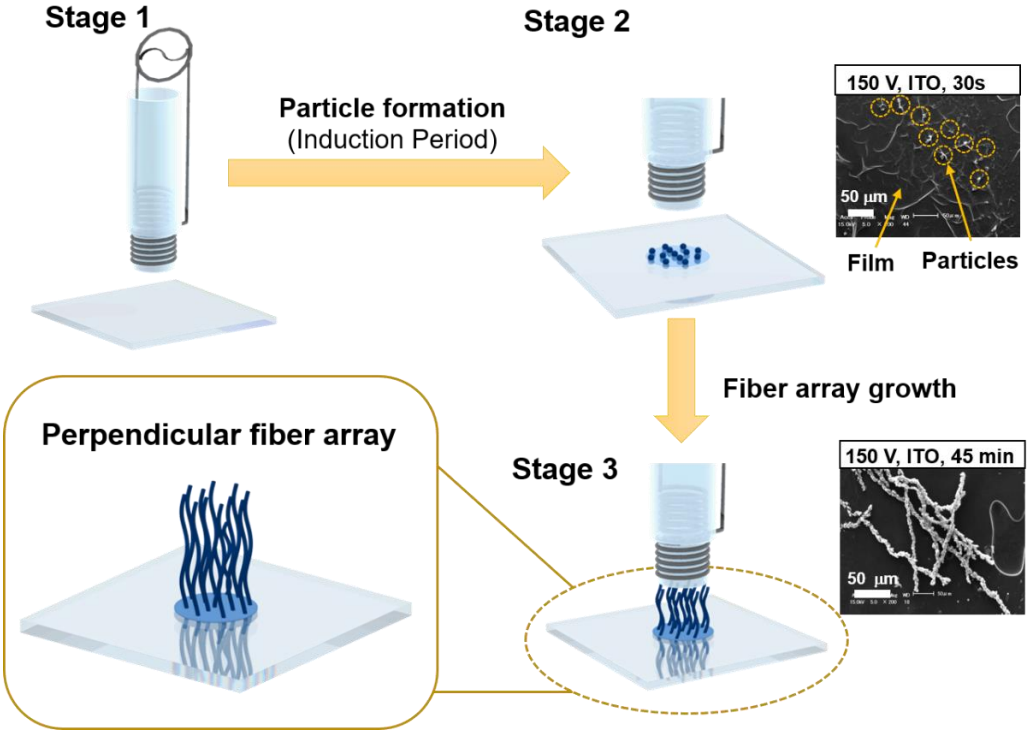

Figure 5. Plausible mechanism for the growth of PEDOT fiber arrays.[12]

COMSOL Simulation to Estimate Potential Difference on the BPE

The limited space in the bipolar cylindrical electrolytic setup impedes the measurement of potential distribution on the BPE surface. To understand the effect of the applied voltage (*E)* and the gap between the cylinder and the bipolar electrode (*d*) on the fiber array growth, computational simulation was carried out. The COMSOL Multiphysics software was introduced to numerically investigate the potential distribution.

The AC/DC module was employed to provide theoretical analysis for exploring the relationship of experimental conditions and the generated electric field distribution. The simulation results showed a mountain-like potential distribution trend on the BPE. As shown in Figure 6, when the driving electrode placed inside the cylinder was a cathode, a circular anodic surface with a surrounding cathodic surface on the BPE formed (anodic moment). The potential distribution was inverted when the voltage was applied in a opposite direction (cathodic moment).

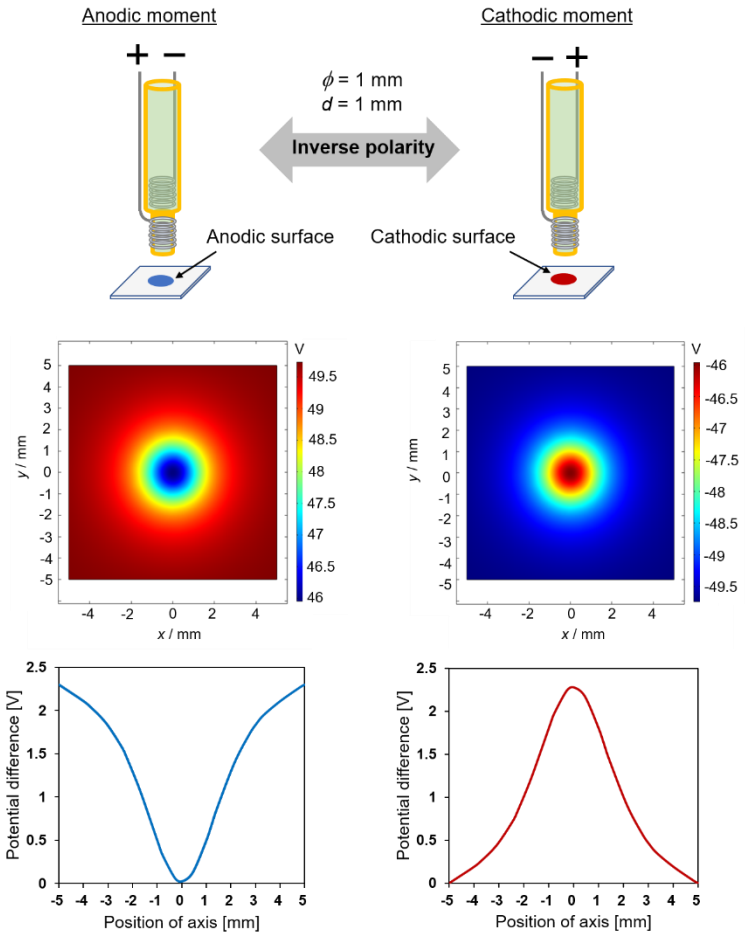

Figure 6. Electric field distribution and potential difference around the BPE surface obtained by COMSOL simulation using a bipolar cylindrical electrolytic setup.[12]

Effect of Applied Voltage

The effect of *E* on the polymerization behavior of EDOT was investigated. The applied potential was gradually increased from 12 V to 150 V. No electropolymerization

occurred on the BPE under a low E of 12 V (Figure 7a). Because formed ΔV_{BPE} on the BPE was insufficient to induce redox reactions. ΔV_{min} of 1.82 V is required to proceed the redox reactions in this bipolar electrochemical system. The polymerization of EDOT can be observed by the application of 50 V, but only a PEDOT film was visual on the BPE in 30 min. SEM analysis revealed that the PEDOT film surface has several small particles (Figure 8). The formed PEDOT fiber array became visible to the naked eye at E = 100 V (Figure 7c). The PEDOT fiber array grew faster at a higher E of 150 V (Figure 7d). However, a more obvious PEDOT film appeared around the circular region of the BPE under the application of a much higher voltage. The length of fibers was *ca.* 1 mm and *ca.* 4 mm under applied voltages of 100 V and 150 V in 30 min (Figure 7c,d). In addition, when the E gradually increased during the electrolytic process, namely 100 V in first 30 min and 50 V in the next 30 min, the speed of fiber growth accordingly slowed down.

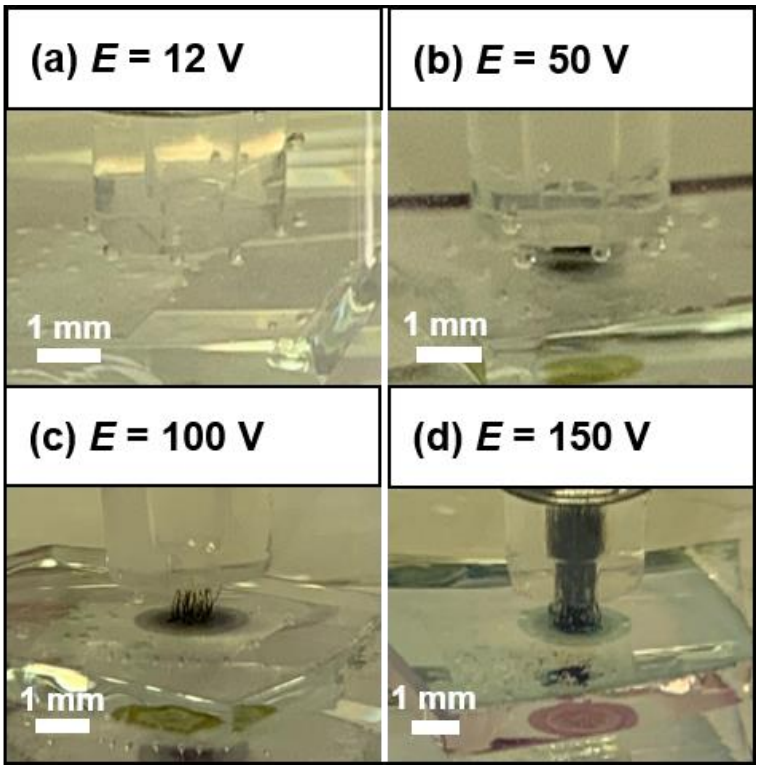

Figure 7. Photographs of the PEDOT fiber array grown in 30 min under different applied potentials (a) 12 V, (b) 50 V, (c) 100 V and (d) 150 V.[12]

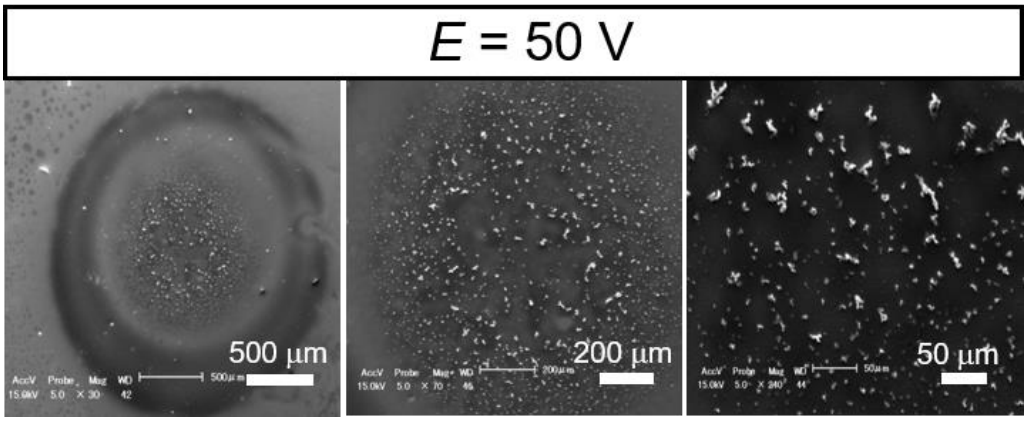

Figure 8. SEM images with various magnitudes a PEDOT film formed under the application of 50 V.[12]

These phenomena were explained by COMSOL simulation. The calculation results revealed when the E increases from 12 V to 150 V, the potential distribution on a BPE and the electric field intensity in the vertical direction gradually improved. Sufficient ΔV_{BPE} is required for successful growth of PEDOT fiber arrays on a BPE (Figure 9a), and a stronger electric field intensity in the z direction accelerated the polymerization process (Figure 9b). Therefore, enhanced E contributes to the growth of PEDOT fiber arrays.

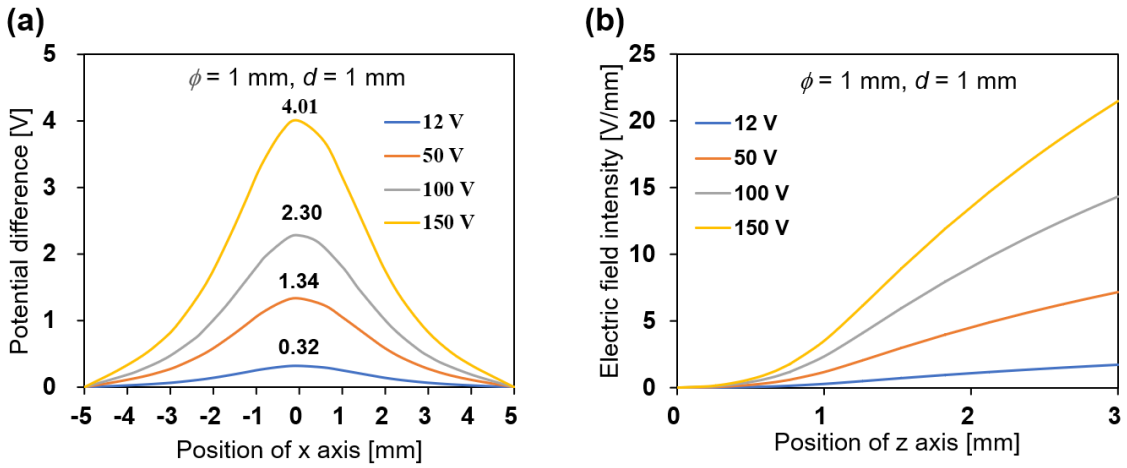

Figure 9. COMSOL Simulations of potential distribution under increased E using an insulating cylinder. (a) ΔV_{BPE} on the BPE. (b) Electric field intensity distribution in the z direction.[12]

Effect of Distance between Cylinder and BPE

The gap distance (d) between the cylinder and the BPE surface is crucial for successful growth of PEDOT fiber array. In experiments, the d value changed from 0 mm (cylinder touched the BPE surface) to 3 mm. When the cylinder contacted the BPE, PEDOT fibers grew very fast. However, the length of the resulting fibers performed a nonuniform feature (Figure 10a). The growth rate of PEDOT fibers was much slower when d increased to 1 mm (Figure 10b), and film formation was observed at d = 2 mm (Figure 10c). At d > 3 mm, PEDOT electropolymerization no longer took place (Figure 10d).

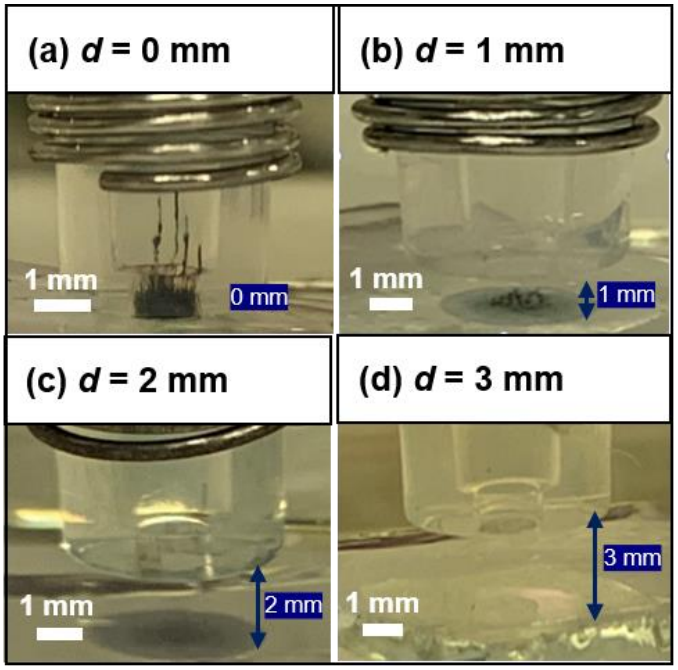

Figure 10. Photographs of PEDOT fibers growth in 15 min under application of 100 V with different d: (a) 0 mm, (b) 1 mm, (c) 2 mm and (d) 3 mm.[12]

Due to the difficulty of estimating ΔV_{BPE} for the cylindrical system, ΔV_{BPE} was based on the simulation results. The ΔV_{BPE} on a BPE and the electric field intensity in the vertical direction were calculated as well under different d values. The values of ΔV_{BPE} at d = 1, 2, 3, 5, and 10 mm were 4.01, 1.78, 0.96, 0.35, and 0.05 V, respectively (Figure 11a). These calculation corresponds to the experimental results, where 150 V of applied voltage was insufficient to generate PEDOT formation when $d \geqslant 3$ mm. Besides, the

electric field intensity in the z direction was obviously decreased with the improvement of *d* (Figure 11b).

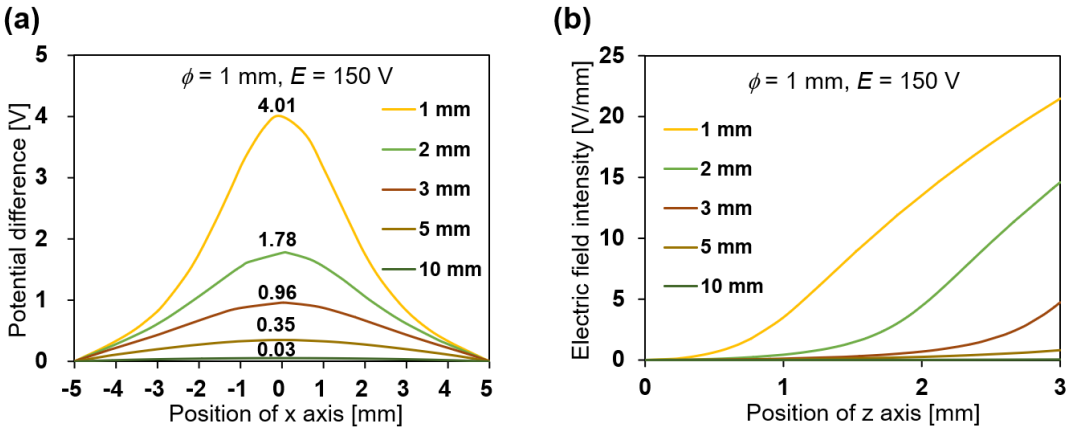

Figure 11. COMSOL Simulations of potential distribution for various *d* using an insulating cylinder. (a) ΔV_{BPE} on the BPE. (b) Electric field intensity distribution in the z direction.[12]

A cylindrical electrolytic cell with driving electrodes at a lower position was employed for the growth of the PEDOT fiber array as well. The polymerization was performed with placing the cell 1 mm apart from BPE as before. However, the position of a pair of driving electrodes was lowered, close to the BPE surface (Figure 12a). The fibers reached the inner driving electrodes quickly to connect each other, which hindered the further growth of PEDOT fibers (Figure 12b), although the later one accelerated the polymerization speed (ca. 1 mm in 7 min) corresponding to the COMSOL simulation (Figure 12c). These results further confirmed that *d* is an important factor for EDOT polymerization, and *d* must be selected at an appropriate value to guarantee the successful growth of a uniform PEDOT fiber array.

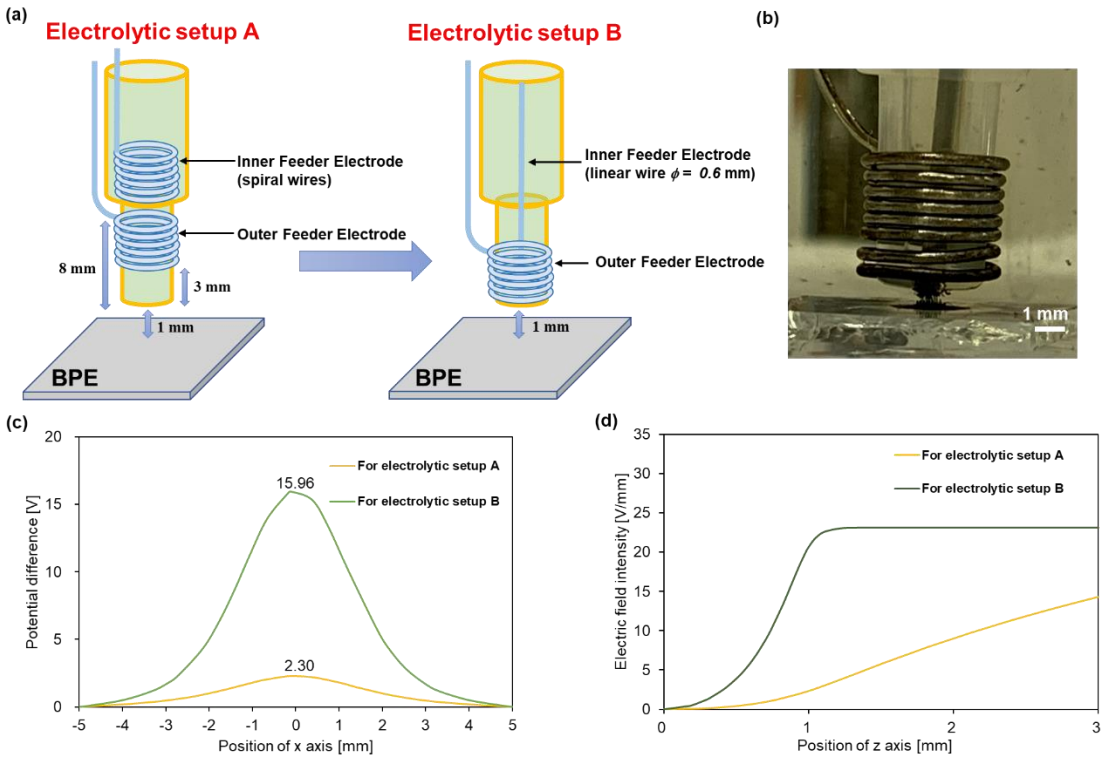

Figure 12. (a) Schematic illustration for original and repurposed electrolytic apparatus. (b) Photograph of PEDOT fiber array formed by using electrolytic setup B. COMSOL simulations of potential distribution of (c) ΔV_{BPE} on the BPE and (d) Electric field intensity distribution in the z direction.[12]

Effect of Concentration, Solvent, Supporting Electrolyte and Frequency

Possible influence factors on the morphologies of the PEDOT fibers were thoroughly investigated, such as concentration of EDOT monomer, solvent, supporting electrolyte and frequency. As for the effect of monomer concentrations, no fiber array was formed on the BPE when a lower monomer concentration of 25 mM EDOT was used (Figure 13a), while fiber arrays were successfully fabricated under higher concentrations of 50 mM and 100 mM EDOT (Figure 13b, c). Besides, a higher concentration of EDOT monomer also produced a greater number of fibers and the average length of the resultant fibers was shorter.

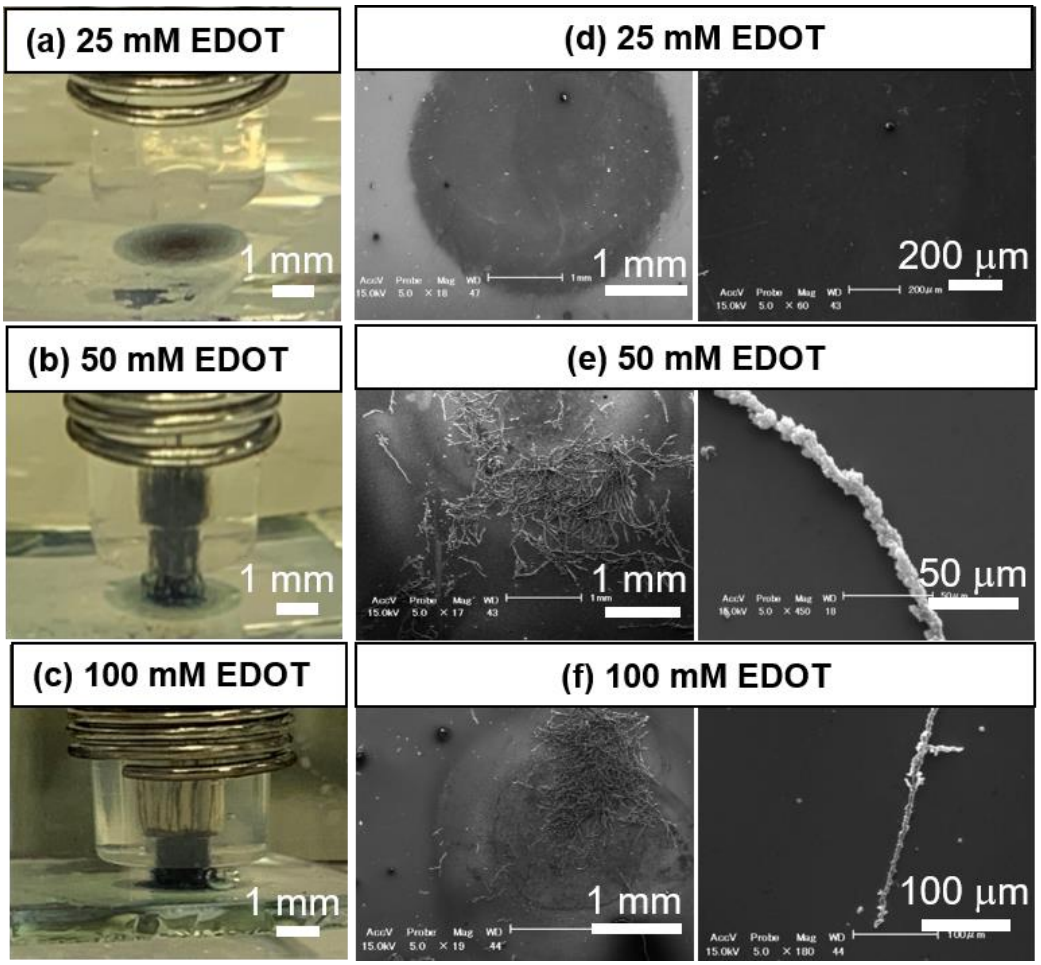

Figure 13. Photographs of polymerized PEDOT (left) and corresponding SEM images (right) when using various EDOT monomer concentrations (a, d) 25 mM, (b, e) 50 mM and (c, f) 100 mM.[12]

The employed solvents affected the growth of PEDOT fiber arrays as well. Dichloromethane (CH_2Cl_2) and methanol (MeOH) were used as solvents to replace MeCN. PEDOT fiber arrays fabricated in CH_2Cl_2 have a snowflake-like microstructure (Figure 14a), while a PEDOT film was observed in the case of MeOH solution (Figure 14b).

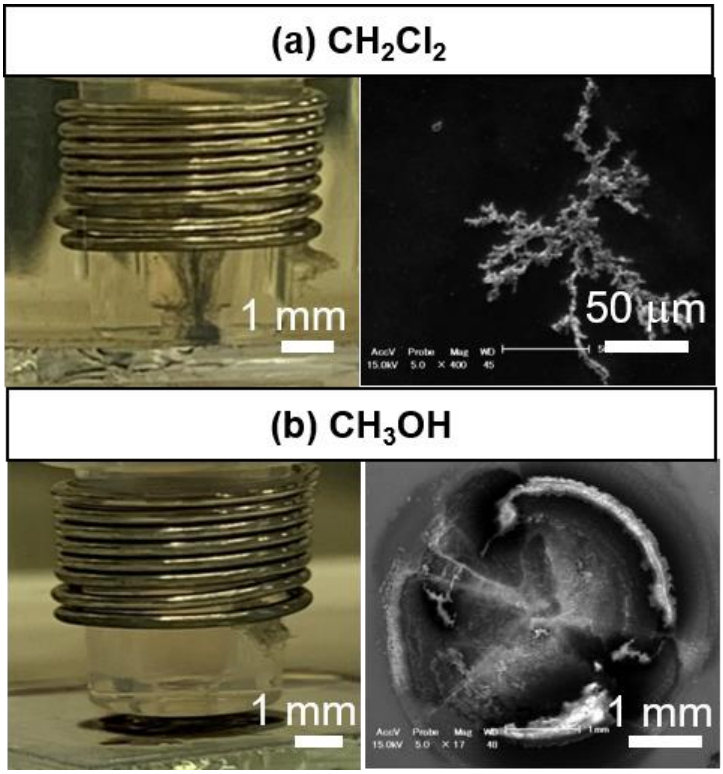

Figure 14. Photographs of polymerized PEDOT (left) and corresponding SEM images (right) using different solvents (a) CH_2Cl_2 and (b) CH_3OH under the application of 150 V.[12]

Although only very low concentration of supporting electrolyte in this bipolar electrolytic system was used, anions still played a significant role in the growth of PEDOT fiber arrays. Bu_4NClO_4, tetrabutylammonium hexafluorophosphate (Bu_4NPF_6) and tetrabutylammonium tetrafluoroborate (Bu_4NBF_4) were used for polymerization. The exist of PF_6^- anions resulted in the formation of several thick perpendicular fibers with a high branching degree with respect to that in ClO_4^- anions (Figure 15a). The use of BF_4^- anions in the electrolyte only generated the formation of a PEDOT film, rather than a vertical PEDOT fiber array. However, many particles were observed on the BPE for BF_4^- case, which indicates that the process kept in the induction stage (Figure 15b).

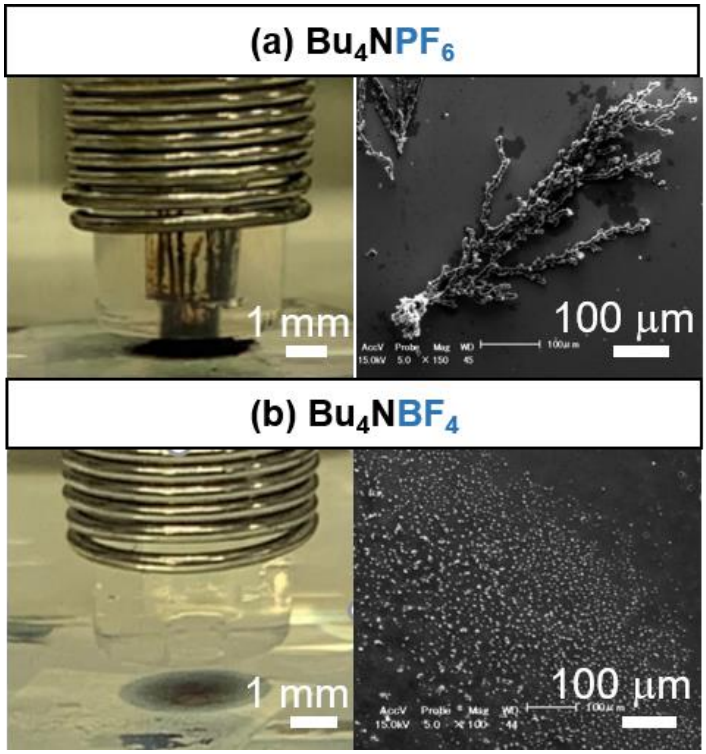

Figure 15. Photographs of PEDOT fiber arrays under 150 V (left) and corresponding SEM images (right) using different electrolytes (a) Bu_4NPF_6 and (b) Bu_4NBF_4.[12]

Besides, the applied frequency also affected the formation of PEDOT fiber array. Under the influence of an external electric field, electrochemically generated charged oligomers undergo the electrophoresis effect. The distinct difference between high and low frequencies is the possible diffusion length of the charged oligomers in the z direction. A lower frequency was considered to offer a longer time for electrochemical reaction on the BPE in every anodic moment and a greater distance of vertical diffusion, which contributes to the perpendicular growth PEDOT fiber arrays. Therefore, low frequency benefits to the growth of PEDOT fiber arrays.

Degree of PEDOT Branching Controlled by Diameter of Cylinder

The morphologies of functional CPs have a direct effect on their properties and performances. Previous studies revealed that the branching degree of PEDOT fibers varies with respect to the free space around the reaction terminals of fibers. The limited space was in favor of the exclusive formation of linear PEDOT fibers.[9] This principle

was also suitable for the PEDOT fiber array in this research. In a limited space (ϕ = 1 mm), a great number of linear fibers formed (Figure 16a,b), while branching fiber appeared in a wide space of ϕ = 2 mm (Figure 16c,d). These results were attributed to the amounts of entered EDOT monomer into the cylinder. When the inner diameter of the cylinder is smaller, there are limited amounts of monomers, so that the monomer sources to the growing terminal of fibers is very limited. In this case, monomers are preferentially consumed at the end of a fiber, where the largest potential difference is applied.

In comparison to the 100 V (Figure 16a,c), the branching degree of PEDOT fibers decreased under the applied voltage of 150 V, and these fibers possessed a relatively smooth surface (Figure 16b,d). In addition, the fiber array grew faster under a higher applied voltage of 150 V. Therefore, it is reasonable to infer that the faster growth rate improved the directionality of fiber growth. When the diameter of cylinder was further increased to 5 mm, branching fibers were performed as well (Figure 17) .

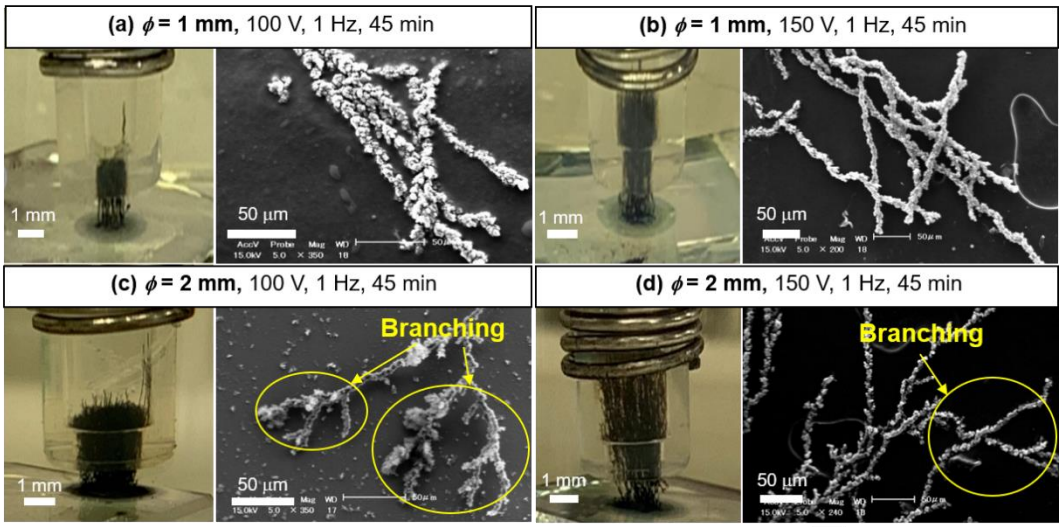

Figure 16. PEDOT fiber arrays formed under different experimental conditions and corresponding SEM images: (a) ϕ = 1 mm, E = 100 V, (b) ϕ = 1 mm, E = 150 V, (c) ϕ = 2 mm, E = 100 V and (d) ϕ = 2 mm, E = 150 V.[12]

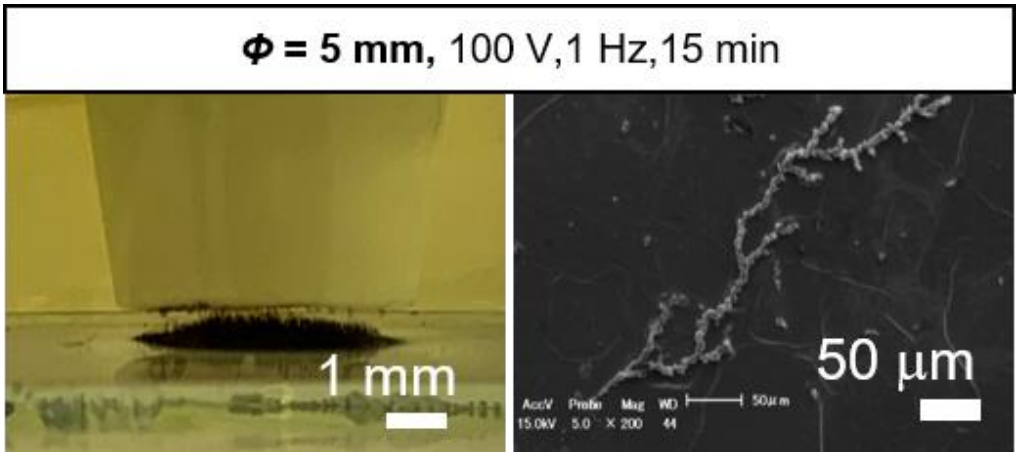

Figure 17. Photograph (left) and corresponding SEM image (right) of the PEDOT fiber array under the applied voltage of 100 V with a cylinder (ϕ = 5 mm).[12]

Perpendicular Growth of PEDOT Derivatives Fiber Array

To expand the family of perpendicular fiber arrays formed by AC electropolymerization, thiophene and other three EDOT derivatives (EDOT-C_1, EDOT-C_{10} and EDOT-Cl, see Experimental Section for the synthesis) were employed. Experimental results demonstrated no fiber array formed from the thiophene system, but a circular film underneath the cylinder was observed. On the other hand, PEDOT-derivatives of EDOT-C_1, EDOT-C_{10} and EDOT-Cl successfully produced fiber arrays having different microstructures (Figure 18). PEDOT-C_1 gave the formation of linear fiber arrays with a rosary-like structure (Figure 18a, d, and g). PEDOT-C_{10} performed the fastest growth, and its fibers showed a relatively rough surface (Figure 18b, e, and h). PEDOT-Cl was rod-like fiber arrays (Figure 18c, f, and i). Here, the morphological features of these PEDOT derivatives fibers resembled those obtained from Au wires in previous work.[8] Hence, the mechanism of fiber formation is regarded to be fundamentally consistent with the previous system.

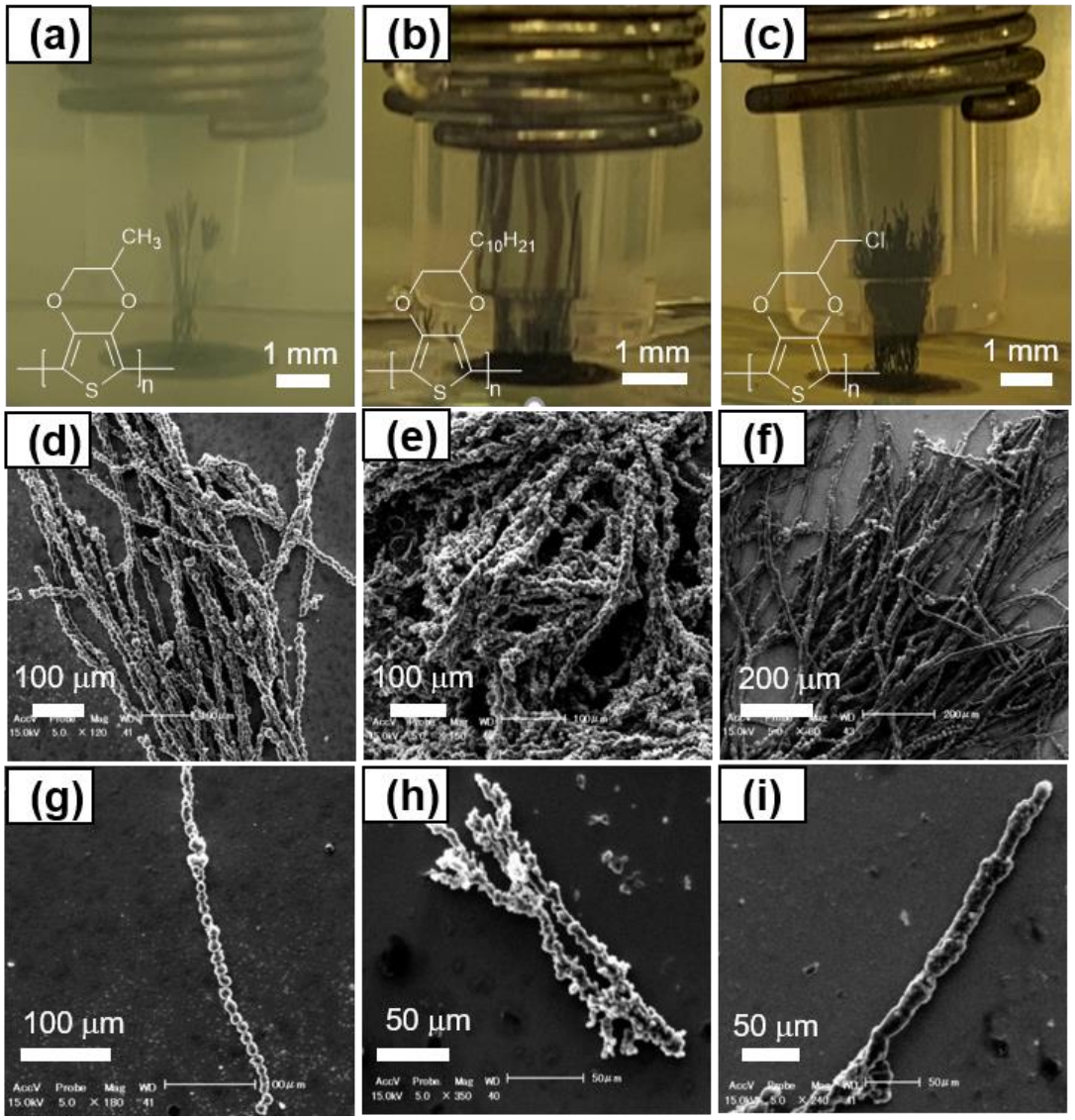

Figure 18. (a,b,c)Photographs of perpendicular fiber arrays, SEM images of (d,e,f) fiber arrays and (g,h,i) single fiber for PEDOT-C_1, PEDOT-C_{10} and PEDOT-Cl.[12]

Growth of Fiber Arrays on Different Materials

This strategy for perpendicular growth of PEDOT fiber arrays has a general applicability on other common electrodes as a BPE material, such as Pt, GC or flat ITO (Figure 19i, k,l), replacing the ITO (Figure 19 j). The fibers obtained on each substrate possessed 10 µm diameter, which is relatively consistent. It should be specially noted that the PEDOT fiber array prepared on the GC surface kept standing after the removal of the cylinder, whereas the PEDOT fiber arrays obtained on Pt, GC and flat ITO surfaces

collapsed. This phenomenon demonstrates that PEDOT fiber arrays grown on a GC substrate should be robust to against the mechanical stress.

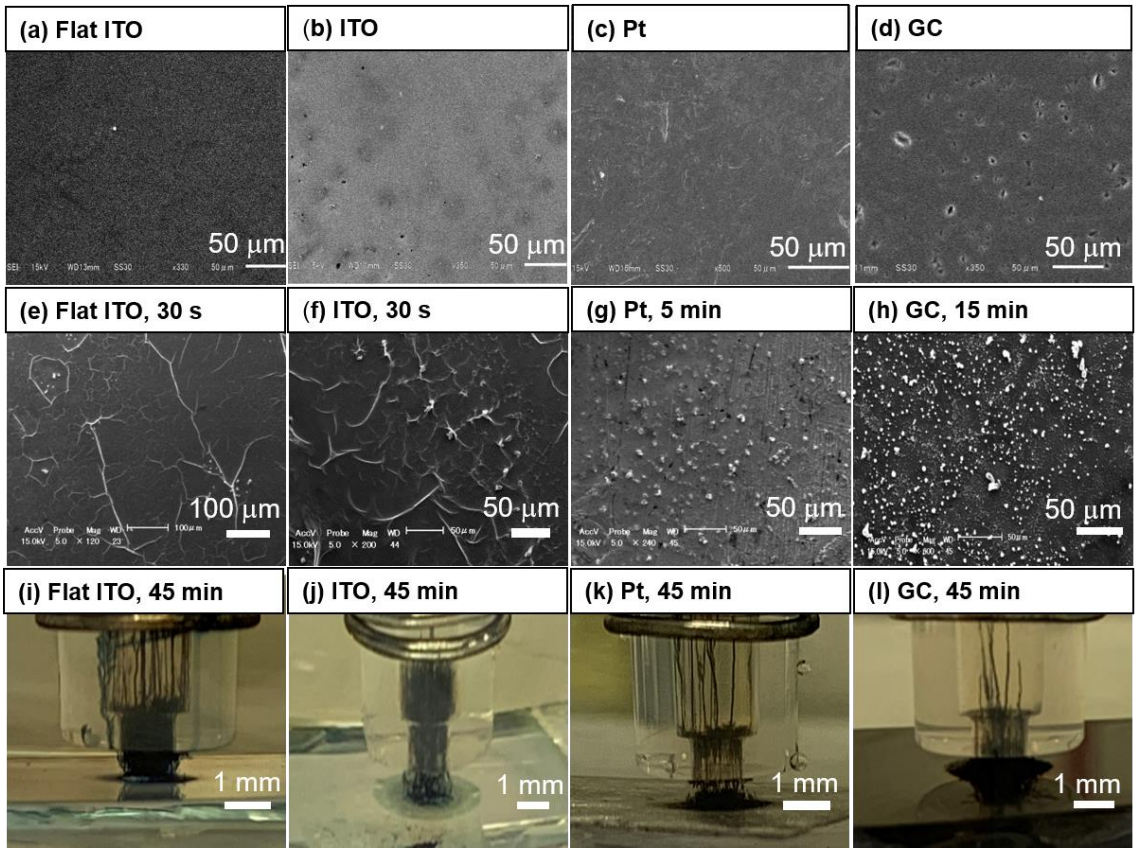

Figure 19. SEM images of pristine substrate surfaces (a–d) and formed films on various substrate surfaces during the induction the period of fiber growth (e–h). (i–l) Photographs of PEDOT fiber arrays grown on different substrates.[12]

To better gain insight into the experimental results, the induction period of fibers growth on various substrates was studied. Compared to the formed particles on other substrates (GC, Pt and flat ITO) (Figure 19e, f, g), the particles formed during induction period on the GC surface were much denser (Figure 19h). On the other hand, the surface roughness of used pristine substrates was also measured by the 3D laser microscope (Figure 19a–d). The GC electrode had the roughest surface, followed by Pt, ITO and flat ITO in sequence (Table 1). Based on these results, it is analyzed that the rough surface of GC benefited to the formation of much more particles, which produced a high density of PEDOT fibers resulting in the great mechanical strength of the vertical fiber array.

Table 1. Surface roughness of the substrates in this work

Substrate	Root mean square roughness (μm)
Flat ITO	0.120
ITO	1.513
Pt	3.133
GC	4.139

Growth of PEDOT Fiber Array on GC Beads-modified Electrode Surface

The perpendicular fiber formation technique was further developed to non-flat surfaces. Many GC microbeads (10–20 μm diameter) were decorated on an ITO surface by the conducting tape. AC-bipolar electrolysis under application of 100 V induced a PEDOT fiber array from these GC beads surface (Figure 20a). The propagation process of the PEDOT fiber array was faster from the surface of GC beads than that from the pristine ITO surface. Presumably because the upper pole of the GC beads could behave as a terminus to initiate the fiber growth. In this case, no induction period was required. As a consequence, the fiber array formed within a shorter period. SEM images revealed that PEDOT fibers connected those GC particles in a network manner, suggesting the fiber growth initiated from poles of GC-particle (Figure 20b). The diameter of these fibers (*ca.* 4.4 μm) was smaller compared to the fibers (*ca.* 10.0 μm) prepared on the pristine ITO surface.

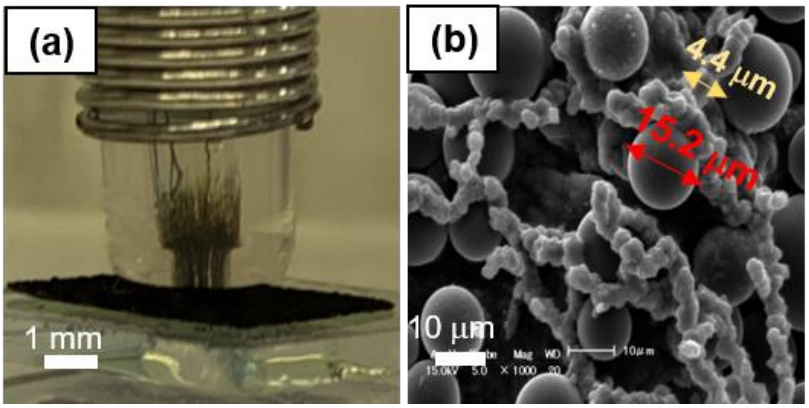

Figure 20. (a) Photograph and (b) SEM image of a PEDOT fiber array fabricated on a GC particle-modified BPE under the applied voltage of 100 V in 15 min.[12]

Conclusion

In summary, the author has demonstrated a general technique to fabricate perpendicular PEDOT fiber arrays on BPE surfaces by AC-bipolar electropolymerization. A particle-induced growth mechanism was proposed based on the investigation of the PEDOT film morphology during the induction period. Narrow gap between the cylinder and the BPE, and high applied voltages favored the formation of fiber arrays due to a bigger potential difference on the BPE surface was generated, which was also proved by COMSOL simulation. The supporting electrolyte, the solvent and the diameter of the cylinder significantly affected the morphologies of the PEDOT fiber arrays. Besides, high monomer concentration and low applied frequency contributed to the fiber array formation. Linear fibers tended to form using a cylinder having a smaller diameter, while branching fibers were fabricated by employing a cylinder having a larger diameter. A family of EDOT derivatives also gave perpendicular fiber arrays under similar conditions. In addition, a wide range of electrode substrates and electrode surfaces were applicable. The proposed strategy here provides a universal, facile and reliable way to prepare CP fiber arrays directly from electrode surfaces without the use of the template. Therefore, the described method in this work opens a new door for designing functional materials to satisfy the need of electronic devices.

Experimental Section

Materials

All reagents and dehydrated solvent were purchased from commercial sources and used without further purification otherwise noted. The electrolytic solutions were deaerated by intensive argon bubbling just before use. EDOT derivatives of EDOT-C_1, EDOT-C_{10} and EDOT-Cl were synthesized according to reported procedures in the literatures.[13] Flat ITO conductive glass, Pt plate, GC plate and GC particle were obtained from commercial sources.

Instruments

An EC1000SA AC/DC power source (NF Corporation) was employed for electropolymerization. Scanning electron microscopy (SEM) observation was carried out with a Shimadzu SS-550 microscope. 3D laser microscope (OLS 4100) and atomic force microscope (Shimadzu SPM-9700) were used to determine the surface morphologies of PEDOT films. ^{1}H nuclear magnetic resonance (NMR) spectra were recorded with a JEOL EX270 NMR spectrometer ($CDCl_3$ as a solvent). COMSOL Multiphysics 5.4 software was used to simulate the electric field distribution.

Synthesis of EDOT-derivatives

The EDOT derivates of EDOT-C_1, EDOT-C_{10} and EDOT-Cl were synthesized by a *p*-toluenesulfonic acid (*p*-TSA)-catalyzed transesterification reaction between 3,4-dimethoxythiophene and 1,2-propanediol, 1,2-dodecanediol or 3-chloropropane-1,2-diol, respectively. The chemical shift for ^{1}H NMR was given in δ (ppm) with respect to that for the internal tetramethylsilane (TMS) as an internal standard. The ^{1}H NMR data of obtained monomers corresponded to the previous reported value.[14]

EDOT-C_1

Under the argon atmosphere, a toluene solution with *p*-toluenesulfonic acid (0.34 g, 1.8 mmol), 1,2-propanediol (1.31 g, 17.3 mmol) and 3,4-dimethoxythiophene (1.00 g, 6.9

mmol) was refluxed for 48 h. After cooling to room temperature, the mixture was filtrated with celite, extracted with dichloromethane, then washed with 5% NaOH solution and brine. The organic phase was dried by anhydrous $MgSO_4$ and concentrated. The crude product was further purified by silica gel chromatography with hexane/ethyl acetate (4/1) to yield 0.22 g of greenish yellow oil (17%).

^{1}H NMR (25 °C, $CDCl_3$, ppm): 1.35(t, J = 6.5 Hz, 3H), 3.85 (dd, *J* = 8.6 Hz, *J* = 8.4 Hz, 1H), 4.25 (m, 2H), 6.27 (s, 2H).

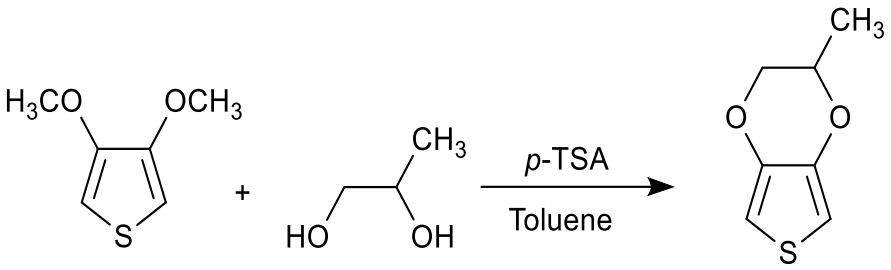

EDOT-C10

Under the argon atmosphere, a toluene solution with1,2-dodecanediol (2.26 g, 11.2 mmol), *p*-toluenesulfonic acid (0.15 g, 0.80 mmol,) and 3,4-dimethoxythiophene (1.08 g, 7.5 mmol) was refluxed for 67 h under an N_2 atmosphere. After cooling to room temperature, the mixture was filtrated with celite, extracted with dichloromethane, and then washed with 5% NaOH solution and brine. The organic phase was dried by anhydrous $MgSO_4$ and concentrated. The crude product was further purified by silica gel chromatography with hexane/ethyl acetate (8/1) to yield 1.74 g of yellow oil (83%).

^{1}H NMR (25 °C, $CDCl_3$, ppm): 0.88 (t, *J* = 6.8 Hz, 3H), 1.40 (m, 18H), 3.86 (dd, *J* = 8.0 Hz, *J* = 8.4 Hz, 1H), 4.16 (m, 2H), 6.32 (s, 2H).

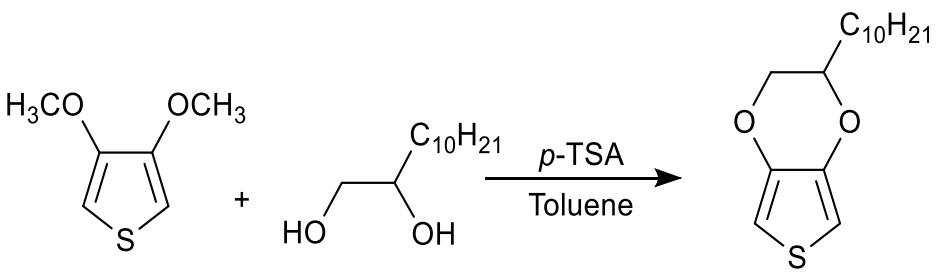

EDOT-Cl

Under the argon atmosphere, a toluene solution with *p*-toluenesulfonic acid (0.20 g, 1.1 mmol), 3,4-dimethoxythiophene (1.00 g, 7.0 mmol) and 3-chloropropane-1,2-diol (1.53 g, 13.9 mmol) was refluxed for 70 h. After cooling to room temperature, the mixture was filtrated with celite, extracted with dichloromethane, then washed with 5% NaOH solution and brine. The organic phase was dried by anhydrous $MgSO_4$ and concentrated. The crude product was purified by silica gel chromatography with hexane/ethyl acetate (6/1) to yield 0.75 g of yellow oil (57%).

^{1}H NMR (25 °C, $CDCl_3$, ppm): 3.7 (m, 2H), 4.15 (dd, J = 6.5 Hz, J = 4.3 Hz, 1H), 4.26 (m, 2H), 6.36 (s, 2H).

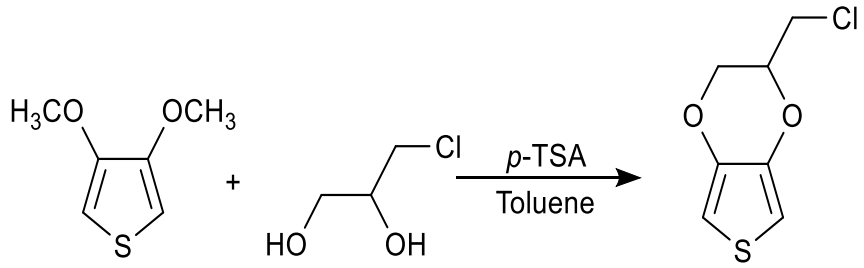

Cell Configuration

A glass container acted as an electrolytic cell and a pair of stainless steel driving electrodes was placed on the insulating cylinder. The driving electrodes were hand-made by shaping stainless steel wires into a spiral to generate a homogeneous electric field. For the cylinder, the inner diameters (ϕ) of the lower and upper cylinders were 1.0 mm and 5.0 mm, with the heights were 8 mm and 60 mm, respectively. A conductive plate (10 mm × 10 mm) composed of ITO, Pt or GC was placed underneath the cylinder as the BPE. An AC power apply was externally connected to driving electrodes (Figure 21a).

When applying an iterative potential on the BPE, the circular anodic or cathodic area appeared alternately underneath the area covered by the cylinder, together with a surrounding cathodic or anodic area having a gradient interface, which depends on the direction of electric potential (Figure 21b).

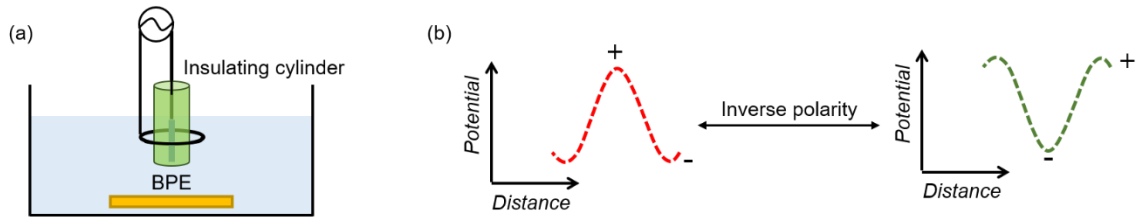

Figure 21. (a) Schematic illustration of the electrolytic cell configuration and (b) potential distribution on the BPE surface under the AC application.[12]

Determination of the Length of PEDOT Fibers

For the short PEDOT fibers (< 1 mm), the length was obtained according to the SEM images. Lengths of four fibers were measured in SEM images and the arithmetic mean value of these fibers was regarded as the length of PEDOT fiber under this condition. For the long fibers (> 1 mm), the length was estimated using an optical image.

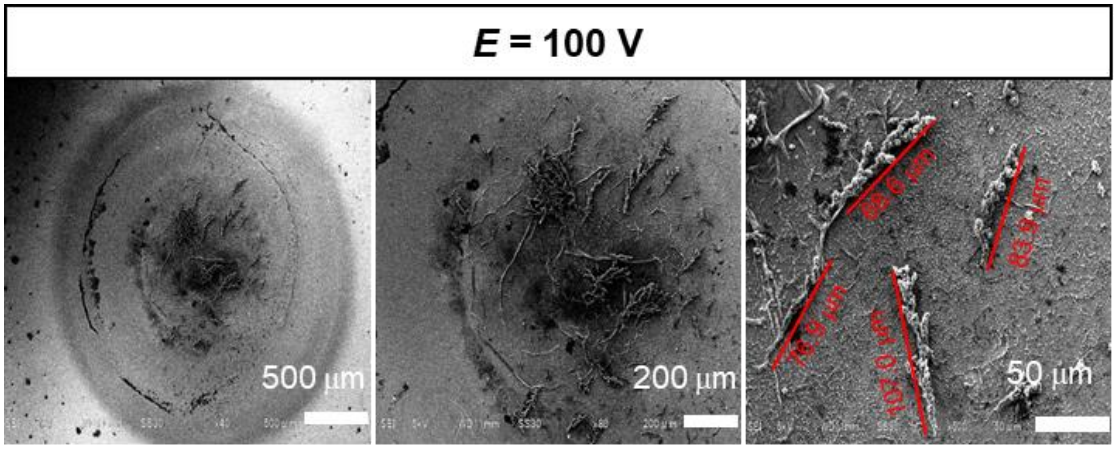

Figure 22. The measurement of PEDOT fiber length based on SEM images.[12]

Estimation of Electric Field Distribution using COMSOL Multiphysics

Geometrical model and simulated calculation were conducted using the COMSOL Multiphysics (Version 5.4) AC/DC module to investigate the electric field distribution and the intensity under different experimental conditions. The geometrical model and material parameters were set according to the practical experimental electrolytic conditions.

References

[1] J. Huang, S. Virji, B. H. Weiller, R. B. Kaner, *Journal of the American Chemical Society*, **2003**, *125*, 314–315.

[2] X. Zhang, W. J. Goux, S. K. Manohar, *Journal of the American Chemical Society*, **2004**, *126*, 4502–4503.

[3] V. Callegari, L. Gence, S. Melinte, S. Demoustier-Champagne, *Chemistry of Materials*, **2009**, *21*, 4241–4247.

[4] S. Il Cho, R. Xiao, S. B. Lee, *Nanotechnology*, **2007**, *18*, 405705.

[5] C. Li, H. Bai, G. Shi, *Chemical Society Reviews*, **2009**, *38*, 2397–2409.

[6] C. L. Curtis, J. E. Ritchie, M. J. Sailor, *Science*, **1993**, *262*, 2014–2016.

[7] M. Fujii, K. Arii, K. Yoshino, *Synthetic Metals*, **1995**, *71*, 2223–2224.

[8] Y. Koizumi, N. Shida, M. Ohira, H. Nishiyama, I. Tomita, S. Inagi, *Nature Communications*, **2016**, *7*, 10404.

[9] M. Ohira, Y. Koizumi, H. Nishiyama, I. Tomita, S. Inagi, *Polymer Journal*, **2017**, *49*, 163–167.

[10] Y. Koizumi, M. Ohira, T. Watanabe, H. Nishiyama, I. Tomita, S. Inagi, *Langmuir*, **2018**, *34*, 7598–7603.

[11] T. Watanabe, M. Ohira, Y. Koizumi, H. Nishiyama, I. Tomita, S. Inagi, *ACS Macro Letters*, **2018**, *7*, 551–555.

[12] Y. Zhou, N. Shida, Y. Koizumi, T. Watanabe, H. Nishiyama, I. Tomita and S. Inagi. *Journal of Materials Chemistry C*, **2019,** *7*, 14745–14751.

[13] H. Randriamahazaka, V. N. C. Chevrot, *Journal of Electroanalytical Chemistry*, **1999**, *472*, 103–111.

[14] D. W. Breiby, E. J. Samuelsen, L. Groenendaal, B. Struth, *Journal of Polymer Science, Part B: Polymer Physics*, **2003**, *41*, 945–952.

Chapter 3

Fabrication of Polymer Nanowires by Templated Bipolar Electropolymerization Assisted by Electrophoretic Effect

Abstract: Fabrication of perpendicular conducting polymer (CP) nanowires on a substrate surface is of significance in the field of energy devices and organic electronics. Although the use of a template with nanopores for electropolymerization of aromatic monomers is a straightforward approach to prepare such materials, limited diffusion of monomers into the narrow nanopores of the hard template impedes the formation of robust polymer nanowires. In this work, successful formation of robust and dense polymer nanowires is presented based on a templated bipolar electrolysis promoted by the electrophoretic effect. Charged monomers used for the bipolar electrolysis can migrate under an external electric field, undergoing forced and directional diffusion into the nanopores of a template. Both of ruthenium-polypyridine and thiophene-based conducting polymer nanowires were obtained by the cathodic reduction and the anodic oxidation, respectively, on a bipolar electrode (BPE). The produced polymer nanowires keep one-dimensional perpendicular form even after the removal of the hard templates due to the great improvement in their mechanical strength.

Introduction

One-dimensional (1D) CP nanostructures in the forms of nanowires and nanorods have been used in various fields of sensor,[1,2] organic phototransistor,[3] lithium ion battery[4] and supercapacitors[5] due to their advantages compared to their bulk counterparts. Many preparation strategies with respect to 1D polymer nanostructures have been developed, such as electrospinning methods,[6] electrodeposition,[7,8] chemical vapor deposition[9] and so on. Among these methods, the electrodeposition is attractive due to the use of a facile setup and the controllability by the applied voltage. A hard template attached on the electrode surface is commonly used to achieve the regular shape and the size of nanostructures. The anodic aluminum oxide (AAO) template is the most popular one for the preparation of nanostructures.

However, the nanopores in the AAO template have a high aspect ratio, which highly limited diffusion of the electroactive monomers into it. Thus, the deposited polymer tends to perform a hollow tubular structure having a lack mechanical strength (Figure 1).[10,11] As a result, collapsed 1D polymer nanotubes are usually obtained, which severely restrict their practical applications. To solve this problem, Atobe and co-workers presented the use of supercritical fluids that have low viscosity and high diffusivity to produce robust CP nanofibers by the templated electropolymerization.[12] This strategy is reliable in response to the improvement of monomer diffusion, but it needs special apparatuses and harsh conditions, which restricted the large-scale application. Constant current electrolysis with direct assembly method also was employed to prepare CP nanowires, but it requires precious control of current density and three-step electrochemical deposition procedure. [13]

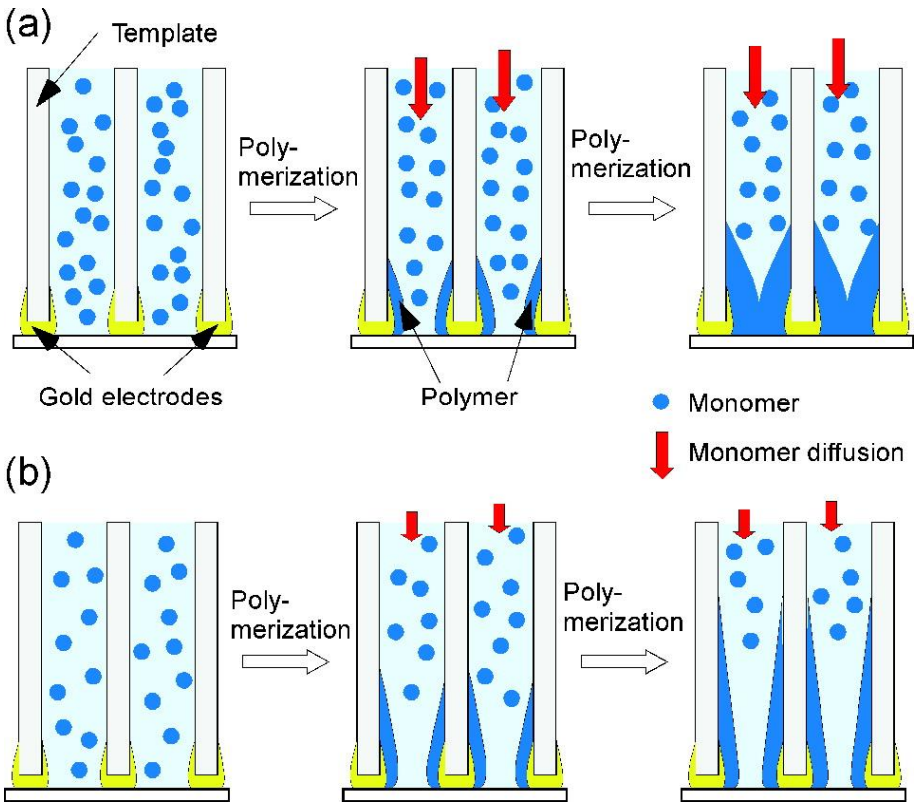

Figure 1. (a) Growth mechanism of PEDOT nanostructures based on diffusion and reaction kinetics for high oxidation potential region (≥ 1.4 V). Two extreme cases are considered: (a) slow reaction rate under sufficient monomer supply and (b) fast reaction rate under insufficient monomer supply.[10]

The introduction of electrophoresis during the electropolymerization process seems a straightforward way to enhance the diffusion ability of charged monomers towards the electrode surface. Electrophoresis relies on an electric field across the bulk electrolyte solution. Therefore, the essential component of supporting salt with a high concentration should be avoid otherwise the applied voltage was mainly consumed on the electric double layers. From this perspective, bipolar electrolysis could be a promising technique.[14–16] Because a low concentration of the electrolyte is employed to offer an electric field across the whole electrolytic solution, which drives the electrochemical reactions on the BPE. Anodic and cathodic reactions occur simultaneously on poles of the BPE. Therefore, bipolar electrochemistry can perform compatible electrolysis and electrophoresis together. In fact, several studies have investigated the preparation of intriguing anisotropic materials benefited from the effect of concurrent electrolysis and

electrophoresis in one bipolar electrochemical system.[16–26]

In this work, fabrication of 1D robust CP nanowires by synergetic effects of electrolysis and electrophoresis in bipolar electrochemistry was conducted. Here, valuable and applicative aromatic monomers of ruthenium polypyridine complexes with positive charges and a thiophene-based salt with a negative charge were employed for electropolymerization. This work devotes to create a facile and efficient approach to prepare robust 1D polymer nanowires.

Result and Discussion

Templated Bipolar Electropolymerization of Cationic Monomers

Reductive electropolymerization was conducted firstly using ruthenium-containing cationic monomers. Polypyridine transition-metal complexes possess attractive photophysical and electrochemical properties. Murray and co-workers have carried out the reductive electropolymerization using vinyl-substituted polypyridine iron and ruthenium complexes on electrode surfaces.[27] Such electropolymerized complex films are widely used in many fields, including electrocatalysis,[28] electrochromic,[29] sensor[30] and electrogenerated chemiluminescence.[31] Zhong and co-workers firstly developed an ligand of 5,5′-divinyl-2,2′-bipyridine (5,5′-dvbpy) to efficiently transform ruthenium complex into its polymeric films.[32–34] And this class of ruthenium complexes performed superior electropolymerization ability, while the fabrication of corresponding polymer nanowires has never been reported so far. Here, $[Ru(5,5'\text{- dvbpy})(bpy)_2](PF_6)_2$ (**1**) and $[Ru(5,5'\text{-dvbpy})_3](PF_6)_2$ (**2**) were synthesized firstly according to the literatures.[32,35,36] The electropolymerization process of both compounds was monitored by cyclic voltammetry (CV) and the current increased with CV cycles, which dedicated successful formation of polymeric films. In comparison of **1** (Figure 2a), reductive electropolymerization of **2** was more efficient due to more vinyl groups in the ligand framework (Figure 2c). The CVs of these conductive polymeric films in the monomer-free electrolyte solution demonstrated a well-defined $Ru^{II/III}$ and redox couples from

ligands (Figure 2b,d). After the characterization of the electrochemical activities, these monomers were employed in the templated bipolar electrolysis.

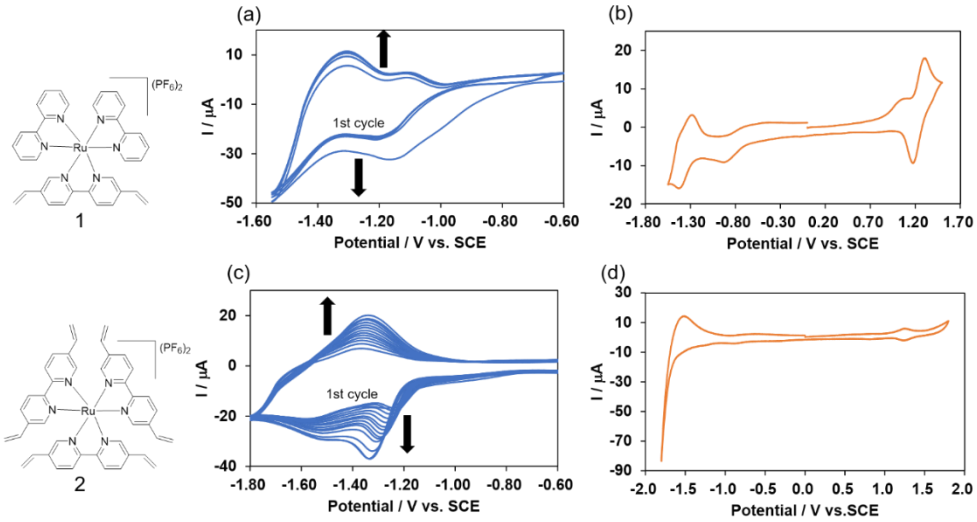

Figure 2. (a) CV measurement of 0.5 mM monomer **1** by repeated cyclic potential scans in acetonitrile (MeCN) with 0.1 M Bu_4NClO_4 using Au disk (ϕ = 3 mm) as a working electrode, a SCE as a reference electrode and a Pt plate (20 mm × 20 mm) as a counter electrode at a scan rate of 200 mV/s. (b) CV measurement of the obtained polymeric film **1** in a monomer-free supporting electrolyte solution at a scan rate of 100 mV/s. (c) CV measurement of 0.5 mM monomer **2** by repeated cyclic potential scans in MeCN with 0.1 M Bu_4NClO_4 using Au disk (ϕ = 3 mm) as a working electrode, a SCE as a reference electrode and a Pt plate (20 mm × 20 mm) as a counter electrode at a scan rate of 100 mV/s. (d) CV measurement of the obtained polymeric film **2** in a monomer-free electrolyte solution at a scan rate of 100 mV/s.[37]

As shown in Figure 3a, the experimental configuration for bipolar electrolysis includes an electrolytic cell (20 mm × 10 mm), driving electrodes (10 mm × 10 mm), a pair of split BPEs and an MeCN electrolytic solution containing hydroquinone (HQ) as a sacrificial reagent and ruthenium-ligand monomers. The AAO membrane was attached on the BPE surface, which was connected to another piece of ITO by an ammeter.[38] This split BPEs was placed in the electrolyte, in which the modified ITO electrode and pristine ITO electrode act as cathode and anode, respectively. Reductive electropolymerization of ruthenium-ligand monomers took place on the BPE cathode, while oxidation of HQ proceeded on the BPE anode simultaneously to keep electronic balance on the BPE (Figure 3b). The applied potential difference on the BPE (ΔV_{BPE}) should be higher than

1.63 V that is the onset potential difference (ΔV_{min1}) of their redox couple (Figure 18). ΔV_{BPE} was fixed to 14 V by controlling the distance (7 mm or 14 mm) between the anode and cathode of BPE. The applied voltage on a pair of driving electrodes is enough to drive the redox reactions (Figure 20). During the reductive electropolymerization, positively charged **1** and **2** moved toward the BPE cathode induced by the external electric field across the solution. Notably, the ruthenium complexes here act as both monomer and supporting electrolyte, which avoid the use of additional supporting electrolyte. The templated bipolar electropolymerzation was proceeded in the following manner: The AAO template-modified BPE was immersed into the electrolytic solution for at least 1 h before a DC applied voltage (20 V or 40 V) on driving electrodes. After templated bipolar electrolysis, the cathode of BPE was washed by MeCN to remove residual monomers. Then, the AAO template was dissolved using 1 M KOH aq. (Figure 3c). Finally, the sample was carefully washed by deionized water and MeCN in sequence, and further used for the characterization.

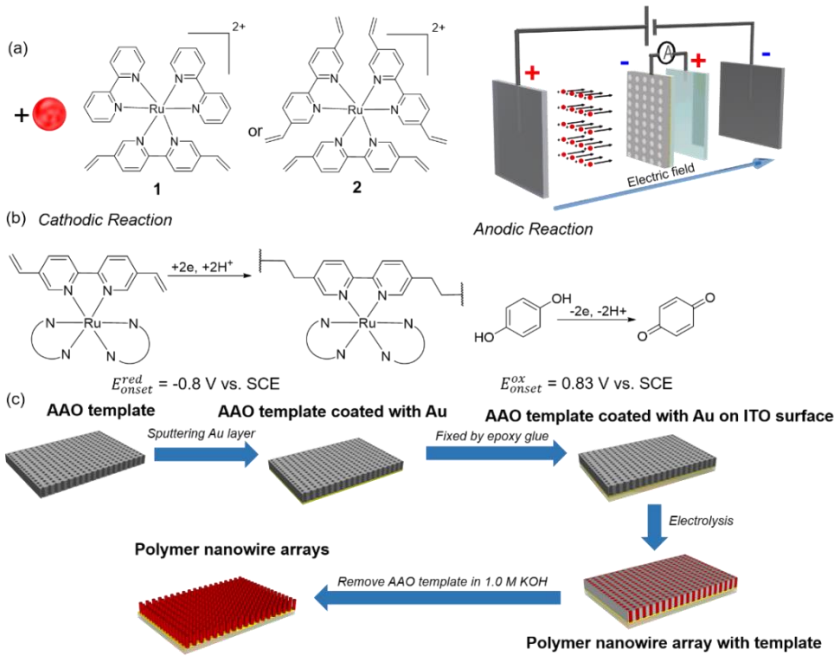

Figure 3. (a) Chemical structures of Ru-contained complexes and schematic illustration of the electrochemical setup for the templated bipolar electrolysis. (b) Reductive polymerization of Ru-contained complexes on BPE cathode and sacrificial oxidation of hydroquinone on BPE anode. (c) Illustration of processes to fabricate polymer nanowire arrays.[37]

Figure 4a demonstrates the SEM image of used AAO membrane with a 200 nm pore diameter. When the templated bipolar electropolymerization of **2** was carried out, an ammeter connecting the split BPE monitored the flowed current between the BPE anode and cathode. The total amount of electricity for the redox couple on the split BPE was 184 mC (Figure 5). The current-time curve displayed the highest current appeared at the beginning of the electrolysis. This is presumably due to the fast reaction of **2** already filled in channels of the template after immersion process, followed by a lower but steady electrolytic current due to the continuous electrolysis of **2** supplied to the channels by electrophoresis. Here, as a control experiment, constant potential electrolypolymerization at −1.2 V vs. SCE also was proceeded, which passed the consistent amount of charge (184 mC). SEM images of the obtained films on both cases revealed the different morphologies of the resulting polymers. 1D poly-$[Ru(5,5'\text{-dvbpy})_3](PF_6)_2$ (poly-**2**) nanowires were fabricated on the ITO surface by the templated bipolar electrolysis (Figure 4b), while the templated constant potential electrolysis produced the aggregated state on the electrode surface, probably due to the poor mechanical strength (Figure 4c). The standing nature of poly-**2** nanowires prepared by the templated bipolar electropolymerization approach represents their good mechanical strength. Considering the concentration of monomers and the electricity were consistent in both cases, it is reasonably summaries that the bipolar electrochemical conditions enabled the more efficient migration of **2** into the nanopores of the AAO membrane, affected by the electrophoretic effect. The cross-sectional image of the electrode surface showed that nanowires kept a vertical geometry to the substrate after removing the template. EDS analysis revealed the chemical compositions of poly-**2** nanowires. Ru element came from poly-**2** and Au element was from the bottom layer (Figure 4d).

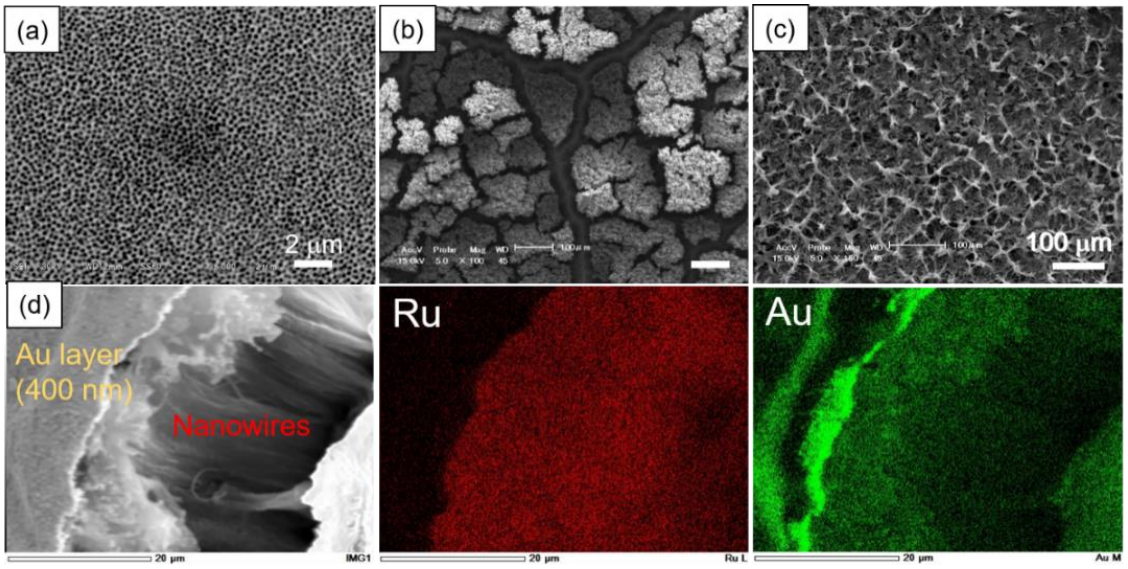

Figure 4. SEM images of (a)AAO membrane and poly-**2** nanowires prepared by (b) the templated bipolar electrolysis or (c) the conventional templated constant potential electrolysis. (d) Cross-sectional SEM image of perpendicular poly-**2** nanowires in (b) and corresponding EDS mappings of Ru and Au elements.[37]

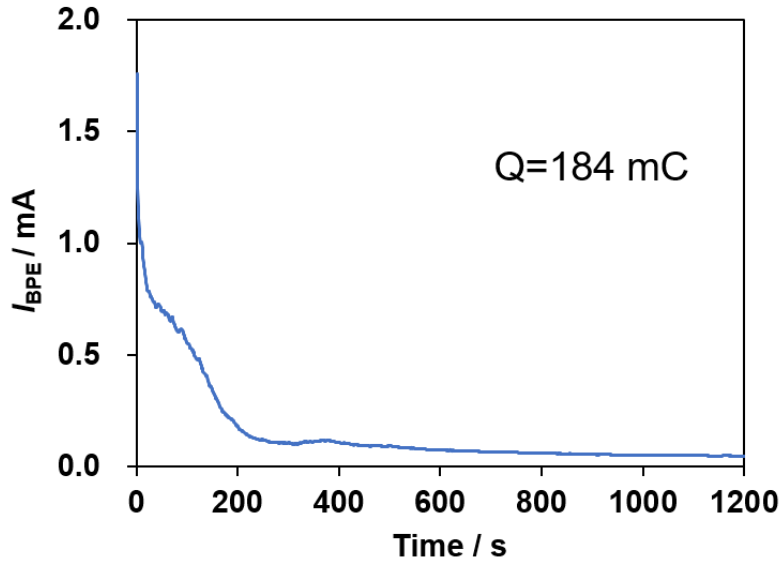

Figure 5. Current-time curve for templated bipolar electropolymerization of monomer **2**.[37]

In addition, the templated bipolar electrolysis of **1** was also conducted. However, the resulting poly-[(5,5′-dvbpy)$(bpy)_2$] (poly-**1**) partially dissolved in KOH solution when the template was removed by KOH solution (Figure 6). It can be explained that poly-**2** has crosslinked structure with the presence of six vinyl groups per monomer, benefiting to

maintain the integrity property. On the other hand, poly-**1** belongs to a linear polymer in principle, leading to the undesired dissolution.

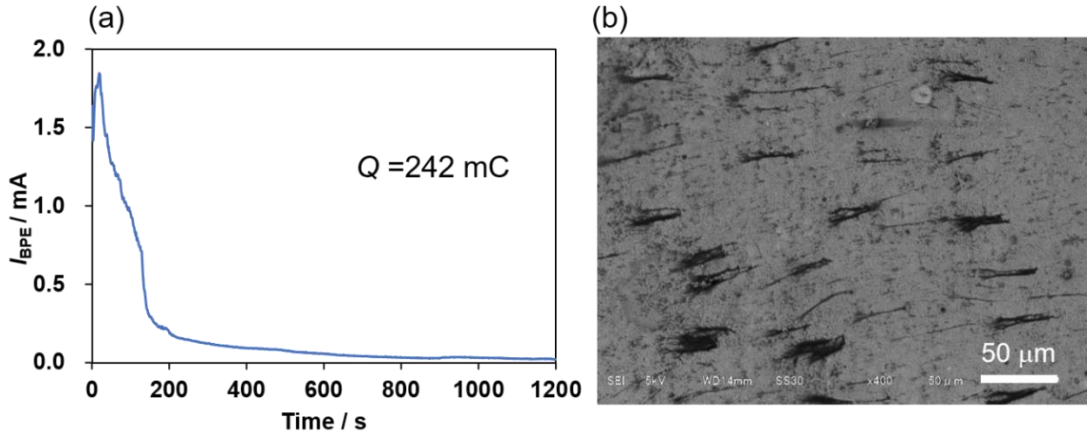

Figure 6. (a) Current-time curve and (b) SEM image for templated bipolar electropolymerization of monomer **1**.[37]

These obtained two ruthenium-contained polymer nanowires were also characterized by IR spectroscopy, which showed a strong peak at 844 cm^{-1} derived from PF_6^-. And the peak at 935 cm^{-1} belongs to out-of-plane deformation vibration of the vinyl group, which disappeared for poly-**1** nanowires due to the vinyl group is absolutely consumed. However, the IR data stated that a part of vinyl groups were still maintained in poly-**2** nanowires (Figure 7).

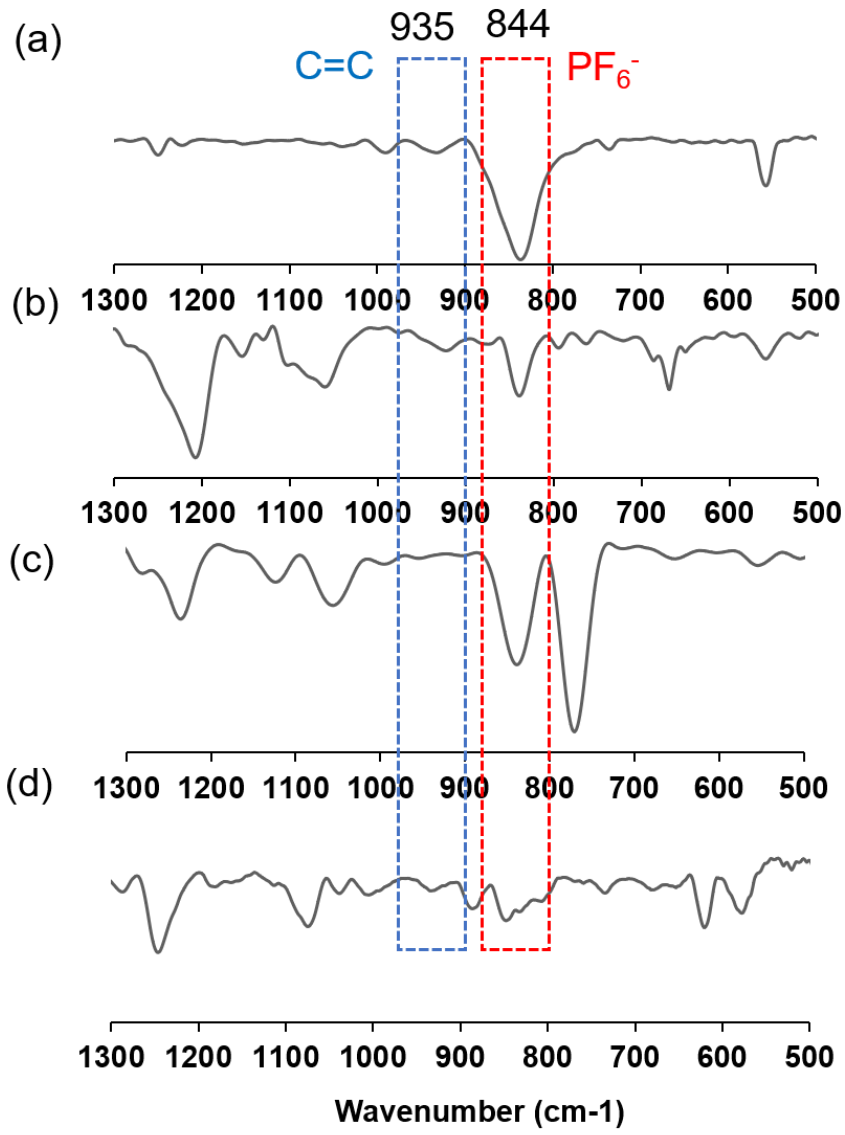

Figure 7. IR spectra of (a) **1**, (b) **2**, (c) poly-**1** nanowires, (d) poly-**2** nanowires.[37]

The templated bipolar electropolymerization of monomer **2** was proceeded under different conditions of electropolymerization time (*T*), monomer concentrations (*C*) and applied electric field intensity (*E*). Morphologies of resulting films were characterized by SEM images (Figure 8). When a low *E* of 10 V/cm was applied, electropolymerizaiton of 0.25 mM of monomer **2** did not conduct smoothly and no polymer nanowire was observed in 4 min (Figure 8a). When *T* was extended from 4 min to 20 min, aggregated polymers was produced having a collapsed structure (Figure 8b). When a higher *E* of 20 V/cm was used for shorter *T* (4 min), the 1D polymer nanomaterials collapsed on the electrode

surface in the form of many aggregated tubular structures, as evidenced in its TEM image (Figure 8c, 9). The thickness of the nanotube wall was *ca.* 30 nm. Extending *T* to 20 min under the same condition, perpendicular 1D poly-**2** nanowires was formed with length (*L*) of 25 μm (Figure 8d), which was estimated from the cross-sectional SEM image (Figure 4d). Previous study explained the formation of hollow tubular structures from the templated electropolymerization because of the limited diffusion of monomers.[39] In contrast, poly-**2** nanowires showed no cavity observed from the top view of high-resolution SEM images (Figure 8d).

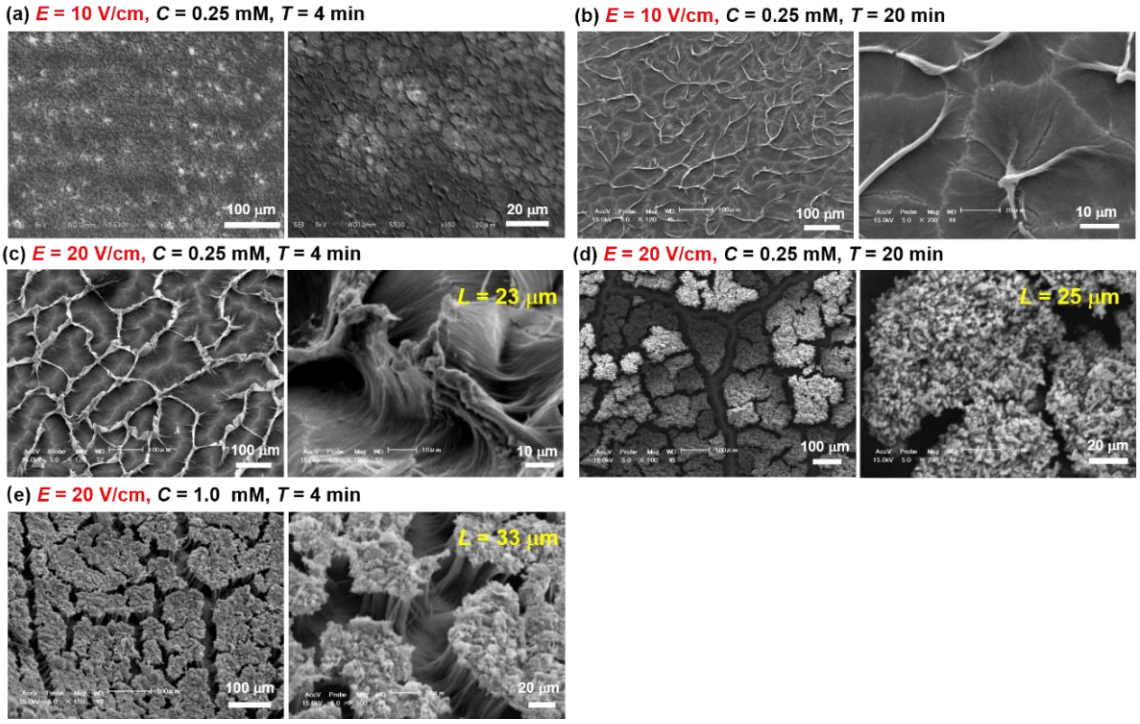

Figure 8. SEM images with low and high magnitude of poly-**2** fabricated under different conditions. (a) *E* = 10 V/cm, *C* = 0.25 mM and *T* = 4 min, (b) *E* = 10 V/cm, *C* = 0.25 mM and *T* = 20 min, (c) *E* = 20 V/cm, *C* = 0.25 mM and *T* = 4 min, (d) *E* = 20 V/cm, *C* = 0.25 mM and *T* = 20 min, (e) *E* = 20 V/cm, *C* = 1.0 mM and *T* = 4 min.[37]

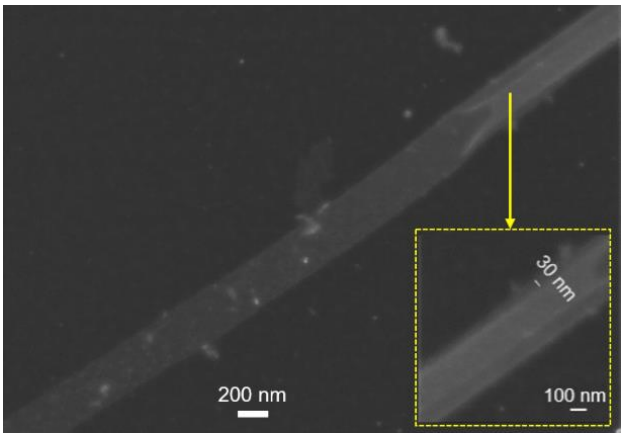

Figure 9. TEM image of poly-**2** nanotube in Figure 8c.

Poly-**2** nanowires were also characterized by a 3D laser microscope, confirming the uniform lengths of fibers (Figure 10a). Vertical poly-**2** nanowires with 33 μm in length were also successfully constructed within 4 min when a higher *C* of 1.0 mM solution was employed (Figure 8e). Again, EDS mappings confirmed the existence of ruthenium in the obtained poly-**2** nanowires (Figure 10b).

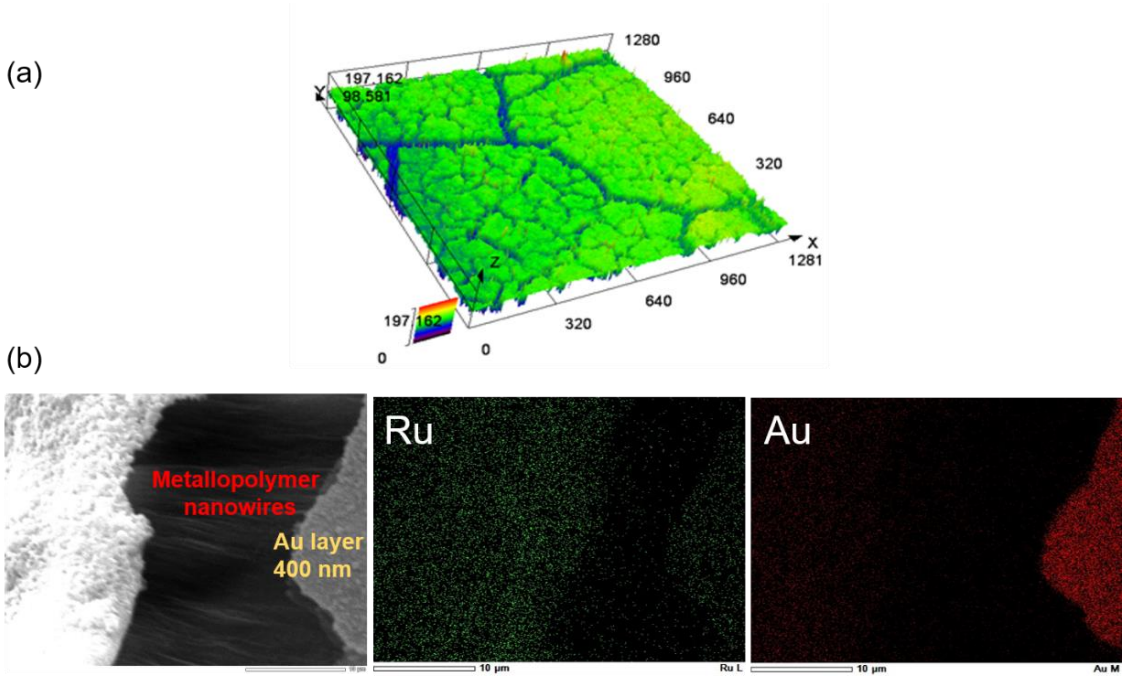

Figure 10. (a) 3D laser microscope image and (b) cross-sectional SEM images of perpendicular poly-**2** nanowires formed in Figure 8e with corresponding EDS mappings of Ru and Au elements.[37]

These results demonstrates that the electrophoresis effect of the cationic monomers plays an important role in the formation of polymer nanowires. *E* is the crucial factor and a higher *C* and a longer *T* generally favor the formation of robust polymer nanowires. Under the application of a lower *E* (10 V/cm), the migration ability of monomers is slow, resulting in a disordered migration of charged monomers toward the template (Figure 11a), while a higher *E* (20 V/cm) intensifies the directed electrophoresis. Under a lower *C* of 0.25 mM and shorter *T* of 4 min, no standing fibers were observed, probably due to the weak mechanical strength (Figure 11b). In this situation, the mass transfer from the bulk solution was slow by the reason of the low monomer concentration. However, migration of charged monomers was effectively promoted by increasing *T* and *C*. when *T* was extended, more charged monomers underwent lasting electrophoresis toward the pores of the template, generating nanowires with a better mechanical strength (Figure 11c). Higher *C* also contributed to the supply of charged monomers into nanopores of the template. Therefore, increased *C* generated longer free-standing polymer nanowires in a short *T* as well (Figure 11d).

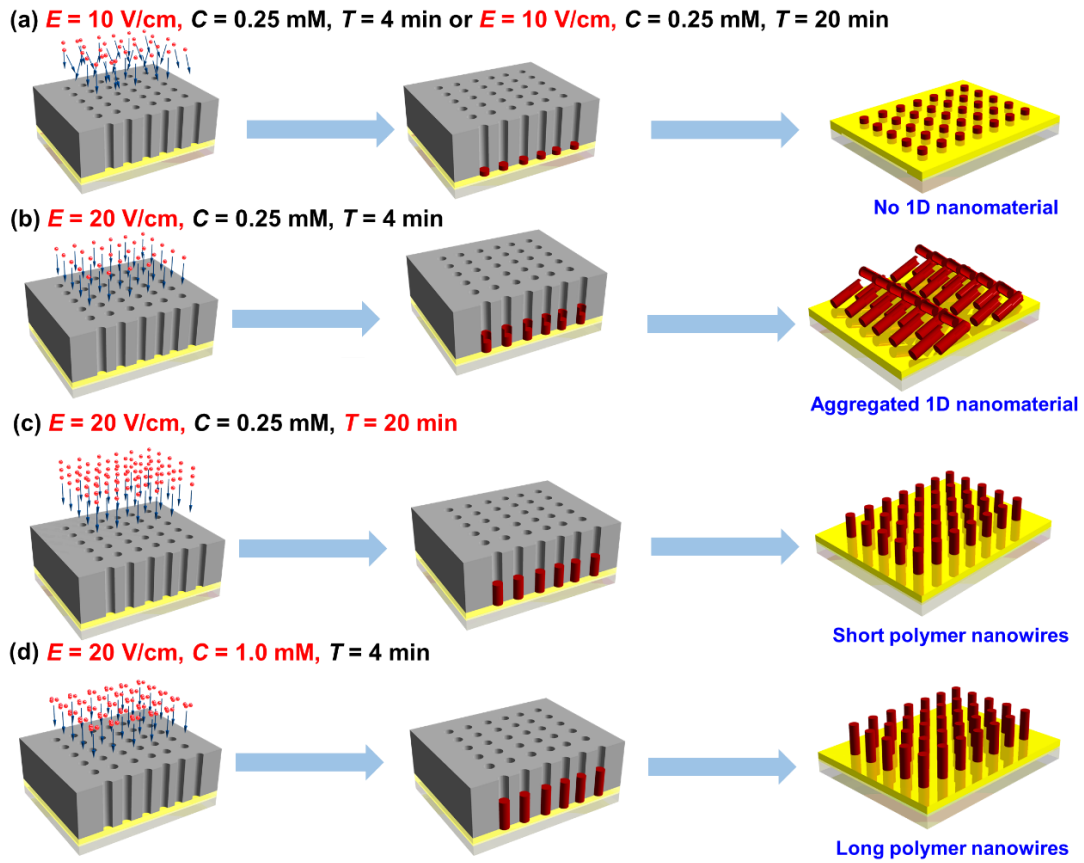

Figure 11. Summary of the templated bipolar electropolymerization of **2** under different conditions.[37]

Templated Bipolar Electropolymerization of Anionic Monomer

The described approach here is expected to have a general applicability on charged monomers. Thus, an anionic thiophene derivative with opposite charge was employed for oxidative electropolymerization promoted by electrophoresis. Polythiophene and its derivatives have attracted considerable concerns for the applications in field-effect transistor,[40] light-emitting diodes[41] and supercapacitors.[42] Modification on 3-position of thiophene is a common approach to endow various functionalities.[43] Here, potassium 3-thiophenetrifluoraborate (**3**) was used as a monomer for the electropolymerization in the boron trifluoride diethyl ether (BFEE) to achieve robust conducting polymer nanowires by the templated bipolar electrolysis. In several thiophene electropolymerization systems, BFEE with a strong Lewis acidity was employed as a

solvent to lower the oxidation potential than that in common solvents.[44–46] The electropolymerization of **3** is hard to proceed in MeCN, but the BFEE enables the efficient electropolymerization. The smooth polymerization was confirmed by CV measurement, which gave a corresponding polymer film (Figure 12). Based on this, we intended to explore the templated bipolar electropolymerization of **3** by employing BFEE as a solvent.

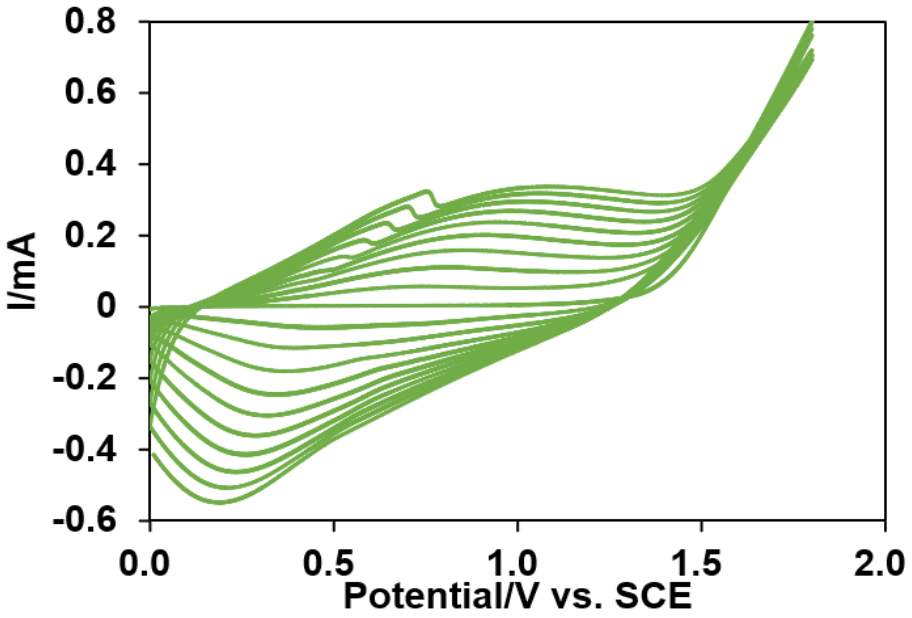

Figure 12. (a) CV measurement of 5 mM monomer **3** by cyclic potential scans in Bu_4NClO_4/ BFEE using an ITO electrode (10 mm×10 mm) as a working electrode, a SCE as a reference electrode and a Pt plate (20 mm × 20 mm) as a counter electrode at a scan rate of 100 mV/s.[37]

The experimental configuration in Figure 13a includes an electrolytic cell (40 mm × 20 mm), driving electrodes (20 mm × 15 mm), a split BPEs and 5 mM **3** in the BFEE solution. The ITO electrode surface modified with the AAO template was employed as a BPE anode. BFEE may contain acidic byproduct during the hydrolysis under atmospheric condition. Thus, oxidative electropolymerization of **3** proceeds on the BPE anode to produce thiophene-containing polymer, and the hydrogen evolution reaction conducted on the BPE cathode. ΔV_{BPE} is supposed to be higher than the onset potential difference of corresponding redox couples (ΔV_{min2} = 1.54 V, Figure 17). ΔV_{BPE} was adjusted at 7 V by controlling the distance (7 mm or 14 mm) between anode and cathode of the BPE, as well

as the applied voltage on driving electrodes. During the bipolar electrolysis, negatively charged **3** was forced to the BPE anode for polymerization. As for the electrolysis process and the followed treatment, which were identical as mentioned before.

In this section, thiophene-containing polymer (poly-**3**) was fabricated by the bipolar electrolysis and the conventional constant potential electrolysis with the help of the AAO template, respectively, keeping equal charge passed (467 mC). The conventional templated constant potential electropolymerization produced nanowires, which bent into disordered domains when the template was removed (Figure 13 b). These nanowires tend to congregate into bundles (2-3 mm) and keep a wide space with each other. On the contrary, bipolar electrolysis made orderly vertical nanowires (Figure 13c).

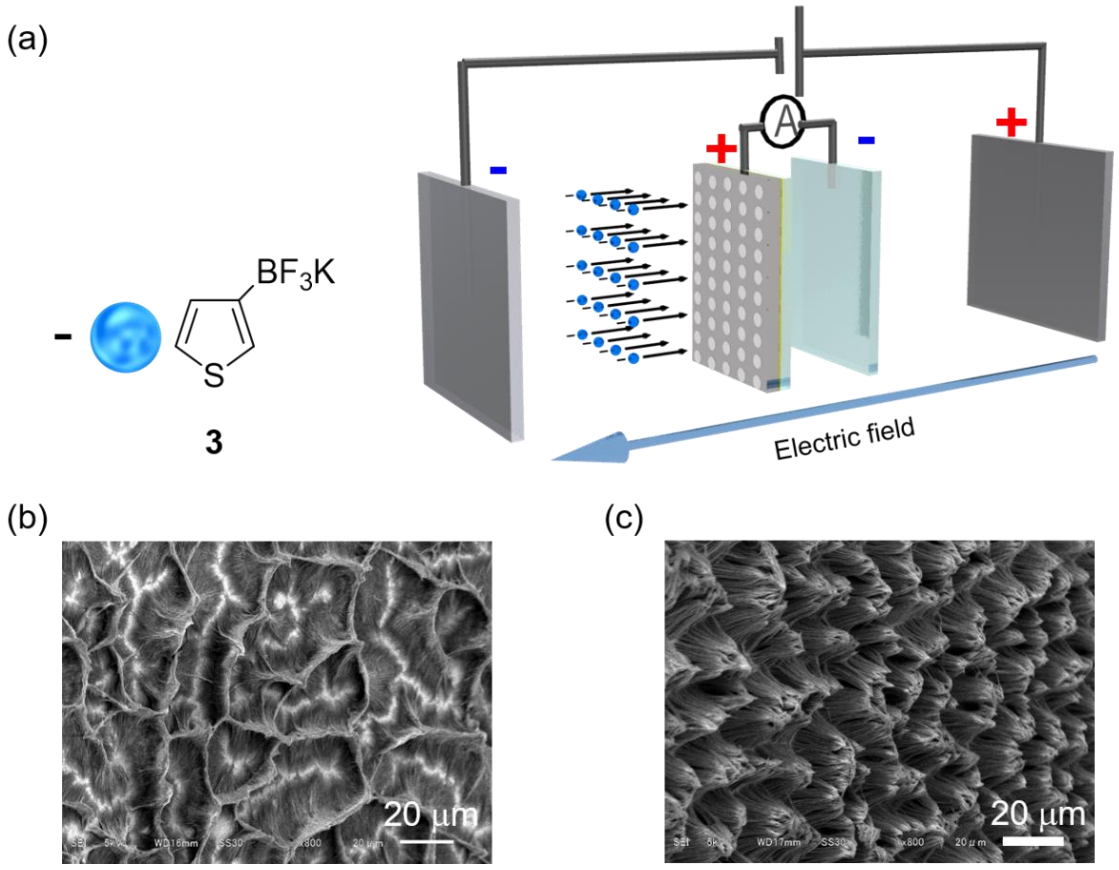

Figure 13. (a) Schematic illustration of the templated bipolar electrochemical setup. Fabrication of poly-**3** nanowires on the AAO modified electrode surface by (b) conventional constant potential electrolysis and (c) bipolar electrolysis.[37]

The effects of *E* and *T* on the morphologies of poly-**3** nanowires were then explored. For 5 V/cm, the electropolymerization occurred, but not in the form of linear nanowires (Figure 14a). With the improved *E* of 10 V/cm, 1D perpendicular polymer nanowires were prepared on an BPE surface (Figure 14b, c). For a longer *T*, higher nanowires were observed (Figure 13c) compared with that in Figure 13b. These results revealed that higher *E* can accelerate the directional migration of charged monomer **3** into the AAO template decorated on the BPE anode, contributing to form robust polymer nanowires. With increased *T*, longer polymer-**3** nanowires were produced.

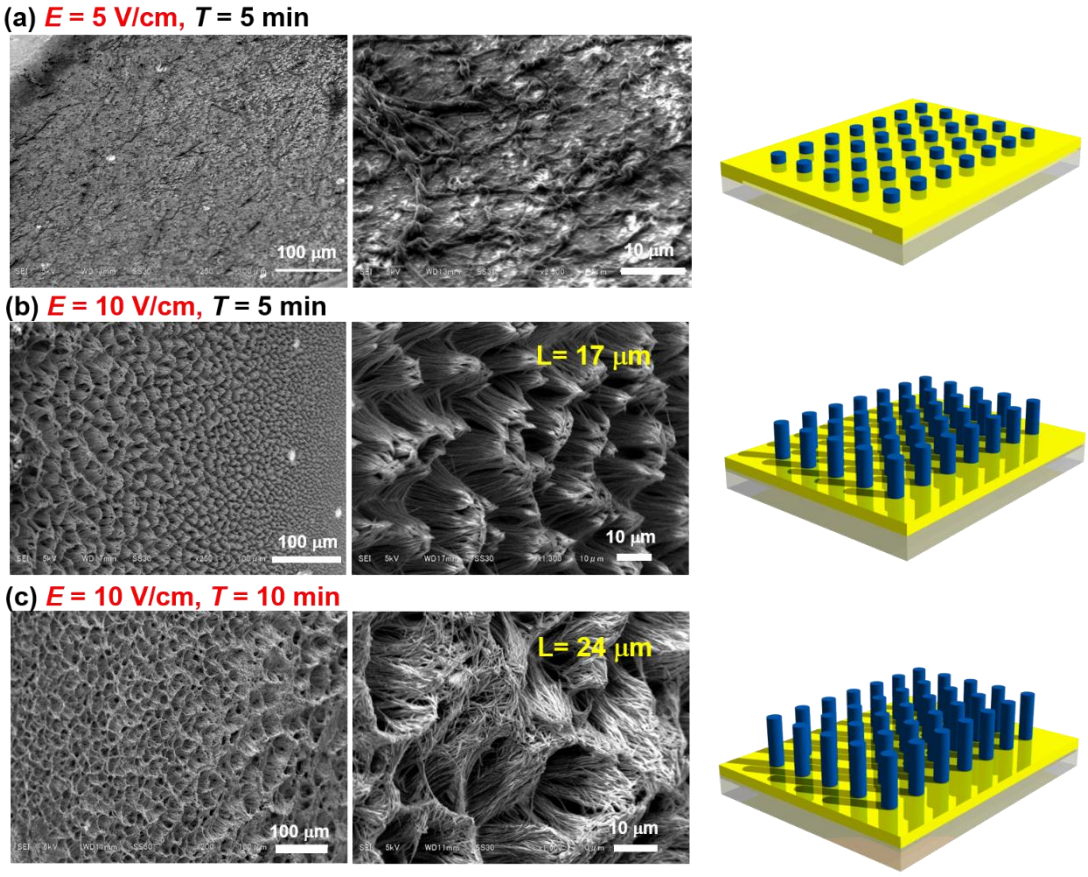

Figure 14. SEM images and schematic illustration of poly-**3** fabricated under various conditions. (a) *E* = 5 V/cm, *C* = 5 mM and *T* = 5 min, (b) *E* = 10 V/cm, *C* = 5 mM and *T* = 5 min, (c) *E* = 10 V/cm, *C* = 5 mM and *T* = 10 min.[37]

IR spectra of monomer **3** and poly-**3** nanowires demonstrated the typical characteristic ring stretching vibration for thiophene. The skeletal vibrations at 1386 cm^{-1}

belongs to C-C bond. 1082 cm^{-1} and 1043 cm^{-1} are attributed to C-S bond. Stretching vibration of in-plane C-H appeared at 1216 cm^{-1} and C-H out-of-plane vibration absorption corresponds to 1072 cm^{-1} and 1041 cm^{-1} (Figure 15).[47] The height and composition of these perpendicular poly-**3** nanowires fabricated in Figure 14b,c were further analyzed by SEM and EDS. The cross-sectional view of SEM images represented that *L* of polymer nanowires was about 17 μm in 5 min (Figure 16a), and 24 μm 10 min (Figure 16b) when *E* was 10 V/cm. Besides, EDS mappings revealed the distribution of sulfur element, in support of the successful preparation of poly-**3** nanowires (Figure 16).

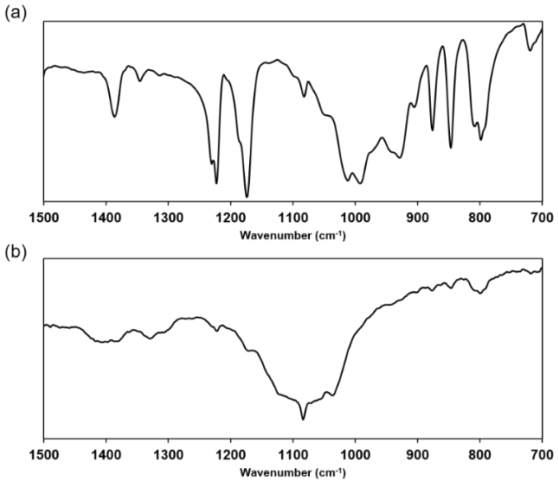

Figure 15. IR spectra of (a) **3** and (b) poly-**3** nanowires.[37]

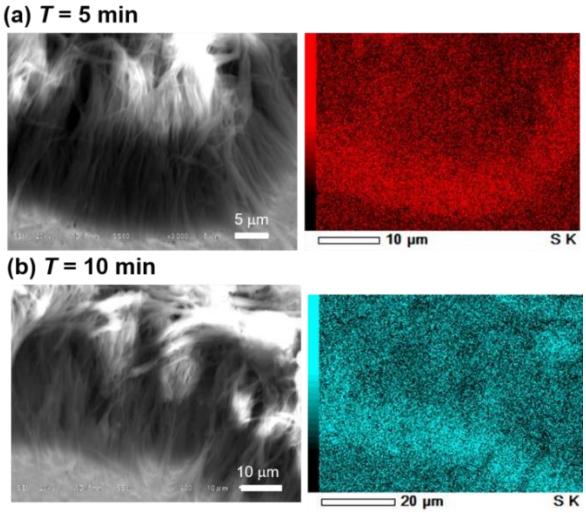

Figure 16. Cross-sectional SEM images of poly-**3** nanowires obtained in (a) Figure 14b and (b) Figure 14c and the corresponding EDS mappings of S.[37]

CV measurements were employed to evaluate the electrochemical properties of obtained robust poly-**3** nanowires. The poly-**3** nanowires were fabricated by the templated bipolar electrolysis (E = 10 V/cm, C = 5 mM and T = 5 min), and by the template constant potential electropolymerization, respectively, keeping the consistent passed quantity of electricity (0.92 C). Therefore, the same amount of poly-**3** was electrodeposited under both cases. As shown in Figure 17, the oxidative current of the poly-**3** nanowires obtained from bipolar electrolysis is bigger than that from constant potential electrolysis, presumably due to the different performances in the electrochemical active surface area.

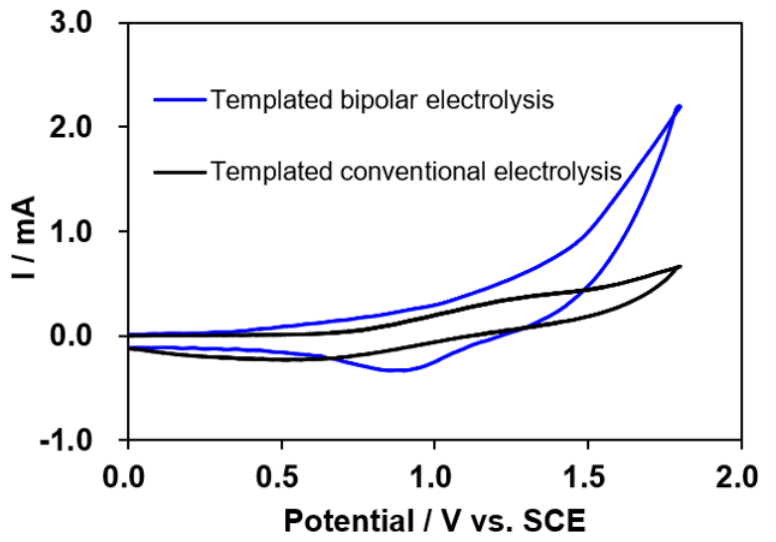

Figure 17. CV measurement of poly-**3** nanowires fabricated by both of conventional electrolysis and bipolar electrolysis. Potential sweep rate of CV is 100 mV s^{-1}.[37]

Conclusion

In conclusion, templated bipolar electrolytic system provides synergetic electropolymerization and electrophoresis effects simultaneously for the preparation of robust CP nanowires. In this work, both of reductive electropolymerization of cationic ruthenium complexes (monomers **1** and **2**) and oxidative electropolymerization of anionic thiophene derivative (monomer **3**) on the templated modified electrode surface were investigated. The produced polymer nanowires with uniform and robust structures were

distinguished from those fabricated by a conventional electropolymerization method. These results were attributed to the reinforced directional migration of these charged monomers into nanopores of the AAO template actuated by the electric field across the bulk solution in bipolar electrochemical system. Electrophoretic effect is critical for templated bipolar electropolymerization. Besides, the length of these polymer nanowires could be well adjusted by changing the electrolysis time and the monomer concentration. The proposed approach offers a general and straightforward strategy to fabricate robust polymer nanowires using charged monomers.

Experimental Section

Materials

Hydroquinone, boron trifluoride diethyl etherate (BFEE), potassium-3-thiophenetrifluoraborate and other starting reagents for the synthesis of ruthenium complexes were purchased from commercial sources and used without further purification otherwise noted. According to the reported procedures in the literatures, ruthenium complexes with vinyl groups were synthesized.[32,35,36] Anodic aluminum oxide (AAO) template (200 nm pore size, 13 mm diameter, 60 μm thickness) was obtained from Whatman. Indium tin oxide (ITO) conductive glass was carefully washed with methanol, deionized water and acetone. The electrolytic solution was deaerated by an argon bubbling just before use.

Instruments

^{1}H nuclear magnetic resonance (NMR) spectra were recorded on a JEOL ECP-300. An EC1000SA AC/DC power applier from NF Corporation was used to procced electrolysis. The PC Link software dedicated to a PC for collecting data from an ammeter was used to record the current. Infrared spectroscopy (IR) Tracer-100 comes from SHIMADZU company. An Olympus OLS4100 3D was employed for the laser microscopy measurement. Energy dispersive X-ray spectroscopy (EDS) measurement

and scanning electron microscopy (SEM) observation were conducted using the JEOL JSM 6610 equipment. Gold thin layer was spattered using an Eiko IB-3 ion coater.

Synthesis of Ru-ligand complexes

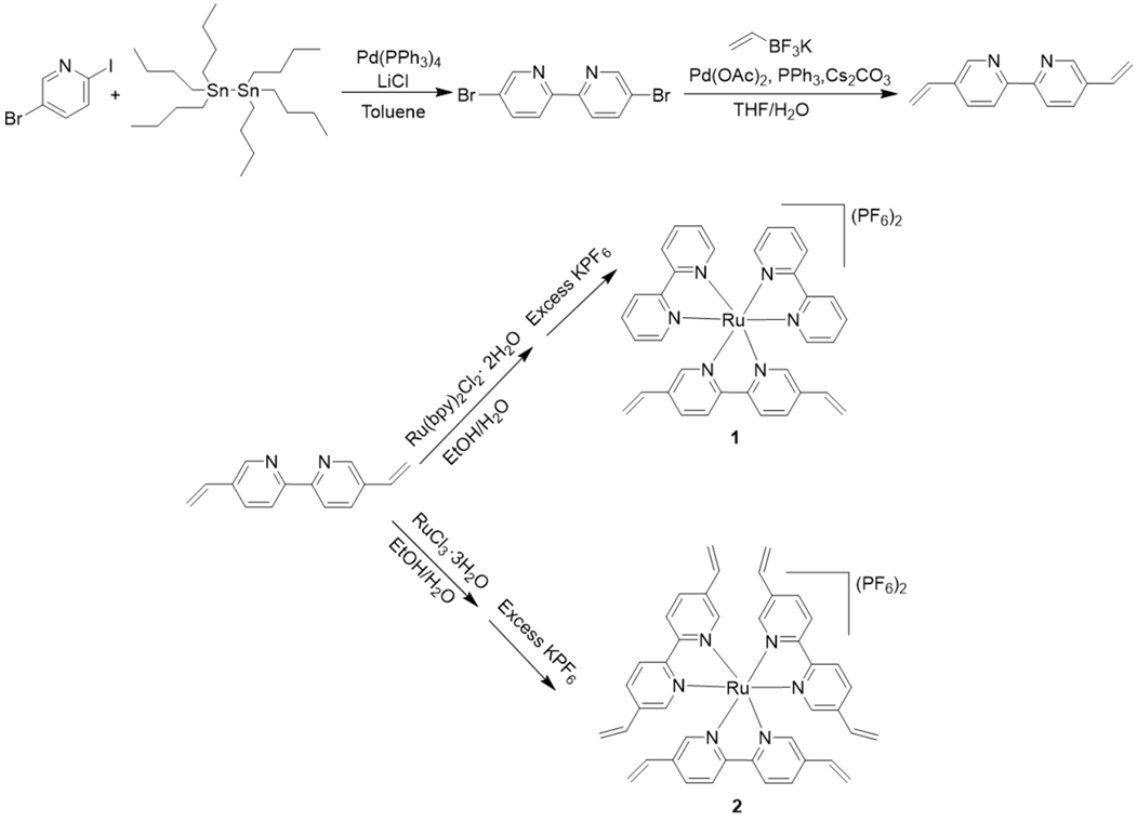

Scheme S1. Synthesis of ruthenium complexes.

The chemical shift for ^{1}H NMR was given in δ (ppm) with respect to that for the internal tetramethylsilane (TMS) as an internal standard.

5,5'-Dibromo-2,2'-bipyridine

In anhydrous toluene (10 mL), bis(tributyltin) (0.64 g, 1.1 mmol), 5-bromo-2-iodopyridine (0.61 g, 2.1 mmol), LiCl (59 mg, 1.4 mmol) and $Pd(PPh_3)_4$ (0.07 g, 0.06 mmol) were refluxed under N_2 atmosphere for 72 h. After cooling to room temperature, the solution was diluted with diethyl ether (Et_2O), then washed with brine and dried over anhydrous $MgSO_4$. The crude product was purified by column chromatography on silica gel (hexane/ethyl acetate = 10:1) to yield 200 mg of white solid (60%). The ^{1}H NMR data

of the product are identical to those in the literature.[36]

^{1}H NMR (25 °C, $CDCl_3$, ppm): δ7.94 (d, J = 7.8 Hz, 2H), 8.29 (d, J = 8.7 Hz, 2H), 8.71 (s, 1H).

5,5′-Divinyl-2,2′-bipyridine (dvbpy)

In THF/H_2O (24:1, 5 mL in total), 5,5′-dibromo-2,2′-bipyridine (0.10 g, 0.3 mmol), potassium vinyltrifluoroborate (0.17 g, 1.3 mmol), PPh_3 (5 mg, 0.02 mmol), Cs_2CO_3 (0.31 g, 1.0 mmol) and $Pd(OAc)_2$ (2 mg, 0.008 mmol) were stirred at 85 °C under N_2 atmosphere for 48 h. After cooling to room temperature, the solution was diluted with 5 mL of H_2O, followed by the extraction with CH_2Cl_2. The organic phase was collected and washed with brine, then dried over Na_2SO_4. The crude product was purified by column chromatography on silica gel (petroleum ether/dichloromethane/NH_4OH = 35:50:1) to yield 57 mg of yellow powder (87%). The ^{1}H NMR data of the product are identical to those in the literature.[32]

^{1}H NMR (25 °C, $CDCl_3$, ppm): 5.42 (d, J = 11.1 Hz, 2H), 5.89 (d, J = 18.6 Hz, 2H), 6.77 (dd, J = 11.1 Hz, 18.0 Hz, 2H), 7.87 (d, J = 6.0 Hz, 2H), 8.37 (d, J = 8.4 Hz, 2H), 8.66 (s, 2H).

[Ru(5,5′-dvbpy)(bpy)$_2$](PF$_6$)$_2$

5,5′-Divinyl-2,2′-bipyridine (0.030 g, 0.1 mmol) and *cis*-$Ru(bpy)_2Cl_2 \cdot 2H_2O$ (0.060 g, 0.1 mmol) were added in the mixture of ethanol/H_2O (10 mL/5 mL). The reaction solution was refluxed under a N_2 atmosphere for 5 h. After cooling to room temperature, ethanol was evaporated, followed by the addition of KPF_6. The resulted precipitate was collected, then washed with water and Et_2O. The solid was then subjected to column chromatography on silica gel (KNO_3/H_2O/CH_3CN = 1/15/150) to give 64 mg of brown-yellow powder having a yield of 59%. The ^{1}H NMR data are identical to those in the literature.[35]

^{1}H NMR (25 °C, $CDCl_3$, ppm): 5.44 (d, J = 11.1 Hz, 2H), 5.84 (d, J = 18.7 Hz, 2H), 6.54 (dd, J = 11.4 Hz, 18.0 Hz, 2H), 7.38 (t, J = 6.0 Hz, 4H), 7.58 (s, 2H), 7.69 (d, J = 5.7

Hz, 2H), 7.75 (d, *J* = 5.7 Hz, 2H), 8.05 (t, *J* = 7.5 Hz, 4H), 8.16 (d, *J* = 8.4 Hz, 2H), 8.41 (d, *J* = 8.4 Hz, 2H), 8.46 (d, *J* = 8.4 Hz, 4H).

[Ru(5,5'-dvbpy)$_3$](PF$_6$)$_2$

5,5′-Divinyl-2,2′-bipyridine (0.050 g, 0.2 mmol) and *cis*-$RuCl_3 \cdot 3H_2O$ (0.04 g, 0.07 mmol) in the mixture of ethanol/H_2O (10 mL/5 mL). The reaction solution was refluxed under a N_2 atmosphere for 24 h. After cooling to room temperature, ethanol was removed and an excess amount of KPF_6 was added. The precipitate was washed with water and Et_2O, then subjected to column chromatography on silica gel ($KNO_3/H_2O/CH_3CN$ = 1/10/400) to give 21mg of brown-yellow powder having a yield of 42%. The ^{1}H NMR data are identical to those in the literature.[32]

^{1}H NMR (25 °C, $CDCl_3$, ppm): 5.46 (d, *J* = 12.3 Hz, 6H), 5.83 (d, *J* = 19.5 Hz, 6H), 6.54 (dd, *J* = 13.2 Hz, 19.5 Hz, 6H), 7.62 (s, 6H), 8.15 (d, *J* = 9.3 Hz, 6H), 8.40 (d, *J* = 9.6 Hz, 6H).

Estimation of ΔV_{BPE}

The minimum applied voltage required to induce a BPE (ΔV_{min}) was estimated from the difference between the oxidation and reduction potentials of the corresponding redox species, E_{ox} and E_{red}, (Eq. 1), as previously reported.[4]

$$\Delta Vmin = |E_{ox} - E_{red}| \quad (1)$$

Ruthenium complexes electrolytic systems

The reductive polymerization of **1** or **2** and the oxidation of HQ proceed simultaneously. Using the onset potentials of these half reactions (Figure 18), ΔV_{min1} was estimated in Eq. 2,

$$\Delta V_{min1} = |E_{ox} - E_{red}| = |0.83\ V - (-0.80\ V)| = 1.63\ V \quad (2)$$

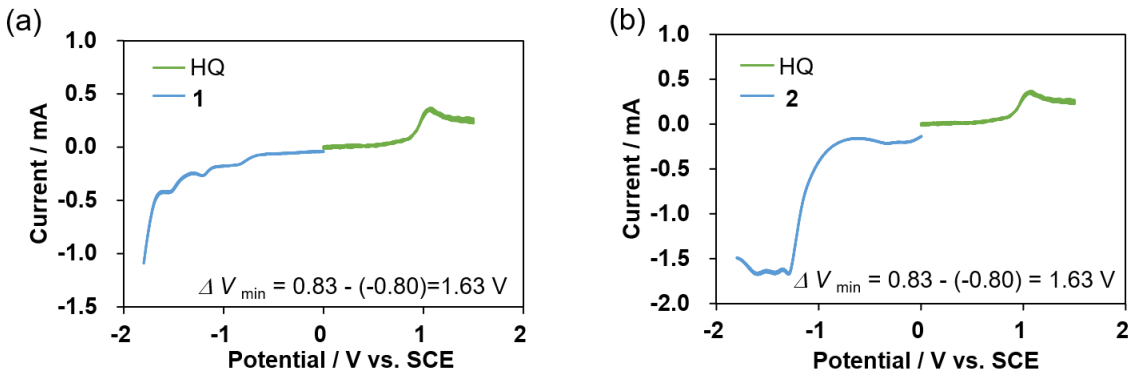

Figure 18. Linear sweep voltammograms of 0.5 mM (a) **1** and (b) **2**, and 0.5 mM HQ measured independently in 0.1 M Bu_4NClO_4/MeCN solution using a Pt working electrode (10 mm × 10 mm). The scan rate is 100 mV/s.[37]

Thiophene derivatives electrolytic system

The oxidative polymerization of **3** and the reduction of acidic byproduct in a BFEE solution proceed simultaneously on the BPE. Using the onset potentials of these half reactions (Figure 19), ΔV_{min2} was estimated in Eq. 3,

$$\Delta V_{min2} = |E_{ox} - E_{red}| = |1.30\ V - (-\ 0.24\ V)\ | = 1.54\ V \quad (3)$$

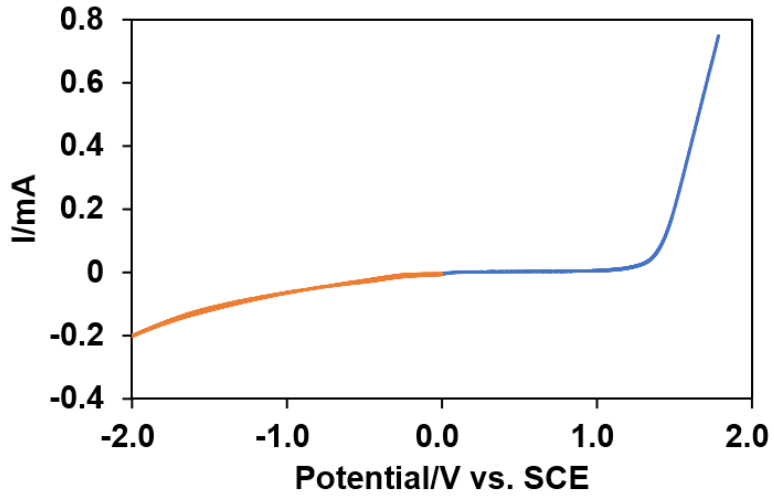

Figure 19. Linear sweep voltammograms of a pure BFEE solution (orange line, cathodic scan) and 5 mM **3** in a BFEE solution (blue line, anodic scan) using an ITO working electrode (10 mm × 10 mm). The scan rate is 100 mV/s.[37]

Cell configuration

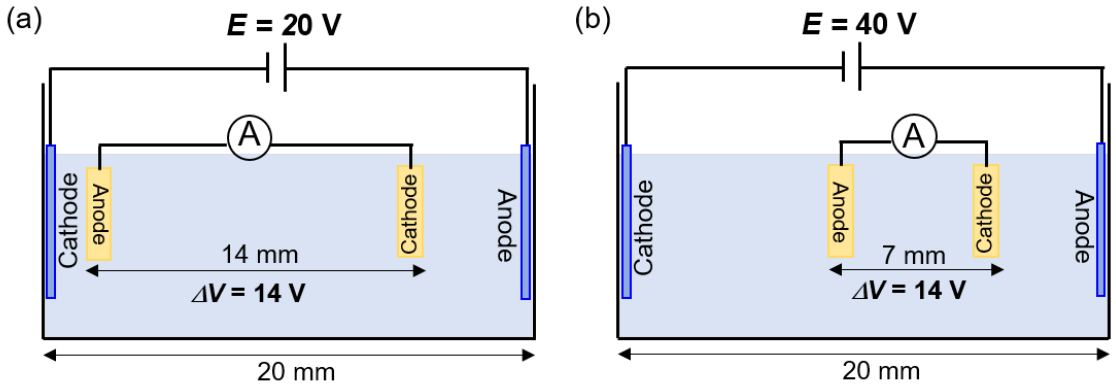

Figure 20. Employed electrolytic setups under various applied voltages (a) 20 V and (b) 40 V.[37]

Preparation of AAO membrane-fixed ITO plate

A hard template of AAO membrane was coated with a gold layer (400 nm) by ion sputtering firstly. The gold-modified side was then attached to an ITO plate and fixed by the epoxy glue to expose an area of 8 mm × 5 mm. The AAO template-decorated electrode was kept under an ambient condition for two days before use.

Templated conventional constant potential electrolysis

Ruthenium complex electrolytic system

0.25 mM monomer **1** or **2** dissolved in 0.1 M Bu_4NClO_4/MeCN solution was used as electrolytic solution. AAO template-modified ITO plate was utilized as a cathode. Before constant potential electrolysis, AAO template-modified ITO plate was immersed in the electrolyte for 30 min to impregnate electrolyte into nanopores of the template. Then, potential of −1.2 V vs. SCE was applied for the electropolymerization using a Pt plate as a counter electrode (20 mm × 20 mm). After reductive polymerization, the AAO template was removed from the ITO substrate by immersing in 1 M KOH aq for at least 12 h. The obtained sample was washed with water and MeCN, then dried in the air.

Thiophene derivatives electrolytic system

5 mM monomer **3** dissolved in BFEE solution was used as electrolytic solution.

AAO template-modified ITO plate was utilized as an anode. Before constant potential electrolysis, the AAO template-modified ITO plate was immersed in the electrolyte for 30 min to impregnate electrolyte into nanopores of the template. Then, potential of 1.0 V vs. SCE was applied for the oxidative electropolymerization using a Pt plate as a counter electrode (20 mm × 20 mm). After oxidative polymerization, the AAO template was removed from the ITO substrate by immersing in 1 M KOH aq. for at least 12 h. The obtained sample was washed with water and MeCN, then dried in the air.

Templated bipolar electrolysis

An AAO membrane modified ITO plate facing to driving cathode/anode acts as a bipolar anode/cathode, while another ITO plate is used as a bipolar cathode/anode. The modified ITO plate and pristine ITO acting as a split BPEs were connected by an ammeter. And the electrolysis was proceeded using a constant voltage between the driving electrodes. After bipolar electrolysis, the piece of template-decorated ITO was immersed in MeCN to remove residual monomers. The AAO template was dissolved by immersing in 1 M KOH aq. for 12 h. The obtained sample was carefully washed several times using the deionized water and MeCN.

References

[1] N. Hui, F. Chai, P. Lin, Z. Song, X. Sun, Y. Li, S. Niu, X. Luo, *Electrochimica Acta,* **2016**, *199*, 234–241.

[2] Y. Dan, Y. Cao, T. E. Mallouk, S. Evoy, A. T. C. Johnson, *Nanotechnology*, **2009**, *20*, 434014.

[3] M. Zhu, S. Lv, Q. Wang, G. Zhang, H. Lu, L. Qiu, *Nanoscale,* **2016**, *8*, 7738–7748.

[4] C. Li, X. Yin, L. Chen, Q. Li, T. Wang, *Chemistry - A European Journal*, **2010**, *16*, 5215–5221.

[5] W. He, C. Wang, F. Zhuge, X. Deng, X. Xu, T. Zhai, *Nano Energy,* **2017**, *35*, 242–250.

[6] Y. Liu, X. Zhang, Y. Xia, H. Yang, *Advanced Materials*, **2010**, *22*, 2454–2457.

[7] J. Huang, K. Wang, Z. Wei, *Journal of Materials Chemistry,* **2010**, *20*, 1117–1121.

[8] D. K. Taggart, Y. Yang, S. C. Kung, T. M. McIntire, R. M. Penner, *Nano Letters*, **2011**, *11*, 125–131.

[9] K. Kim, J. I. Jin, *Nano Letters,* **2001**, *1*, 631–636.

[10] I. C. Seung, B. L. Sang, *Accounts of Chemical Research*, **2008**, *41*, 699–707.

[11] K. Singh, A. Ohlan, P. Saini, S. K. Dhawan, *Polymers for Advanced Technologies*, **2008**, *19*, 229–236.

[12] M. Atobe, N. Yoshida, K. Sakamoto, K. Sugino, T. Fuchigami, *Electrochimica Acta,* **2013**, *87*, 409–415.

[13] L. Liang, J. Liu, C. F. Windisch, Jr., G. J. Exarhos, Y. Lin, *Angewandte Chemie International Edition,* **2002,** *41*, 3665-3668.

[14] G. Loget, D. Zigah, L. Bouffier, N. Sojic, A. Kuhn, *Accounts of Chemical Research,* **2013**, *46*, 2513–2523.

[15] L. Bouffier, D. Zigah, C. Adam, M. Sentic, Z. Fattah, D. Manojlovic, A. Kuhn, N. Sojic, *ChemElectroChem,* **2014**, *1*, 95–98.

[16] N. Shida, Y. Zhou, S. Inagi, *Accounts of Chemical Research,* **2019,** *52,* 2598–2608.

[17] Y. Koizumi, N. Shida, M. Ohira, H. Nishiyama, I. Tomita, S. Inagi, *Nature*

Communications, **2016**, *7*, 10404.

[18] J. Roche, G. Loget, D. Zigah, Z. Fattah, B. Goudeau, S. Arbault, L. Bouffier, A. Kuhn, *Chemical Science*, **2014**, *5*, 1961–1966.

[19] M. Ohira, Y. Koizumi, H. Nishiyama, I. Tomita, S. Inagi, *Polymer Journal*, **2017**, *49*, 163–167.

[20] T. Watanabe, M. Ohira, Y. Koizumi, H. Nishiyama, I. Tomita, S. Inagi, *ACS Macro Letters*, **2018**, *7*, 551–555.

[21] Y. Zhou, N. Shida, Y. Koizumi, T. Watanabe, H. Nishiyama, I. Tomita, S. Inagi, *Journal of Materials Chemistry C*, **2019**, *7*, 14745–14751.

[22] Y. Koizumi, H. Nishiyama, I. Tomita, S. Inagi, *Chemical Communications*, **2018**, *54*, 10475–10478.

[23] J.C. Bradley, H. M. Chen, J. Crawford, J. Eckert, K. Ernazarova, T. Kurzeja, M. Lin, M. McGee, W. Nadler, S. G. Stephens. *Nature*, **1997,** *389*, 268–271

[24] J. C. Bradley, Z. Ma, S. G. Stephens, *Advanced Materials*, **1999**, *11*, 374–378.

[25] J. C. Bradley, *Journal of The Electrochemical Society*, **1999**, *146*, 194-198.

[26] G. Loget, J. J. Roche, E. Gianessi, L. Bouffier, A. Kuhn, *Journal of the American Chemical Society* , **2012,** *134*, 20033–20036.

[27] H. D. Abruña, P. Denisevich, M. Umaña, T. J. Meyer, R. W. Murray, *Journal of the American Chemical Society*, **1981**, *103*, 1–5.

[28] C. M. Elliott, J. R. Dunkle, S. C. Paulson, *Langmuir*, **2005**, *21*, 8605–8608.

[29] R. M. Leasure, W. Ou, J. A. Moss, R. W. Linton, T. J. Meyer, *Chemistry of Materials*, **1996**, *8*, 264–273.

[30] M. C. DeRosa, P. J. Mosher, G. P. A. Yap, K. S. Focsaneanu, R. J. Crutchley, C. E. B. Evans, *Inorganic Chemistry*, **2003**, *42*, 4864–4872.

[31] K. M. Maness, R. H. Terrill, T. J. Meyer, R. W. Murray, R. M. Wightman, *Journal of the American Chemical Society*, **1996**, *118*, 10609–10616.

[32] H. J. Nie, J. Y. Shao, J. Wu, J. Yao, Y. W. Zhong, *Organometallics*, **2012**, *31*, 6952–6959.

[33] M. Li, J. Zhang, H. J. Nie, M. Liao, L. Sang, W. Qiao, Z. Y. Wang, Y. Ma, Y. W. Zhong, K. Ariga, *Chemical Communications,* **2013**, *49*, 6879–6881.

[34] A. Kajikawa, T. Togashi, Y. Orikasa, B. Bin Cui, Y. W. Zhong, M. Sakamoto, M. Kurihara, K. Kanaizuka, *Dalton Transactions,* **2015**, *44*, 15244–15249.

[35] H. J. Nie, J. Yao, Y. W. Zhong, *Journal of Organic Chemistry*, **2011**, *76*, 4771–4775.

[36] Z. He, M. Li, W. Que, P. J. Stang, *Dalton Transactions*, **2017**, *46*, 3120–3124.

[37] Y. Zhou, N. Shida, Y. Koizumi, K. Endo, I. Tomita and S. Inagi. *Macromolecules,* **2020,** *53*, 8123–8130.

[38] K. Miyamoto, H. Nishiyama, I. Tomita, S. Inagi, *ChemElectroChem,* **2019**, *6*, 97–100.

[39] R. Umeda, H. Awaji, T. Nakahodo, H. Fujihara, *Journal of the American Chemical Society*, **2008**, *130*, 3240–3241.

[40] G. W. Hsieh, Z. R. Lin, C. Y. Hung, S. Y. Lin, C. R. Yang, *Organic Electronics*, **2018**, *54*, 27–33.

[41] D. B. Romero, M. Schaer, L. Zuppiroli, B. Cesar, B. François, *Applied Physics Letters*, **1995**, *67*, 1659–1661.

[42] A. Laforgue, P. Simon, J. F. Fauvarque, *Synthetic Metals,* **2001**, *123*, 311–319.

[43] H. P. Welzel, G. Kossmehl, H. Boettcher, G. Engelmann, W. D. Hunnius, *Macromolecules*, **1997**, *30*, 7419–7426.

[44] S. Jin, G. Xue, *Macromolecules,* **1997**, *30*, 5753–5757.

[45] W. Chen, G. Xue, *Progress in Polymer Science,* **2005**, *30*, 783–811.

[46] T. Kurioka, H. Nishiyama, I. Tomita, S. Inagi, *ChemElectroChem,* **2018**, *5*, 753–755.

[47] R. Liu, Z. Liu, *Chinese Science Bulletin,* **2009**, *54*, 2028–2032.

Chapter 4

Fabrication of Gradient and Patterned Organic Thin Films by Means of Bipolar Electrolytic Micelle Disruption Method Using Redox-active Surfactants

Abstract: Benefiting from the feature of a wireless controllable potential distribution on the bipolar electrode (BPE), bipolar electrochemistry could be regarded as a powerful approach to achieve selective surface modification. In this Chapter, a bipolar electrolytic micelle disruption (BEMD) approach for the fabrication of gradient and patterned organic films is proposed. A U-shaped bipolar electrolytic setup having a sigmoidal potential distribution on the BPE produced gradient thin films composed of various interesting organic compounds, including a polymerizable monomer with a vinyl group, an organic dye and three kinds of aggregation-induced emission (AIE) molecules. Their gradient feature was well characterized by UV-vis absorption, surface morphology analysis and thickness measurement. In addition, related patterned films were also prepared with the help of a cylindrical bipolar electrolytic setup that is capable of site-selective potential application on the BPE surface. Such a facile BEMD method provides a general and facile way to prepare organic films.

Introduction

Bipolar electrochemistry has regained a considerable interest in the last two decades because of its widespread application ranging from analytical chemistry[1,2] to materials science[3–5] and beyond.[6–9] For bipolar electrochemical technique, it generates electrochemical reactions on the BPE in a wireless manner relative to the conventional electrochemical method.[10] In regard to electrochemical setup, it has a couple of driving electrodes linked to an external power source, and a BPE placed in an electrolytic solution. Here, the driving electrodes forming an electric field across the solution with a low concentration of salt induces electrochemical reactions on the BPE without a direct ohmic contact. Based on the principles of bipolar electrochemistry, the potential distribution on the BPE surface can be adjusted by the electrolytic cell design, the applied voltage, as well as the position and the shape of the driving electrodes. Therefore, the BPE on bipolar electrochemical system can act as an in situ template to modify gradient surfaces.[11–14] Inagi and co-workers originally developed electrolytic setups that effectively produced different gradient materials,[15] such as gradient electrochemical doping of the conducting polymer,[16,17] electrochemical chlorination in a gradient manner across polythiophene films,[18] the fabrication of a 3D gradient polymer brush using electrochemically mediated atom transfer radical polymerization[19] and gradient electrochemical modifications of a poly(3,4-ethylenedioxythiophene)-based polymer by an electro-click reaction.[20] Besides, another electrolytic system having an insulating cylinder has been studied. The pair of driving electrodes are separated using a plastic shielding cylinder, which gave a mountain-like potential distribution on the BPE. The cylindrical setup was employed to achieve wireless site-selective patterns on the BPE.[19,21,22] These proposed bipolar electrolytic setups offer a greatly effective and facile approach to prepare gradient and patterned films. However, all of fabricated gradient or patterned films here underwent electrochemical reactions in the process of the film-formation. In this context, the resulting gradient or patterned thin films on the electrode surface could keep an original chemical composition during the film formation process is a challenge but has the

potential to extend the application scope of the described bipolar electrochemical technique.

The preparation approach of organic thin films is crucial due to its attractive applications in electronic devices such as transistors,[23] photovoltaic cells[24] and sensors.[25] The common methods of preparing organic small molecules films are dry processes, such as physical vapor deposition (PVD) and chemical vapor deposition (CVD).[26,27] However, these methods require expensive equipments and complicated processes. On the other hand, a practical and unique wet process, named as the electrolytic micelle disruption method was developed from Soji's group, in which various organic thin films formed after the deposition of released organic molecules during the oxidative process of electroactive surfactants having a ferrocene moiety.[28–30] The approach is based on the disruption of these micelles formed by redox-active surfactants when they are oxidized on the electrode surface. Solubilizates (organic compounds) are released from the micelles, then gradually deposited on the electrode surfaces, forming a thin film. The film formation process is very simple and can be widely extended to many compounds. Furthermore, it is not only available for the family of organic compounds,[30,31] but also for fullerenes[32] and polymers.[33,34] Unlike common electrochemical film formation process on the electrode surface by electrochemical reactions that the starting organic compounds undergo reactions, this method gives thin films of intact organic molecules loaded by micelles. For this technique, no organic solvents are required, thus belongs to an environmentally friendly technology.

The author demonstrates that the electrolytic micelle disruption process can be ideally introduced to bipolar electrolytic system by several experiments, known as the bipolar electrolytic micelle disruption (BEMD) method. With the help of BEMD method, the preparation of various gradient and patterned organic thin films in a wireless manner is possible. In this work, *N*-vinylcarbazole (NVC) was solubilized in the cationic surfactant of (11-ferrocenylundecyl)trimethylammonium bromide (FTMA) micelles, while the nonionic surfactant of α-(11-ferrocenylundecyl)-ω-hydroxypoly(oxyethylene)

(FPEG) micelles are applicative to copper phthalocyanine (CuPc) and three aggregation-induced emission (AIE) compounds. When these FTMA micelles solubilizing NVC, and FPEG micelles incorporating CuPc or AIE in an aqueous solution were employed to the BEMD system, these organic compounds were unfettered in the oxidation process of electroactive surfactants due to hydrophilicity and electrostatic repulsion of positively charged ferrocenyl head groups. Due to the sigmoidal potential distribution on the BPE in the U-shaped electrolytic setup and the mountain-like potential distribution on the BPE in the cylindrical electrolytic cell, the location and the quantity of disrupted micelles were accordingly regulated, which prompted deposited organic films with a gradient or patterned characteristic. The gradient NVC film can be further photopolymerized under UV irradiation, realizing a post-functionalization in a facile way. In this contribution, the presented methodology here provides a reliable way to prepare various gradient and patterned organic thin films, which is not only used to organic molecules, but potentially expanded to others, such as functional polymers and carbon-based materials.

Result and Discussion

Fabrication of Gradient NVC Films and Post-functionalization

A ferrocene-decorated cationic surfactant of FTMA was obtained on the basis of a reported procedure.[30,35] The redox-active surfactant of FTMA can form to a micelle and solubilize the well-known NVC compound for the film formation (Figure 1a). The preparation of electrolytic solution as follows: an excess amount of NVC was added to an aqueous micellar solution containing 0.1 M lithium sulfate (Li_2SO_4) and 2.0 mM FTMA. The suspension system was sonicated for 2 h, then kept stirring for 5 days to reach a solubilization equilibrium. Next, undissolved NVC compounds were removed using centrifugation (2000 rpm, 1 h) and the separated solution was used for electrolysis. A home-made U-shaped electrolytic setup having a couple of platinum (Pt) driving

electrodes (20 mm×20 mm), and a piece of indium tin oxide (ITO) as a BPE (40 mm×10 mm) was employed for bipolar electrolysis (Figure 15a). A half of the ITO surface was covered with a tape for facilitating the thickness measurement of the film (Figure 17). In the NVC micellar system, FTMA oxidized on the anode, while $FTMA^+$ or H_2O reduced on the cathode to maintain electrons in balance on the BPE. Considering the $FTMA^+$ species formed at the anodic surface of the driving electrode could electrophorese to the cathodic surface of the BPE, the minimum potential difference (ΔV_{min1}) of *ca.* 0.15 V is required (Figure 16a and eq (2)). This bipolar electrolysis was carried out in an aqueous medium. Thus, water as the most abundant compound, should be noted in the reduction pole of the BPE, which performed the potential difference of about 1.16 V (eq 3). The U-shaped setup consisted of a shielding wall separates the driving electrodes, which well controlled the electric field distribution and generated a sigmoidal-like potential distribution on the BPE. IR-drop around the BPE surface can be measured with the help of a reference electrode array. The measurement points near the ITO surface at every 5 mm interval were collected (Figure 15b). Meanwhile, COMSOL simulation was conducted to gain theoretical values with respect to the interfacial potential distribution between the electrolyte and the BPE (Figure 1b). The experimental and simulation results performed a good agreement with each other. In fact, the validation has a great significance, especially for other bipolar electrolytic setups that are difficult to measure the potential distribution, such as a cylindrical cell presented later. For that one, simulation results could reveal the experimental phenomena. According to these results, the maximum potential difference formed on the ITO surface is over ΔV_{min1}, which illustrates that the applied voltage on driving electrodes was sufficient to generate redox reactions on the BPE. When the BEMD process started, FTMA was firstly oxidized to its cation on the anodic area of the BPE, followed by the disruption of FTMA micellar structures. Release of NVC compounds from these micelles happened in this process, simultaneously. As a consequence, free NVC compounds were deposited on the electrode surface. Because the potential difference on the BPE surface is sigmoidal, the differential

degree of FTMA oxidation occurred at each position, which resulted in NVC deposition along the BPE surface in a gradient manner. A thickness-gradient NVC thin film was formed (Figure 1c).

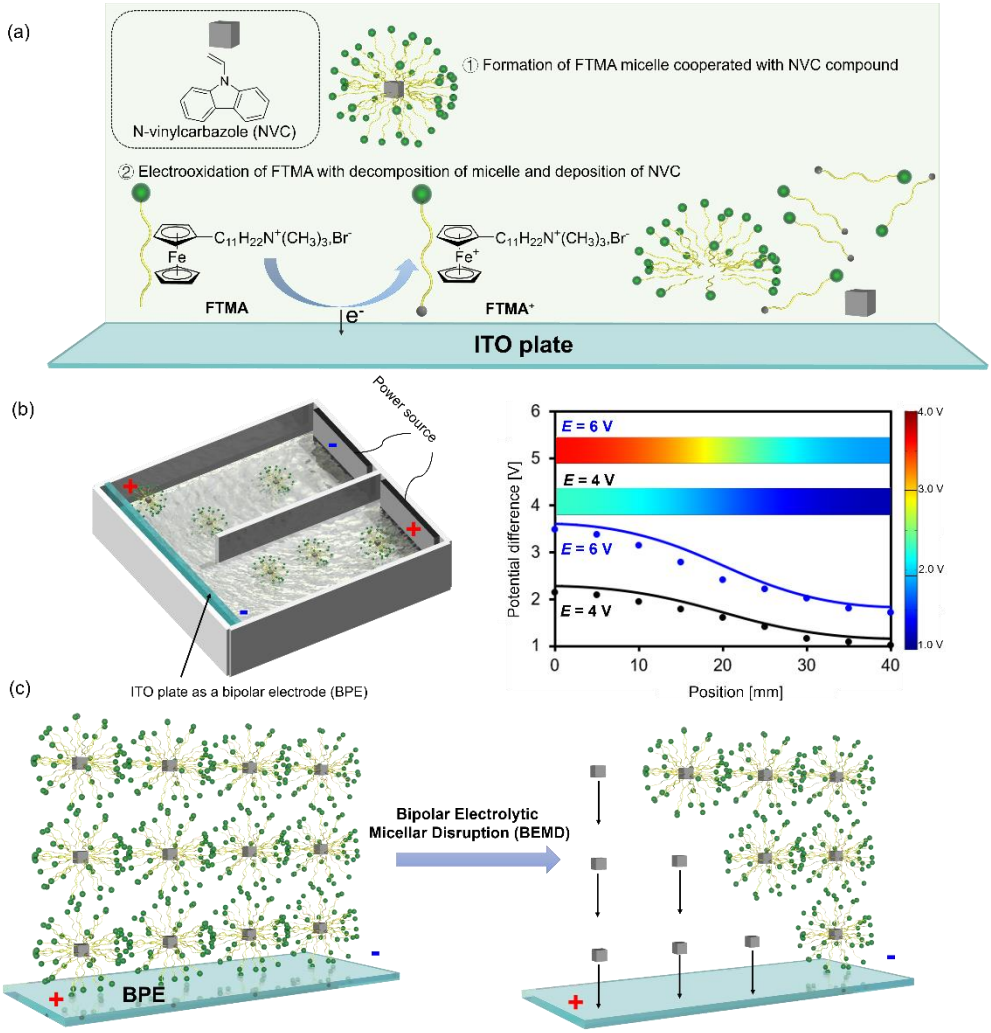

Figure 1. (a) A FTMA micelle incorporated with NVC in an aqueous solution. Here, reduced and oxidized forms of the FTMA are named FTMA and $FTMA^+$, respectively. The FTMA micelle is disrupted to release NVC during the oxidation process of FTMA. (b) In a U-shaped electrolytic setup, voltage profiles along the BPE surface were obtained from the experimental measurement (dot plots) and the corresponding simulation results (two-dimensional diagram and solid line). (c) A gradient NVC film was formed, reflecting the sigmoidal potential distribution on the BPE surface.[36]

Using the BEMD method, NVC organic thin films were fabricated under various conditions. In general, the improvement of an inorganic salt concentration to an ionic surfactant decreases the critical micelle concentration (CMC) of micelle, thus influences

the micelle formation and the solubilization.[37,38] Therefore, depending on the concentration of electrolyte salt (*C*) in micellar solutions, the film thickness can be fine-tuned. When *C* was 50 mM Li_2SO_4, dynamic light scattering (DLS) results demonstrated that the mean diameter of micelles was *ca.* 13 nm in a broad size distribution, while performed a narrower size distribution having a mean diameter (ca. 15 nm) for 100 mM Li_2SO_4 (Figure 2). The influence factor on the size distribution width was proposed to the electrostatic interactions around the micellar surface and the hydrophobic interactions between alkyl chains.[39]

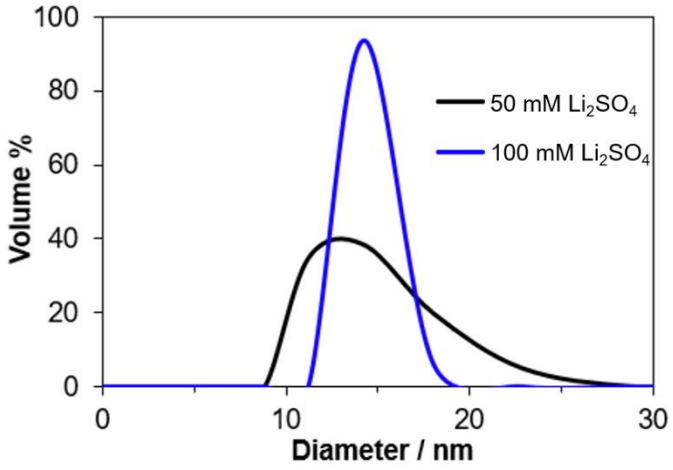

Figure 2. Diameter characterization of FTMA micelles with solubilized NVC under different *C* by dynamic light scattering.[36]

Micellar electrolytic solutions were used in the BEMD approach, thin NVC films were successfully prepared on the BPE surface in all cases. These films showed consistent UV-Vis absorption peaks at *ca.* 349 nm and 336 nm, corresponding to the UV absorption of NVC dissolved in dichloromethane. For the UV spectrometer, the exposed width for the film measurement is 3 mm. Therefore, UV absorption spectra of the NVC film were recorded in every 3 mm, calculating from the most anodic pole of the BPE. When *C* was 50 mM, a white NVC film formed under an applied voltage (*E*) of 6 V for 1.5 h electrolysis time (*T*), which faded toward the cathodic pole of the BPE (Figure 3a). The maximum UV-Vis absorption appeared at the very edge of the anodic area, and the contiguous area orderly decreased towards the right direction, suggesting a gradient NVC

film. And a much thicker NVC film was observed (Figure 3b) when the employed micellar solution has a higher *C* (100 mM). This gradient film performed a stronger UV absorption than that in Figure 3a. Meanwhile, the ratio of broken micelles under this condition was estimated by comparing the UV absorption of solution before and after bipolar electrolysis, which almost reached 53% (Figure 4). Figure 3c demonstrated a lower *E* generated a small amount of NVC released during the BEMD process, thus gave a thinner film. Accordingly, UV characterization showed a relatively weak absorbance, but kept a gradually decreased tendency. In brief, the thickness of the gradient NVC film can be easily tuned by controlling the electrolytic conditions and/or adjusting the micellar solutions.

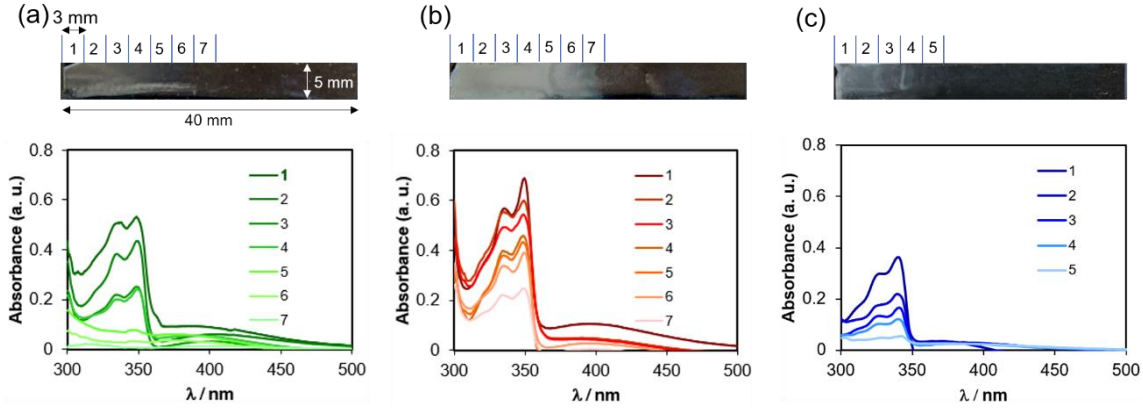

Figure 3. Gradient NVC films were fabricated using the BEMD method under different conditions of (a) *E* = 6 V and *C* = 50 mM, (b) *E* = 6 V and *C* = 100 mM, and (c) *E* = 4 V and *C* = 100 mM, and UV absorption spectra of corresponding films at each area (3 mm × 5 mm) from the anodic terminal of the BPE.[36]

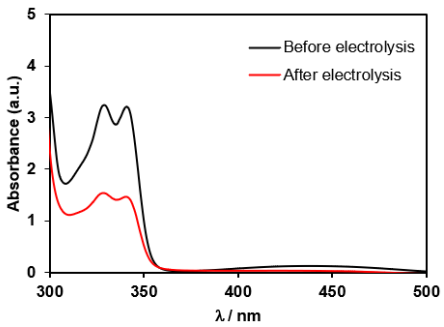

Figure 4. UV absorption spectra of electrolytic solution before and after bipolar electrolysis (*E* = 6 V and *C* = 100 mM).

The gradient profile of NVC films was further evaluated by measuring thickness using a laser scanning microscope. Here, film thickness was confirmed by the height difference between the thin film and previously masked area. The covered BPE area was exposed after the BEMD electrolysis and was carefully washed. The height difference at a specific location was measured ten times to obtain an average value, exhibiting the thickness distribution of films. According to the measurement results, all films possess a gradient feature in height, where the thickness was constantly reduced towards the cathodic edge of the BPE. In the case of 100 mM (*C*), a shorter and thinner NVC film was observed when 4 V was applied. And a higher *E* of 6 V gave a thicker film (Figure 5a). Under *E* of 6 V, the thickness of the film improved with increased *C* (Figure 5b). Even though an increased *C* performed a narrow size distribution, a bigger micelle formed (Figure 2). A bigger micelle contributes to carry more NVC compounds, producing more released NVC compounds on the BPE surface after electrolysis. The result corresponded well to the previous UV absorption measurement of these films. As a matter of fact, the thickness of the NVC film is on the behalf of different amounts of accumulated NVC at positions. From this point, it was speculated that the roughness and the surface morphology at various locations could give a better understand on the accumulation process of NVC molecules. For this reason, atomic force microscopy (AFM) measurement was proceeded in a tapping mode for the characterization of the film surface (Figure 5c). The film in Figure 3b was observed at 1 mm, 10 mm, 15 mm and 20 mm along the NVC film length. At the rightmost area around 20 mm, several grains formed and the root-mean-square (RMS) roughness at this position was higher than pristine ITO. Overall, the RMS value demonstrated an increase trend from 20 mm to 15 mm because more debris having apparent rectangular edges randomly stacked on the electrode surface. From 15 mm to 1 mm, the RMS value performed a slow decrease, which may be due to the small NVC molecules was continuously inserted into the debris spaces as electrolysis proceed at the electrode surface. After constant NVC molecules entered into these debris, the whole surface tended to be smoother. In a word, the surface microtopography showed

that the changed surface morphologies well reflected the gradual accumulation of the NVC on the BPE surface.

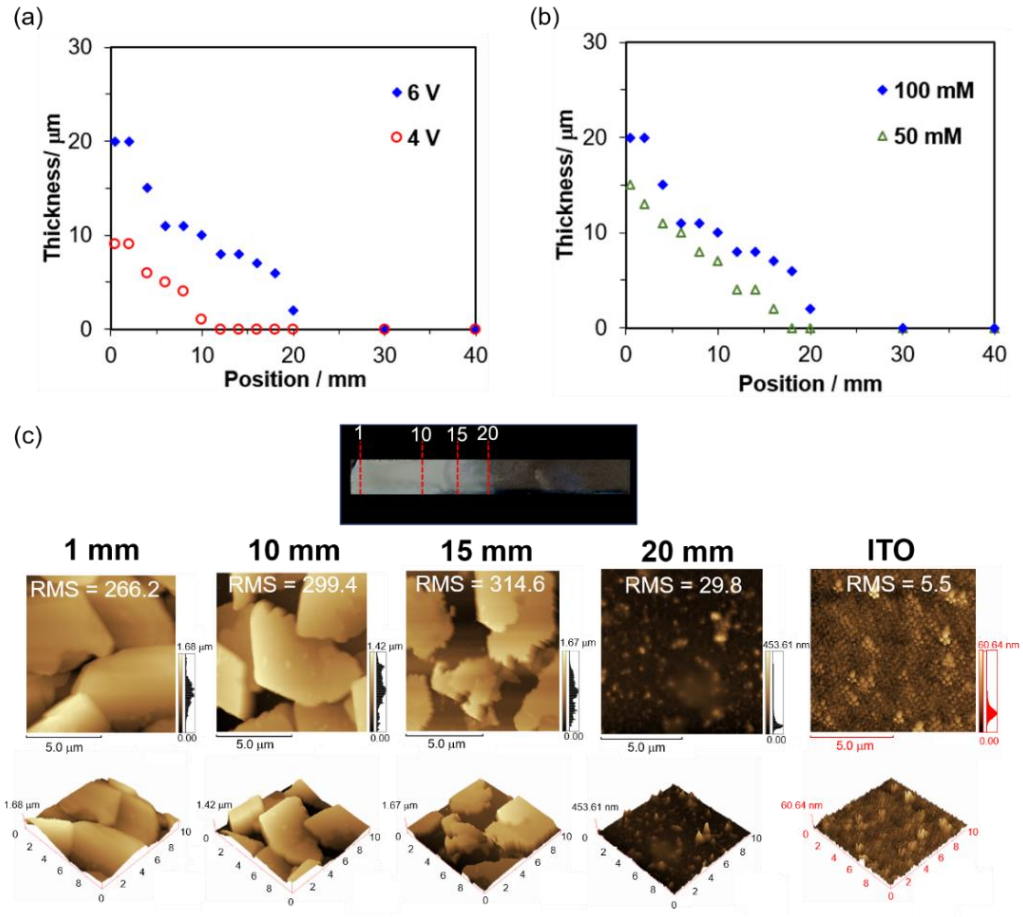

Figure 5. Film thickness profile of the NVC film fabricated under conditions of (a) C = 100 mM and E = 4 V/6 V and (b) E = 6 V and C = 50 mM/100 mM. (c) AFM images of the NVC film at various positions in Figure 2b.[36]

Inspired by the work from Usanmaz et al., where solid-state photopolymerization of NVC was achieved,[40] we attempted to proceed photopolymerization for both the commercially obtained NVC powder and the prepared gradient NVC film. These samples were exactly sealed in glass bottles and evacuated for 5 h before the UV irradiation. The distance between samples and the UV source kept at 10±1 cm and UV irradiation lasted for 50 h. After polymerization, the starting material of NVC powder, poly-NVC powder and poly-NVC film were well dissolved in chloroform ($CHCl_3$). Both of poly-NVC

powder and poly-NVC film demonstrated a red-shift of peak in the UV spectra, compared with the starting material of NVC (Figure 6a). In infrared (IR) spectroscopy measurements, the intensity of characteristic absorption peaks belonging to NVC at 845 cm^{-1}, 962 cm^{-1} and 1636 cm^{-1}reduced to a relatively low intensity for poly-NVC film, which assured the progress of photopolymerization (Figure 6b). Molecular weight analysis by gel permeation chromatography (GPC) presented a number-average molecular weight (M_n) for both poly-NVC powder (6500) and the poly-NVC film (4500). Therefore, it is proposed that the followed photopolymerization of the gradient NVC film is feasible, which would improve the application value of the BEMD method. Such a film preparation strategy and the followed post-functionalization process is not only very simple, but also eco-friendly without use of volatile solvents.

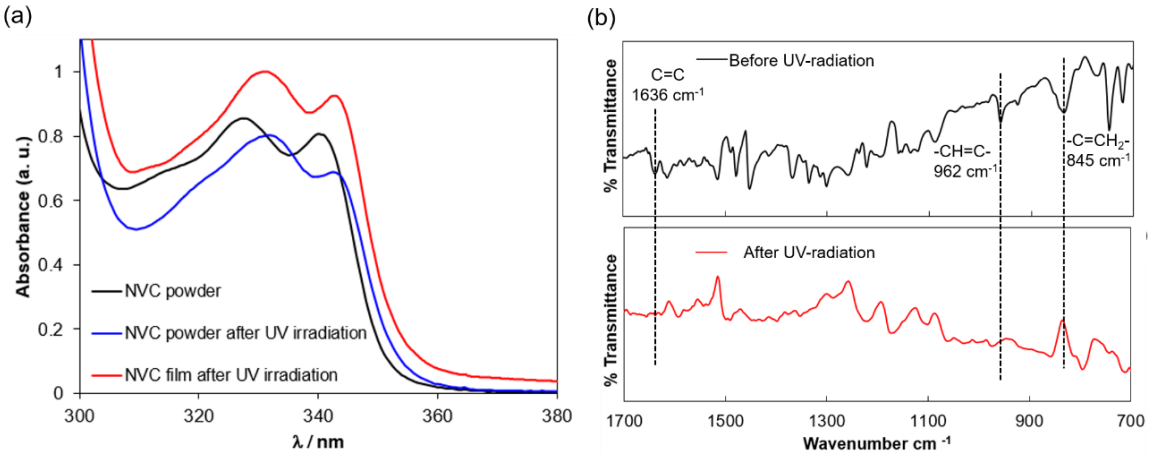

Figure 6. (a) UV-Vis absorption spectra of NVC before and after UV irradiation, dissolved in $CHCl_3$. (b) IR spectra of the gradient NVC films before and after UV irradiation.[36]

Patterning of NVC Circular Films

Towards the objective of patterning organic films by the BEMD approach in a wireless manner, an electrolytic system using an insulating cylinder was established, in which the BPE placed underneath the cylinder and a circular potential distribution formed on it.[21] Figure 7a shows the experimental configuration consisting of a glass container, an cylinder (diameter: 1 mm) that kept about 1 mm distance away from the ITO surface,

a pair of stainless steel driving anode and cathode placed outside and inside the cylinder, respectively. This electrochemical setup offered an anodic circular surface in the area underneath the cylinder. During the micelle disruption as the oxidation of FTMA, NVC molecules were released around the anodic region of the BPE surface, forming a circular NVC film (Figure 7b). In the cylindrical setup, the driving anode was located close to the BPE surface, thus generated $FTMA^+$ from the anode of driving electrode could easily migrate to the cathode of the BPE, acting as a sacrificial species. And the required minimum potential difference kept consistent with that in the U-shaped cell. However, the space in the cylindrical electrolytic setup is too narrow to measure potential distribution on the BPE. Therefore, the interfacial potential distribution was numerically estimated using COMSOL Multiphysics, which performed a mountain-like feature in which the center area possesses the highest potential difference (Figure 7c). The maximum potential difference was 0.2 V under the E of 6 V, which was sufficient to initiate BMED on the BPE (ΔV_{min1} = 0.15 V). As a result, a round white film having a diameter of 2 mm was formed, which reflected the original shape of the cylinder in proportion (Figure 7d). When the E was increased, the diameter of the circular film became larger. The result can be explained based on the numerical simulation results. Generally, the trend was that a stronger E generated a bigger ΔV_{BPE} on the BPE surface, producing an enlarged circular NVC film, correspondingly.

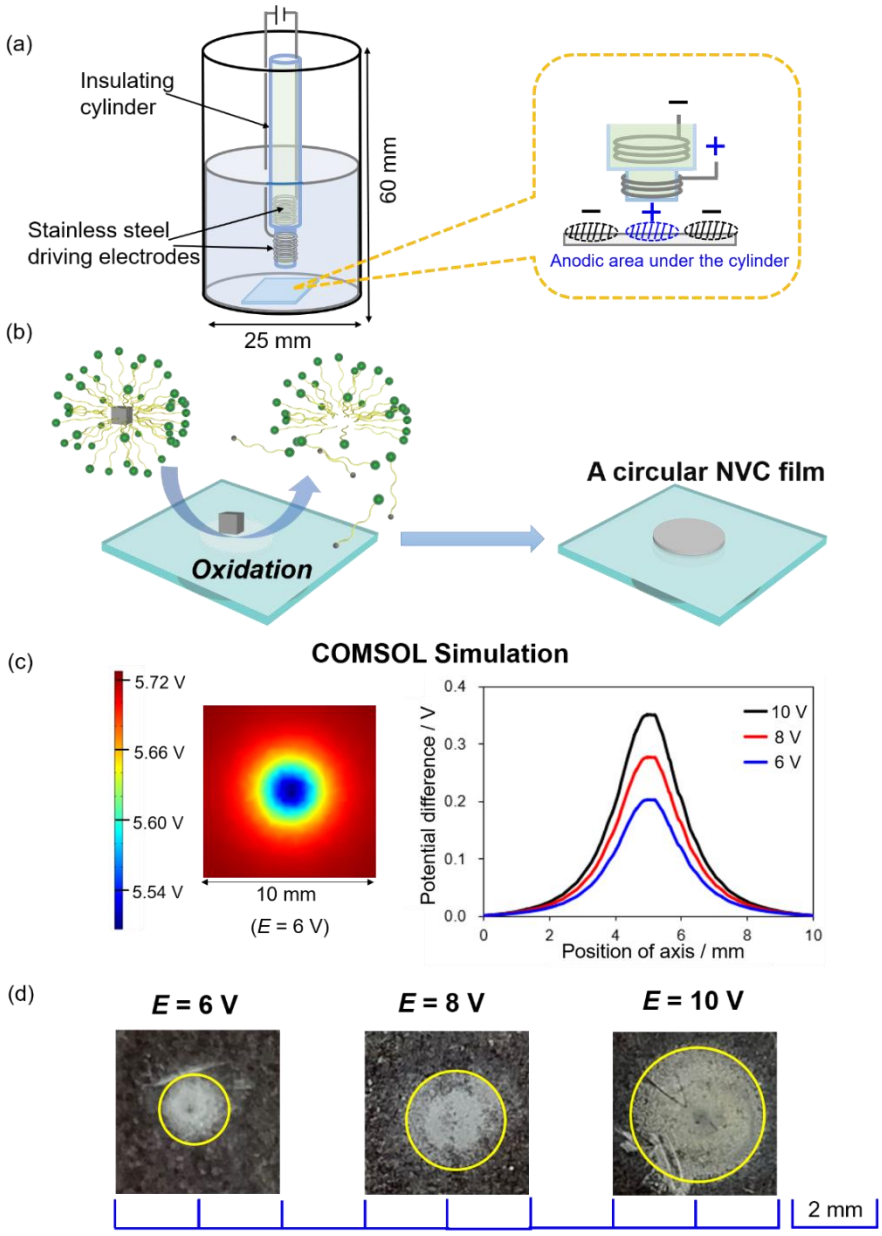

Figure 7. (a) Schematic illustration of a cylindrical bipolar electrochemical setup employed to induce a circular anodic region and surrounding cathodic region on a BPE. (b) Release and deposition processes of NVC molecules from the disrupted FTMA micelle to generate a circular film. (c) Electric field distribution and potential difference around the BPE surface from COMSOL simulation using the cylindrical setup. (d) Photographs of circular NVC films formed in 1 h under different *E*. The rim of circular deposition is highlighted using a yellow circle.[36]

Fabrication of Gradient CuPc Dye Film

Encouraged by the successful application of this BEMD approach in fabricating gradient and patterned NVC films, the author then aimed to extend the range to more

interesting organic compounds. A colored macrocycle of copper phthalocyanine (CuPc), is well known due to its strong Q-band absorption and outstanding efficiency of photoinduced charge generation. Nowadays, CuPc is widely applied to optoelectronic devices, mainly as a thin film. In reported work, gradient heterojunctions on the thickness based on CuPc/3,4,9,10-perylenetetracarboxylic bisbenzimidazole (PTCBI) or CuPc/C_{60} have been prepared by a mechanically controlled shutter having a gradual replacement along the longitudinal direction, which exhibited the position sensing.[41,42] However, the preparation approach relies on expensive equipments and harsh experimental conditions. The method described in this work may provide a new way to prepare it. Here,α-(11-ferrocenylundecyl)-ω-hydroxypoly(oxyethylene) (FPEG) surfactant with a ferrocenyl moiety was employed, which possesses a good dispersion ability for organic compounds having a large size in aqueous solution.[30] 2.0 mM FPEG, 10 mM CuPc and 0.1 M Li_2SO_4 were added to aqueous solution and sonicated for 2 h, followed by stirring for 5 days. The supernatant of resulting solution was separated as an electrolyte. The size of FPEG micelles incorporated with CuPc distributed from 180 nm to 440 nm (Figure 8a). The electrochemical reaction was firstly measured by the cyclic voltammetry (Figure 16b and eq (4)). In the FPEG system, the oxidation of FPEG proceeded at the anodic region, while the reduction of $FPEG^+$ and/or water occurred on the cathodic region. Depending on the CV measurement, ΔV_{min2} should be 0.12 V. According to the obtained potential distribution in employed U-shaped electrolytic cell, the voltages applied to driving electrodes can ensure the redox reactions on the BPE proceed smoothly (Figure 8b). As a consequence, the FPEG micelle incorporating CuPc was gradually disrupted at the anodic area of the BPE, corresponding to the sigmodal potential distribution. Simultaneously, released CuPc molecules deposited on the electrode surface to produce a gradient CuPc thin film (Figure 9).

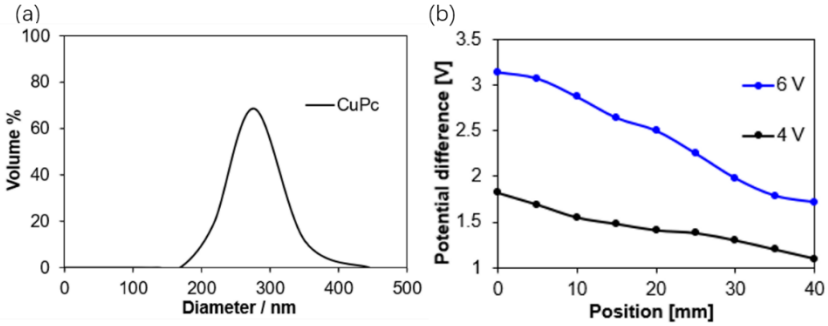

Figure 8. (a) Diameter characterization of FPEG micelles with cooperated CuPc by dynamic light scattering. (b) Measurement of potential distribution around the BPE surface in a U-type electrolytic setup for CuPc solution.

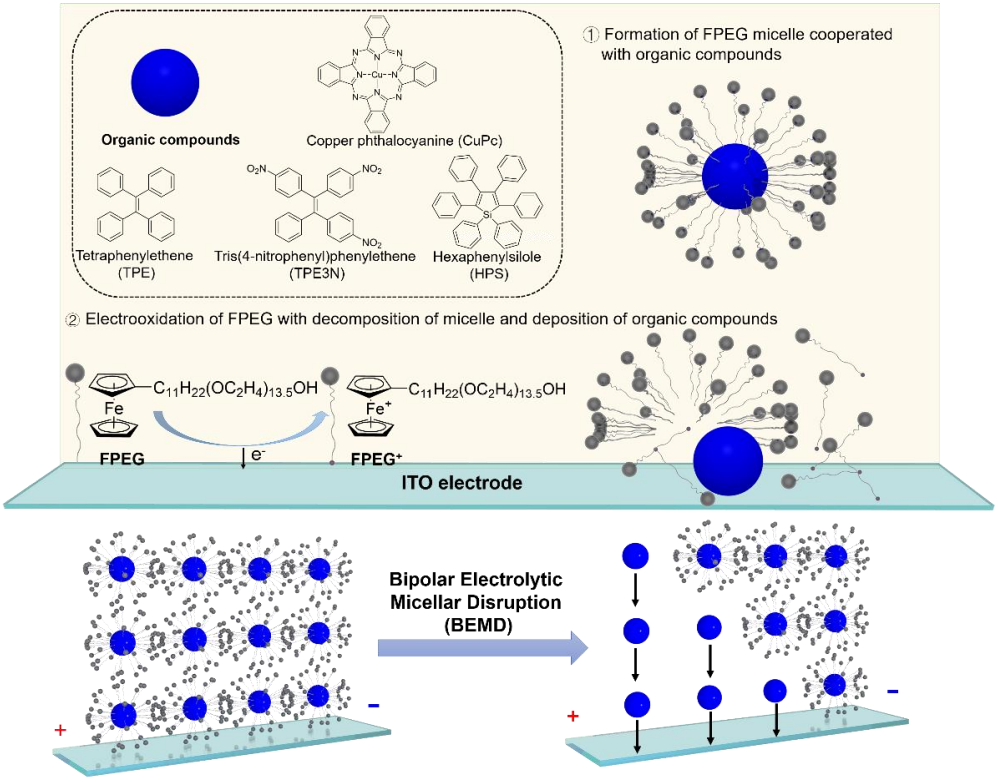

Figure 9. A FPEG micelle dispersed with an organic dye of CuPc or AIE molecules in aqueous solution. Reduced and oxidized forms of FPEG are named FPEG and $FPEG^{+}$, respectively. The FPEG micelle is disrupted to release CuPc during the oxidation process of FPEG. A gradient CuPc film formed, reflecting the sigmoidal potential distribution on the BPE surface.[36]

Photographs of CuPc films prepared under different electrolytic conditions are shown in Figures 10a, b. These films showed a gradually varied blue color changing from the anodic part towards the cathodic part of the BPE. The measurement of UV absorption along the CuPc film at every 3 mm spaced intervals performed consistent absorption

peaks at *ca.* 700 nm and 623 nm with a decreased absorption characteristic, while the rangeability of absorbance in the middle region of these CuPc films was slight. For the thickness measurement of these films, the thickest area appeared at the location that has the highest potential difference. Then, the thickness gradually decreased toward the opposite position of the film. Comparing with 4 V, a higher *E* of 6 V produced a thicker CuPc film after electrolysis, of which the thickest part of 27 μm was almost five times than the other one in the same position of the film (5 μm) obtained under 4 V (Figure 10c).

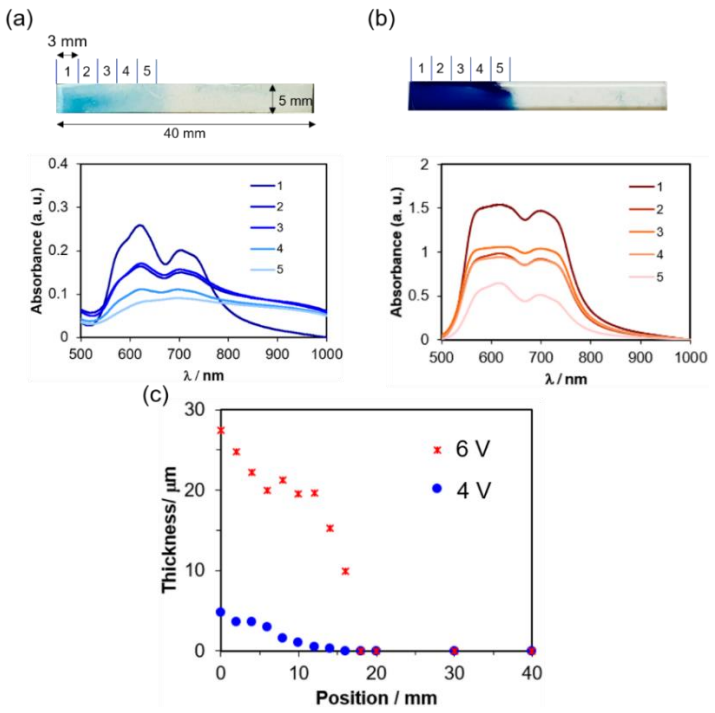

Figure 10. Photographs of CuPc films obtained by the BEMD method in 1.5 h under different *E* of (a) 4 V and (b) 6 V, and their UV absorption spectra (3 mm×5 mm). (c) The thickness profile of CuPc films in figure 9a,b.[36]

With respect to the CuPc film in Figure 9b, its surface morphology was characterized by AFM measurement. Moving from the 15 mm to the 1 mm of the film surface, the RMS values increased because more grains aggregated and stacked (Figure 11). This variation tendency was opposite to NVC film, presumably, due to different grain accumulation manners of molecules. For the NVC film, sheet growth manner was observed, while the

CuPc film performed a granular stacking.

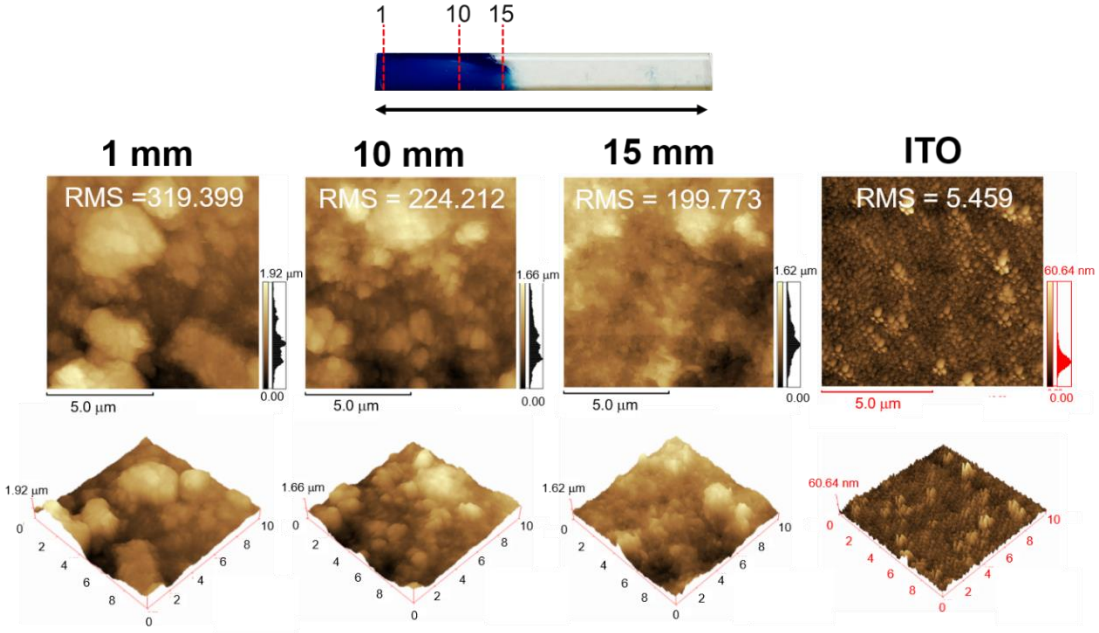

Figure 11. AFM images of the CuPc film at various positions.[36]

Fabrication of Gradient and Circular Luminescent Films with a Variety of Colors.

Next, luminescent organic compounds were introduced to BEMD system. It is well known that the aggregation induced emission (AIE) phenomenon is preferred in the solid state. The AIE effect has been widely used in sensory and optoelectronic systems.[43,44] Therefore, the established method in this work has the application potential to fabricate such AIE thin films in a facile way. To the author's knowledge, there have been no reports on the electrochemically controlled micellar system carrying AIE compounds. The family of AIE luminogens is large and the first candidate here was tetraphenylethene (TPE). TPE belongs to an archetypal luminogen having a very simple molecule structure.[45,46] The prepared electrolytic solution consisting of 2.0 mM FPEG, 10 mM TPE and 0.1 M Li_2SO_4 was sonicated for 2 h and stirred for 5 days, which was used for BEMD electrolysis in a U-shaped electrolytic setup. The size of micelles distributed from 136 nm to 351 nm (Figure 12a). In the process of BEMD, redox reactions on the BPE are identical to the CuPc system. The estimation of minimum potential difference based on the cyclic

voltammogram in Figure 16c and eq (6) was 0.12 V (ΔV_{min3}). Combined with the sigmoidal potential distribution on the BPE surface (Figure 12b), the E of 6 V should be enough to generate corresponding redox reactions. When the bipolar electrolysis proceeded for 1.5 h, deposited TPE molecules covered almost half of the ITO surface and emitted a bright blue light under 365 nm UV irradiation (Figure 13a). Thus, the distribution of accumulated TPE molecules can be visually monitored from the luminescent position and intensity. From the initiating left terminal of the BPE to the 10 mm, the blue emission maintained at a basically stable level. Then, it performed a nonuniform and weakening emission until the end of the TPE film. As mentioned before, 3D laser scanning microscopy was used to measure the height profile of the luminous TPE film. The results showed the thickness kept about 4 μm within the first 8 mm and became thinner later. The gradient profile of generated TPE film from visible observation and height measurement corresponded well with each other.

The AIE properties could be easily changed by modifying the molecular structure. In the subsequent study, a TPE derivative of tris(4-nitrophenyl)phenylethene (TPE3N) was investigated, which can be structurally decorated by one-step reaction from the commercial product of TPE.[47] TPE3N has a yellow emission due to the electron-withdrawing property of the nitro groups. The preparation process of FPEG micellar solution including TPE3N is the same with TPE system. The size of micelles mainly located at 220 nm having a shoulder about 140 nm (Figure 12a). The ΔV_{min4} was 0.14 V (Figure 16d and eq (8)) and the maximum potential difference formed on the BPE can be 1.34 V (Figure 12c), which illustrated the redox reactions in TPE3N system can proceed. The TPE3N thin film was only formed after a long electrolytic time of 5 h. Consequently, a weaker and shorter luminescent TPE3N film was produced. The luminescence intensity of this film was relatively uniform within the range of 10 mm. Beyond the distance of 10 mm, it became weaker and the height of the TPE3N film also gradually decreased towards the rightmost part of the film (Figure 13b).

Another classic AIE luminogen, hexaphenylsilole (HPS) emitting sky-blue light was

also investigated.[44] An FPEG micellar solution with HPS was electrolyzed for 1.5 h under the E of 6 V. The ΔV_{min5} from the FPEG oxidation and $FPEG^+$ reduction was 0.12 V (Figure 16e and eq (10)). Actually, the potential difference formed on the BPE (1.51 V) was enough to generate the redox reactions (Figure 12d). After BEMD electrolysis, a gradient HPS film having a bright sky-blue emission was observed when exposing to UV irradiation. The deposited length of the film was *ca.* 22 mm, whose luminescent intensity decreased from the anodic part to the cathodic part. For the thickness measurement of the HPS film, it kept at a relatively stable level within 14 mm, then decreased to the end of the film, which was consistent to the gradient luminescence of the HPS film (Figure 13c).

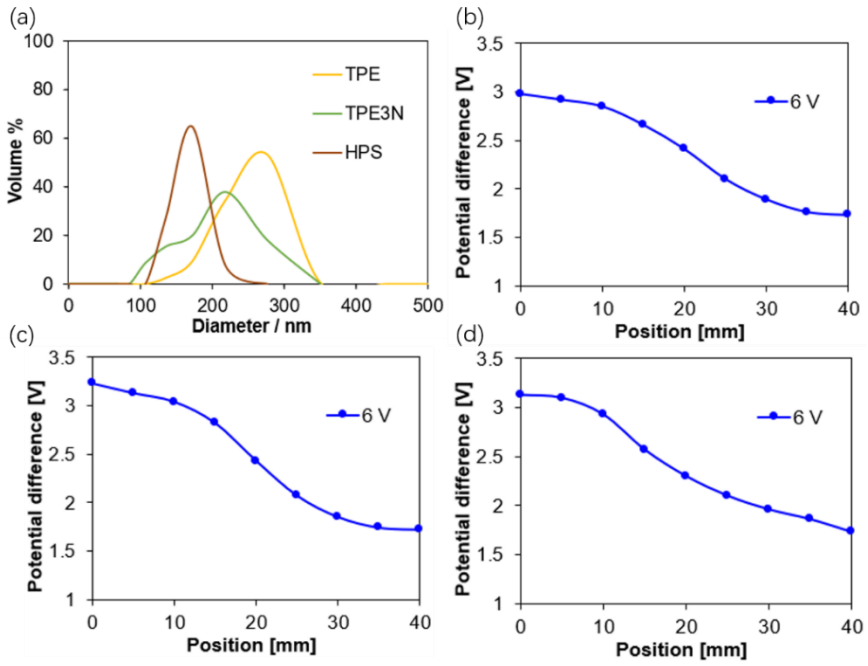

Figure 12. (a) Diameter characterization of FPEG micelles with containing TPE, TPE3N or HPS by dynamic light scattering. Measurement of potential distribution around the BPE surface in a U-type electrolytic setup for (b) TPE, (c) TPE3N or (d) HPS solution.[36]

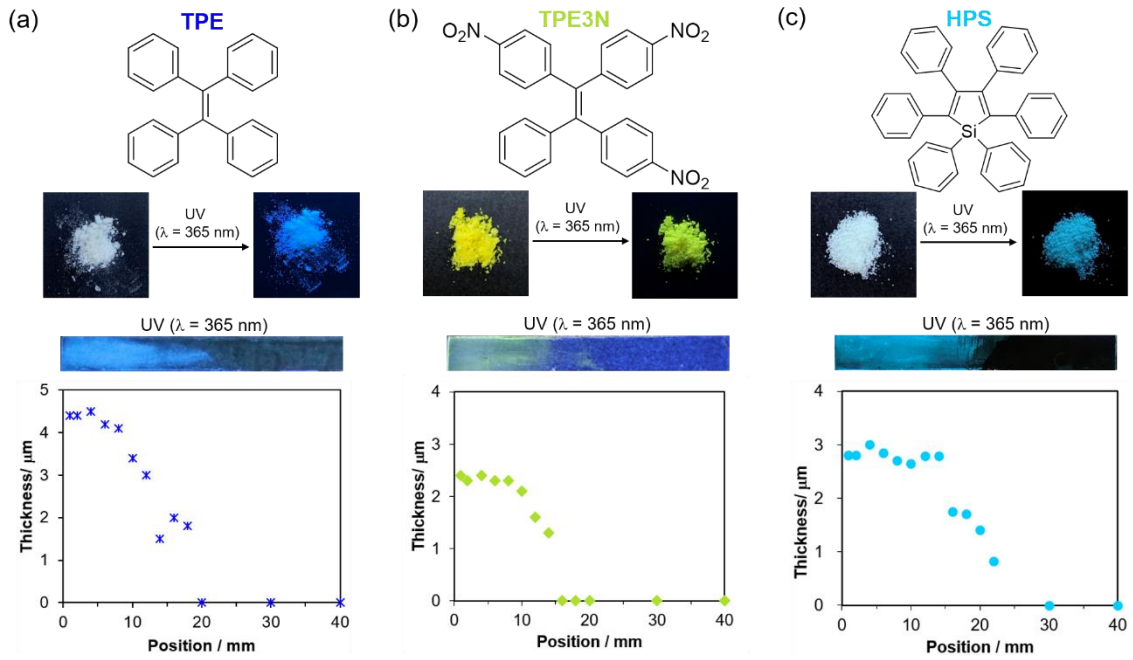

Figure 13. (a) Various emissions of AIE compounds under 365 nm UV irradiation. AIE films with gradient luminescent intensities were prepared using the BEMD method and the thickness of AIE film was determined at various positions (a) TPE, (b) TPE3N and (c) HPS.[36]

TPE thin film in figure 13a was analyzed by AFM observation. Obtained images were distinguished compared to that on bare flat ITO surface. At 1 mm, the image with closely packed grains was presented, while only low-density grains appeared at 10 mm. When moving to the 15 mm or 20 mm, the RMS roughness significantly reduced because of the very limited quantity of aggregated particles on the location (Figure 14). The results corresponded to the thickness of TPE film and the luminescent intensity, which gradually decreased from 8 mm.

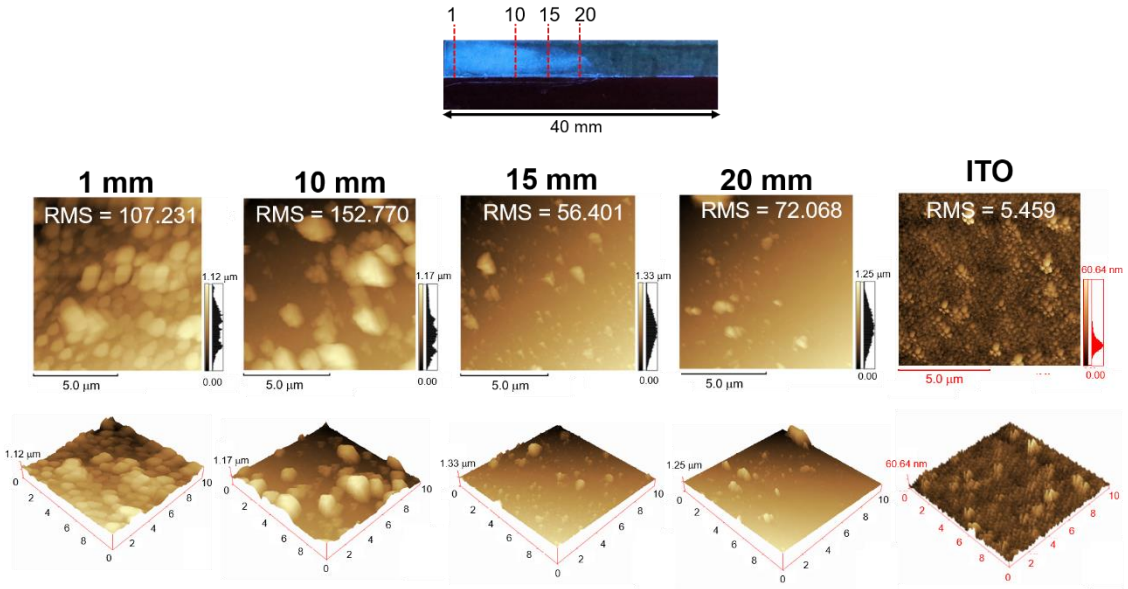

Figure 14. AFM images of HPS film at various positions.[36]

Finally, the preparation of patterned luminescent AIE films was aimed by using a cylindrical electrolytic installation. This setup can generate a circular anodic surface underneath the cylinder, where the oxidation of FPEG proceeded. Then, the released AIE molecules stacked on the electrode surface in a circular shape as the FPEG micelles broken up during the electrolysis process (Figure 15a). After the bipolar electrolysis (E = 6 V), the formation of AIE thin films was observed by the visual examination. The TPE, TPE3N or HPS films had a blue, yellow or sky-blue emission under the UV irradiation of 365 nm, which corresponded to its starting material (Figure 15b). Under a higher E of 8 V, the diameter of the film improved accordingly. It can be clarified based on our previous study that a higher E employed in this cylindrical electrolytic setup, a bigger potential difference formed to possess a larger region to satisfy ΔV_{min}, which generates a broader anodic area.[22]

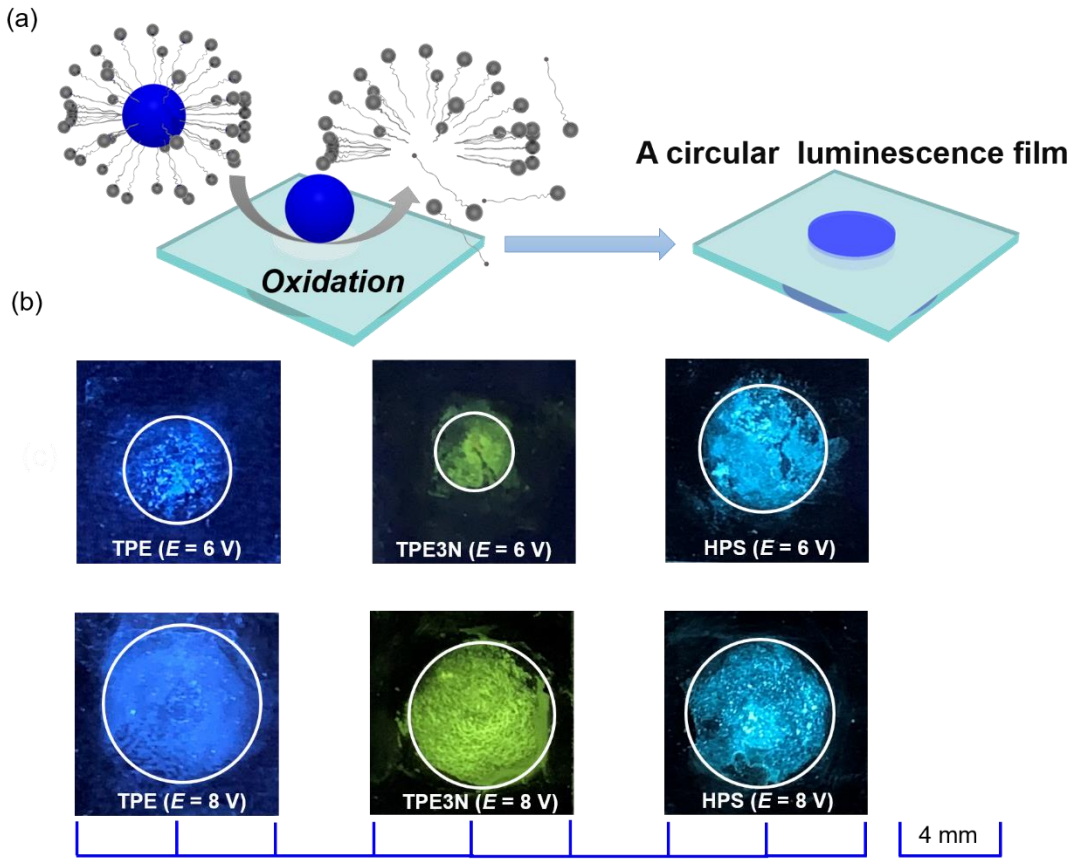

Figure 15. (a) Disruption and deposition of AIE molecules from FPEG micelles for the formation of a circular AIE film. (b) Under 365 nm UV irradiation, photographs of circular AIE films fabricated under different *E*. The rim of circular deposition is highlighted using a white circle.[36]

Conclusion

Combining bipolar electrochemistry with an electrochemically controlled micelle disruption process, a BEMD approach was successfully established. A variety of organic compounds were well incorporated into micelles formed by ferrocene-modified electroactive cationic and nonionic surfactants. During the electrochemical oxidation process of these surfactants, organic molecules were simultaneously released onto the BPE to generate thin films, corresponding to the distribution of potential on the BPE surface. These starting organic compounds as the film-forming materials did not undergo any electrochemical reaction, because the electroactive surfactants contain a ferrocene moiety that has a low oxidation potential to be oxidized firstly. The major advantage of the BEMD approach attributes to the intrinsic feature of bipolar electrochemistry, which

has a possible wireless operation on the potential distribution regulation. For the U-shaped bipolar electrolytic setup, the sigmoidal potential distribution assisted the formation of gradient thin films. By modulating the applied voltage to the driving electrodes or changing the electrolytic solution, the film thickness can be controlled. Besides, the cylindrical bipolar electrolytic setup offered circular films because the distinguishing anodic and cathodic regions on the BPE. The diameter of these circular films was easily adjusted by the applied voltage from the external power supply. In several proof-of-concept experiments, various gradient and circular organic thin films were prepared. NVC compound has an olefinic double bond, thus the generated gradient NVC film can undergo the solid-state polymerization using the UV light. Patterned NVC films having a variety of sizes were fabricated as well. An organic dye of CuPc was dispersed in the micelles formed by the nonionic surfactant of FPEG, which gave gradient blue thin films after BEMD. Three kinds of AIE compounds (TPE, TPE3N and HPS) were also dispersed in FPEG micelles to produce gradient luminescent thin films. Besides, the corresponding colorful and bright circular AIE films were obtained. The wide range of produced thin films confirmed the validity of the established BEMD approach.

The straightforward and facile method can be generalized to more interesting chemical molecules if they can be well solubilized or dispersed by the redox-active surfactants. By adapting bipolar electrolytic configurations or electrolytic conditions, the customization of gradient or patterned films can be achieved. Thus, this method has a broad prospect, not only in the fields of organic dye and luminescence, but also for more sophisticated system, such as biosensor, due to this approach was used on a mild condition without organic solvents. In addition, personalized electrode substrates with different materials and sizes are possible to be employed flexibly to fabricate gradient or circular films, which could satisfy the actual demands in various situations.

Experimental Section

Materials

N-vinylcarbazole, copper phthalocyanine, tetraphenylethene, hexaphenylsilole, lithium sulfate and solvents were purchased from commercial sources and used without further purification. Cationic surfactant of (11-ferrocenylundecyl)trimethylammonium bromide, nonionic surfactant of α-(11-ferrocenylundecyl)-ω-hydroxypoly(oxyethylene) and tris(4-nitrophenyl)phenylethane were synthesized according to literatures.[30,35,46] The aqueous solution was deaerated by intensive Ar bubbling just before use.

Instruments

An EC1000SA AC/DC power applier from NF Corporation was used for bipolar electrolysis. ^{1}H nuclear magnetic resonance (NMR) spectra were recorded on a Bruker biospin AVANCE III 400A. Film thickness was determined by an Olympus OLS4100 3D laser microscope. Dynamic light scatterer (Wyatt DAWN HELEOS II) was used to evaluate the size distribution of micelles. The absorption of organic thin films was characterized by Ultraviolet spectrophotometer (Shimadzu UV-1800). The surface morphologies of films were characterized using atomic force microscope (Shimadzu SPM-9700).

Synthesis of electroactive surfactants and AIE compound

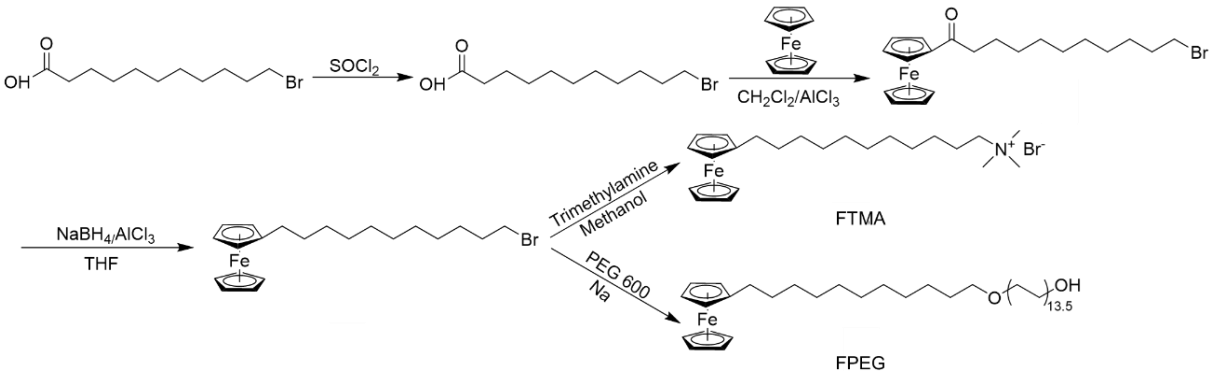

Scheme S1. Synthesis of redox-active surfactants.

The redox-active surfactants were synthesized according to reported procedures.[30,35] The chemical shift for ^{1}H NMR was given in δ (ppm) with respect to that for the internal tetramethylsilane (TMS) as an internal standard.

11-Bromoundecanoyl ferrocene

Under an argon atmosphere, 11-bromoundecanoic acid (5.00 g, 18.9 mmol) added in 8.5 mL of thionyl chloride ($SOCl_2$) refluxed for 5 h. Excess $SOCl_2$ was evaporated to produced 11-bromoundecanoyl chloride (5.04 g, 17.8 mmol) as a clear oil. Then, crude 11-bromoundecanoyl chloride (5.04 g, 17.8 mmol) was dissolved in 7 mL CH_2Cl_2 and slowly added into 34 mL CH_2Cl_2 with a mixture of $AlCl_3$ (2.83 g, 21.2 mmol) and ferrocene (3.81 g, 20.5 mmol) for about 1 h. After stirring overnight, the reaction solution was poured into ice water, and the organic layer was extracted using CH_2Cl_2, washed by water and brine, then dried with anhydrous $MgSO_4$ and concentrated. The crude product was purified by column chromatography (hexane/ethyl acetate = 10:1) to yield 4.00 g of yellow solid (52%).

^{1}H NMR (25 °C, 400 MHz, $CDCl_3$): δ1.39 (m, 12H), 1.70 (m, 2H), 1.85 (m, 2H,), 2.69 (t, *J* = 8.0 Hz, 2H), 3.40 (t, *J* = 4.0 Hz, 2H), 4.19 (s, 5H), 4.49 (s, 2H) and 4.78 (s, 2H).

11-Bromoundecyl ferrocene

11-Bromoundecanoyl ferrocene (3.99 g, 9.2 mmol) in 20.0 mL THF was slowly added to a suspension of $AlCl_3$ (2.45 g, 18.4 mmol) and $NaBH_4$ (1.40 g, 37.0 mmol) in 28 mL THF under an argon atmosphere and stirred for 4 h at room temperature. 10 mL ice water was added to the mixture and the organic layer was extracted using ethyl acetate, then washed twice with water and brine, dried with anhydrous $MgSO_4$ and concentrated. The crude product was purified by column chromatography (hexane/ethyl acetate = 20:1) to yielded 3.72 g of yellow solid (93%).

^{1}H NMR (25 °C, 400 MHz, $CDCl_3$): δ1.28–1.51 (m, 16 H), 1.86 (m, 2 H), 2.30 (t, *J* = 8.0 Hz, 2H), 3.41 (t, *J* = 8.0 Hz, 2H) and 4.0 (m, 9H).

(11-Ferrocenylundecyl) trimethylammonium bromide (FTMA)

Trimethylamine (3.0 M) in ethanol (0.77 mL, 2.3 mmol) was added to 11-bromoundecyl ferrocene (0.96 g, 2.3 mmol) dissolved in 6.0 mL ethanol. The mixture was stirred for 2 days at 60 °C. Then, the solvent was evaporated and washed with hexane , then recrystallized from acetone-hexane to yield 0.56 g of yellow solid (51%).

^{1}H NMR (25 °C, 400 MHz, $CDCl_3$): δ1.28–1.49 (m, 16H), 1.71 (t, J = 16.0 Hz, 2H), 2.28 (t, J = 8.0 Hz, 2H), 3.45 (s, 9H), 3.56 (t, J = 8.0 Hz, 2H) and 4.08–4.13 (m, 9H).

α-(11-Ferrocenylundecyl)-ω-hydroxypoly (oxyethylene) (FPEG)

A piece of sodium metal (40.0 mg, 1.7 mmol) and poly(oxyethylene) with an average molecular weight of 600 (6.00 g, 10.0 mmol) were added to flask under an argon atmosphere. The mixture was stirred for 6 h at 90 °C, followed by adding 11-bromoundecyl ferrocene (0.50 g, 1.2 mmol). The resultant solution maintained at 110 °C for 10 h and cooled to room temperature. The solution was extracted using 50% butanol-water. The organic layer was washed twice with brine, then dried with anhydrous $MgSO_4$ and concentrated. The crude product was purified by column chromatography twice (toluene/ethanol = 6:1) to yield 0.40 g of yellow oil (33%).

^{1}H NMR (25 °C, 400 MHz, $CDCl_3$): δ1.2-1.4 (m, 18 H), 2.30 (t, J = 8.0 Hz, 2H), 3.46 (t, J = 8.0 Hz, 2H), 3.5-3.7 (m, 54H) and 4.0–4.1 (m, 9H).

Tetraphenylethene derivate

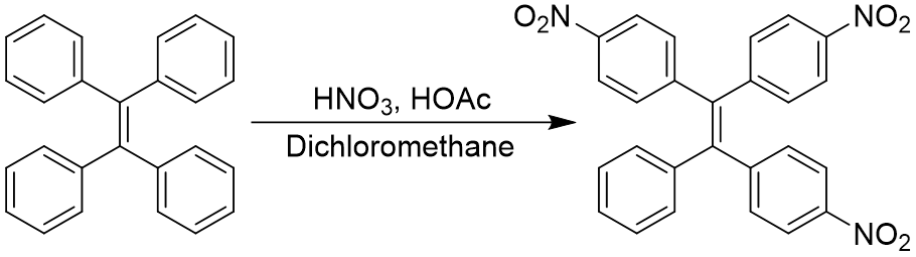

Scheme S2. Synthesis of tris(4-nitrophenyl) phenylethane.

Synthesis of tris(4-nitrophenyl) phenylethane (TPE3N)

Tetraphenylethene (2.49 g, 7.5 mmol) was dissolved in a mixture of dichloromethane

and acetic acid (30 mL/15 mL). 15 mL concentrated nitric acid was slowly added to the resultant solution and stirred at room temperature for 16 h. The solution was extracted using dichloromethane (50 mL) twice, and the organic layer was washed with brine, then dried with anhydrous $MgSO_4$ and concentrated. The crude product was purified by column chromatography (dichloromethane/hexane = 1:1) to yield 1.58 g of yellow powder (45%).[46]

^{1}H NMR (25 °C, 400 MHz, $CDCl_3$): δ6.98 (d, J = 4.0, 2H), 7.15–7.24 (m, 9H), 8.01–8.06 (m, 6H).

Measurement of the voltage profile around the BPE surface in a U-shaped electrolytic setup

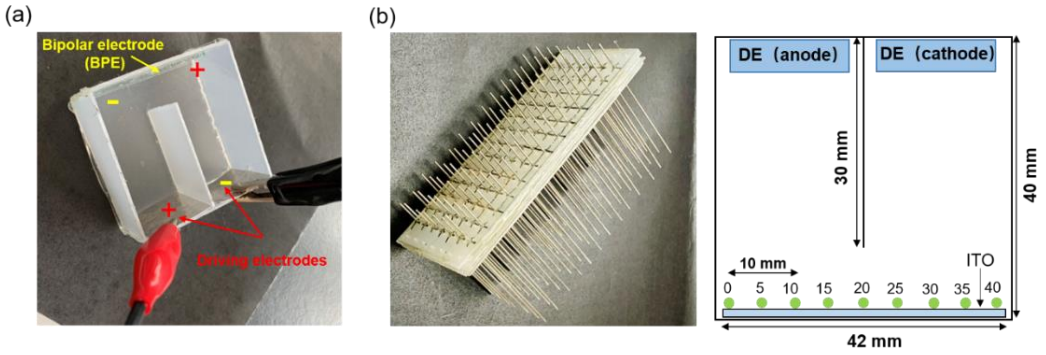

Figure 16. (a) Photograph of the employed U-shaped electrolytic setup. (b) measurement of the voltage profile around the BPE surface using the reference electrode array.[36]

Estimation of required minimum potential difference (ΔV_{BPE}) on the BPE surface

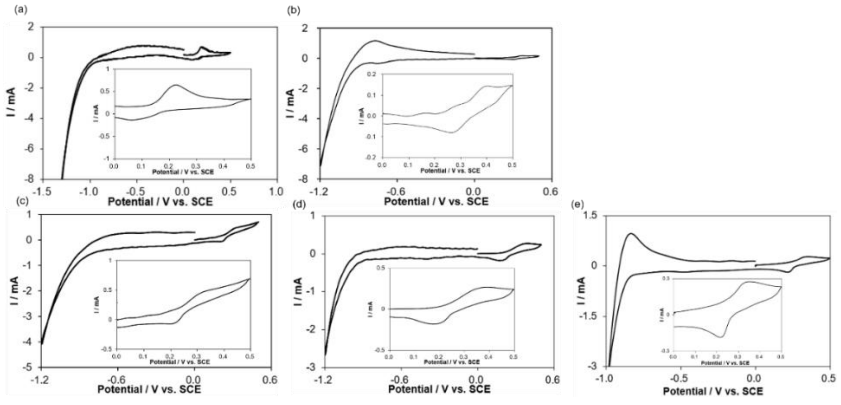

Figure 17. (a) CV measurements of different micellar systems (a) NVC, (b) CuPc and AIE compounds of (c) TPE, (d) TPE3N and (e) HPS, using a Pt plate (10 mm × 10 mm) as a working electrode, a SCE as a reference electrode and a Pt plate (20 mm × 20 mm) as a counter electrode at a scan rate of 100 mV/s.[36]

The required minimum applied voltage to induce electrochemical reactions on the BPE (ΔV_{min}) was estimated according to the potential difference between the oxidation potential and reduction potential of the species, E_{ox} and E_{red}, (Eq. 1).

$$\Delta V_{min} = |E_{ox} - E_{red}| \quad (1)$$

In the NVC electrolytic system, the oxidation of FTMA occurred on the anode of the BPE and the reduction of $FTMA^+$ or H_2O proceeded on the cathode of the BPE, simultaneously.

$$\Delta V_{min1} = |E_{ox} - E_{red}| = |0.22\ V - 0.07\ V| = 0.15\ V \quad (2)$$

$$\Delta V_1 = |E_{ox} - E_{red}| = |0.22\ V - (-0.82\ V)| = 1.16\ V \quad (3)$$

In the CuPc electrolytic system, the oxidation of FPEG occurred on the anode of the BPE and the reduction of $FPEG^+$ or H_2O proceeded on the cathode of the BPE, simultaneously.

$$\Delta V_{min2} = |E_{ox} - E_{red}| = |0.39\ V - 0.27\ V| = 0.12\ V \quad (4)$$

$$\Delta V_2 = |E_{ox} - E_{red}| = |0.39\ V - (-0.83\ V)| = 1.22\ V \quad (5)$$

In the TPE electrolytic system, the oxidation of FPEG occurred on the anode of the BPE and the reduction of $FPEG^+$ or H_2O proceeded on the cathode of the BPE, simultaneously.

$$\Delta V_{min3} = |E_{ox} - E_{red}| = |0.33\ V - (0.21\ V)| = 0.12\ V \quad (6)$$

$$\Delta V_3 = |E_{ox} - E_{red}| = |0.33\ V - (-0.80\ V)| = 1.13\ V \quad (7)$$

In the TPE3N electrolytic system, the oxidation of FPEG occurred on the anode of the BPE and the reduction of $FPEG^+$ or H_2O proceeded on the cathode of the BPE, simultaneously.

$$\Delta V_{min4} = |E_{ox} - E_{red}| = |0.34\ V - (0.20\ V)| = 0.14\ V \quad (8)$$

$$\Delta V_4 = |E_{ox} - E_{red}| = |0.30\ V - (-0.88\ V)| = 1.28\ \text{V} \quad (9)$$

In the HPS electrolytic system, the oxidation of FPEG occurred on the anode of the BPE and the reduction of $FPEG^+$ or H_2O proceeded on the cathode of the BPE, simultaneously.

$$\Delta V_{min5} = |E_{ox} - E_{red}| = |0.37\ V - (0.20\ V)| = 0.12\ V \quad (10)$$

$$\Delta V_5 = |E_{ox} - E_{red}| = |0.37\ V - (-0.83\ V)| = 1.20\ \text{V} \quad (11)$$

Bipolar electrolysis

Preparation of micellar electrolytic solutions

For cationic surfactant of FTMA, the electrolytic solution was prepared as follows: to an aqueous solution, 2.0 mM FTMA, an excess amount of NVC and 0.1 M lithium sulfate (Li_2SO_4) were added. The suspension was sonicated and then stirred for 5 days to obtain a solubilization equilibrium. Undissolved NVC in the solution was carefully removed by centrifugation (2000 rpm, 1 h) and the resultant solution was employed as the electrolyte solution.

For nonionic surfactant of FPEG, the electrolytic solution was prepared as follows: 2.0 mM FPEG, 10 mM compound (CuPc, TPE, TPE3N or HPS) and 0.1 M Li_2SO_4 were added to an aqueous solution. The solution was sonicated and stirred for 5 days. The supernatant of the solution was separated for BEMD electrolysis. All of these electrolytic solutions were deaerated before use by bubbling Ar.

Bipolar Electrolysis in a U-shaped Electrolytic setup

A U-shaped electrolytic setup (40 mm × 42 mm) contains an ITO plate (40 mm × 10 mm) as the BPE and a pair of Pt driving electrodes (20 mm × 20 mm). The driving electrodes were connected to an external power supply. During the bipolar electrolytic, the solution was slightly stirred for FTMA system and was not stirred for FPEG system. After electrolysis, the BPE was very carefully washed using the deionized water, and then dry for the further characterization.

Bipolar Electrolysis in a Cylindrical Electrolytic setup

A cylindrical electrolytic setup contains an insulating cylinder, an ITO plate (10 mm × 10 mm) as the BPE and stainless steel driving electrodes connected to a power source. And the cylinder with a diameter of 1 mm kept about 1 mm from the BPE surface. During the bipolar electrolysis, the electrolytic solution was kept still without stirring. After electrolysis, the BPE was very carefully washed using the deionized water, and then dry for the further characterization.

Measurement of the film thickness

A half of the ITO surface was covered with a tape to facilitate the thickness measurement. After electrolysis, the tape was removed, and the covered area was carefully washed. The height difference between the film and covered area determined the thickness of film, which was measured ten times at a specific location to obtain an average value.

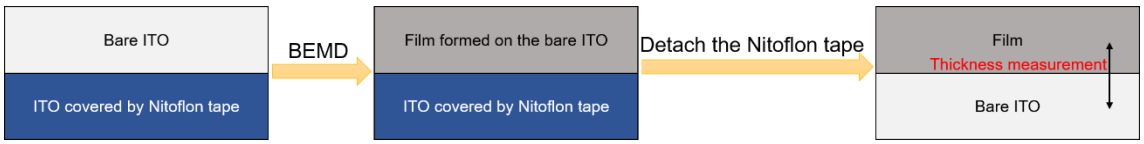

Figure 18. The procedure of measuring film thickness.[36]

References

[1] C. Liu, D. Wang, C. Zhang, *Sensors and Actuators, B: Chemical,* **2018**, *270*, 341–352.

[2] M. S. Wu, Z. Liu, H. W. Shi, H. Y. Chen, J. J. Xu, *Analytical Chemistry,* **2015**, *87*, 530–537.

[3] C. Ulrich, O. Andersson, L. Nyholm, F. Björefors, *Angewandte Chemie International Edition*, **2008**, *47*, 3034–3036.

[4] S. Yadnum, J. Roche, E. Lebraud, P. Négrier, P. Garrigue, D. Bradshaw, C. Warakulwit, J. Limtrakul, A. Kuhn, *Angewandte Chemie International Edition,* **2014**, *53*, 4001–4005.

[5] Y. Zhou, N. Shida, Y. Koizumi, K. Endo, I. Tomita, S. Inagi, *Macromolecules*, **2020**, *53*, 8123–8130.

[6] G. Loget, A. Kuhn, *Journal of the American Chemical Society*, **2010**, *132*, 15918–15919.

[7] C. C. Mayorga-Martinez, B. Khezri, A. Y. S. Eng, Z. Sofer, P. Ulbrich, M. Pumera, *Advanced Functional Materials*, **2016**, *26*, 4094–4098.

[8] B. Gupta, B. Goudeau, P. Garrigue, A. Kuhn, *Advanced Functional Materials*, **2018**, *28*, 1705825.

[9] L. Zhang, B. Gupta, B. Goudeau, N. Mano, A. Kuhn, *Journal of the American Chemical Society,* **2018**, 140, 15501–15506.

[10] M. Li, S. Liu, Y. Jiang, W. Wang, *Analytical Chemistry,* **2018**, *90*, 6390–6396.

[11] G. Loget, D. Zigah, L. Bouffier, N. Sojic, A. Kuhn, *Accounts of Chemical Research,* **2013**, *46*, 2513–2523.

[12] S. E. Fosdick, K. N. Knust, K. Scida, R. M. Crooks, *Angewandte Chemie International Edition*, **2013**, *52*, 10438–10456.

[13] R. M. Crooks, *ChemElectroChem,* **2016**, *3*, 357–359.

[14] N. Shida, Y. Zhou, S. Inagi, *Accounts of Chemical Research,* **2019**, *52*, 2598–2608.

[15] S. Inagi, *Polymer Journal,* **2016**, *48*, 39–44.

[16] S. Inagi, Y. Ishiguro, N. Shida, T. Fuchigami, *Journal of The Electrochemical Society*, **2012**, *159*, G146–G150.

[17] Y. Ishiguro, S. Inagi, T. Fuchigami, *Langmuir*, **2011**, *27*, 7158–7162.

[18] S. Inagi, Y. Ishiguro, M. Atobe, T. Fuchigami, *Angewandte Chemie International Edition*, **2010**, *122*, 10334–10337.

[19] N. Shida, Y. Koizumi, H. Nishiyama, I. Tomita, S. Inagi, *Angewandte Chemie International Edition*, **2015**, *54*, 3922–3926.

[20] N. Shida, Y. Ishiguro, M. Atobe, T. Fuchigami, S. Inagi, *ACS Macro Letters*, **2012**, *1*, 656–659.

[21] Y. Ishiguro, S. Inagi, T. Fuchigami, *Journal of the American Chemical Society*, **2012,** *134*, 4034-4036.

[22] Y. Zhou, N. Shida, Y. Koizumi, T. Watanabe, H. Nishiyama, I. Tomita, S. Inagi, *Journal of Materials Chemistry C*, **2019**, *7*, 14745–14751.

[23] Y. Kanbur, H. Coskun, E. D. Głowacki, M. Irimia-Vladu, N. S. Sariciftci, C. Yumusak, *Organic Electronics*, **2019**, *66*, 53–57.

[24] J. Nelson, *Current Opinion in Solid State and Materials Science*, **2002**, *6*, 87–95.

[25] T. Miyata, S. Kawaguchi, M. Ishii, T. Minami, *Thin Solid Films*, **2003**, *425*, 255–259.

[26] M. Purica, E. Budianu, E. Rusu, M. Danila, R. Gavrila, *Thin Solid Films*, **2002**, *403*, 485–488.

[27] D. Yu, C. Wang, X. Cheng, F. Zhang, *Thin Solid Films*, **2009**, *517*, 4950–4955.

[28] T. Saji, K. Hoshino, S. Aoyagui, *Journal of the Chemical Society*, **1985**, *107*, 6865-6868.

[29] K. Hoshino, T. Saji, *Journal of the American Chemical Society*, **1987**, *109*, 5881–5883.

[30] T. Saji, K. Hoshino, Y. Ishii, M. Goto, *Journal of the American Chemical Society*, **1991,** *113*, 450–456.

[31] K. Hoshino, T. Karato, S. K. Kim, Y. Yamada, T. Ebine, *Electrochimica Acta*,

2008, *53*, 7655–7660.

[32] T. Hino, Y. Ogawa, N. Kuramoto, *Carbon*, **2006**, *44*, 880–887.

[33] J. Jayasree, C. S. Narayanan, *Bulletin of the Chemical Society of Japan*, **1995**, *68*, 89–94.

[34] Y. Hasegawa, T. Sugawara, T. Nakanishi, Y. Kitagawa, M. Takada, A. Niwa, H. Naito, K. Fushimi, *ChemPlusChem*, **2016**, *81*, 187–193.

[35] C. Li, B. Ren, Y. Zhang, Z. Cheng, X. Liu, Z. Tong, *Langmuir*, **2008**, *24*, 12911–12918.

[36] Y. Zhou, N. Shida, I. Tomita and S. Inagi. *Angewandte Chemie - International Edition*, **2021,** *60*, 14620–14629.

[37] D. Yu, X. Huang, M. Deng, Y. Lin, L. Jiang, J. Huang, Y. Wang, *Journal of Physical Chemistry B*, **2010**, *114*, 14955–14964.

[38] U. P. Preiss, P. Eiden, J. Łuczak, C. Jungnickel, *Journal of Colloid and Interface Science*, **2013**, *412*, 13–16.

[39] H. Nomura, S. Koda, T. Matsuoka, T. Hiyama, R. Shibata, S. Kato, *Journal of Colloid and Interface Science*, **2000**, *230*, 22–28.

[40] A. Usanmaz, A. M. Onal, S. Bostan, *British Polymer Journal*, **1989**, *21*, 71–76.

[41] J. Cabanillas-Gonzalez, O. Peña-Rodríguez, I. Suarez Lopez, M. Schmidt, M. I. Alonso, A. R. Goñi, M. Campoy-Quiles, *Applied Physics Letters*, **2011**, *99*, 97–100.

[42] G. Liu, M. Chen, J. Wang, X. Xi, W. Dong, G. Chen, L. Chen, R. Chen, *Optics Communications*, **2018**, *429*, 60–64.

[43] Y. Hong, J. W. Y. Lam, B. Z. Tang, *Chemical Communications*, **2009**, *29*, 4332–4353.

[44] Y. Hong, J. W. Y. Lam, B. Z. Tang, *Chemical Society Reviews*, **2011**, *40*, 5361–5388.

[45] M. Wang, G. Zhang, D. Zhang, D. Zhu, B. Z. Tang, *Journal of Materials Chemistry*, **2010**, *20*, 1858–1867.

[46] Z. Zhao, J. W. Y. Lam, B. Z. Tang, *Journal of Materials Chemistry*, **2012**, *22*, 23726–23740.

[47] T. Yu, D. Ou, Z. Yang, Q. Huang, Z. Mao, J. Chen, Y. Zhang, S. Liu, J. Xu, M. R. Bryce, Z. Chi, *Chemical Science*, **2017**, *8*, 1163–1168.

Chapter 5

General Conclusion

The development of materials science is important to the progress of the society, which significantly supports the innovation in science and technology. Electrochemistry is exactly a green technology that has been widely used to materials science. In this thesis, the author employed bipolar electrochemistry for synthesis of conducting polymers (CPs) and modification of electrode surfaces. Firstly, the author found a facile approach to directly fabricate perpendicular CP fiber arrays on the electrode surface by bipolar electropolymerization, while CP films with a granular or particulate morphology are typically obtained by conventional electropolymerization. It is the reason that the formed charged oligomer can diffuse in a specific direction under bipolar electrochemical conditions. Next, electrophoresis of charged monomers could highly promote the migration of charged monomers into the template; thus the synergetic electropolymerization and electrophoresis effects in one bipolar electrochemical system were regarded as an effective way to make robust CP nanowires, unlike the formation of hollow CP tubular structures using conventional electrochemical method. Finally, the author proposed a new and general approach for the preparation of organic thin films by taking full advantage of bipolar electrochemistry. Because of the controllable potential distribution (gradient and mountain-like) on the bipolar electrode (BPE), a variety of gradient and patterned functional organic thin films were fabricated.

In Chapter 1, the background and the purpose of the thesis were described.

In Chapter 2, the author achieved template-free perpendicular growth of poly-(3,4-ethylenedioxythiophene) (PEDOT) fiber array by bipolar electrolysis under iterative potential application (Figure 1). A cylindrical bipolar electrolytic setup was employed to induce simultaneous anodic and cathodic areas on the BPE surface. A uniform CP fiber

array made of PEDOT grown on the anodic region covered by the cylinder. The applied voltage and the distance between the cylinder and the BPE decided the growth of a PEDOT array. The supporting electrolyte, the solvent and the diameter of the cylinder affected the morphology of the fibers. The methodology offered a facile and efficient approach to fabricate conductive fiber arrays.

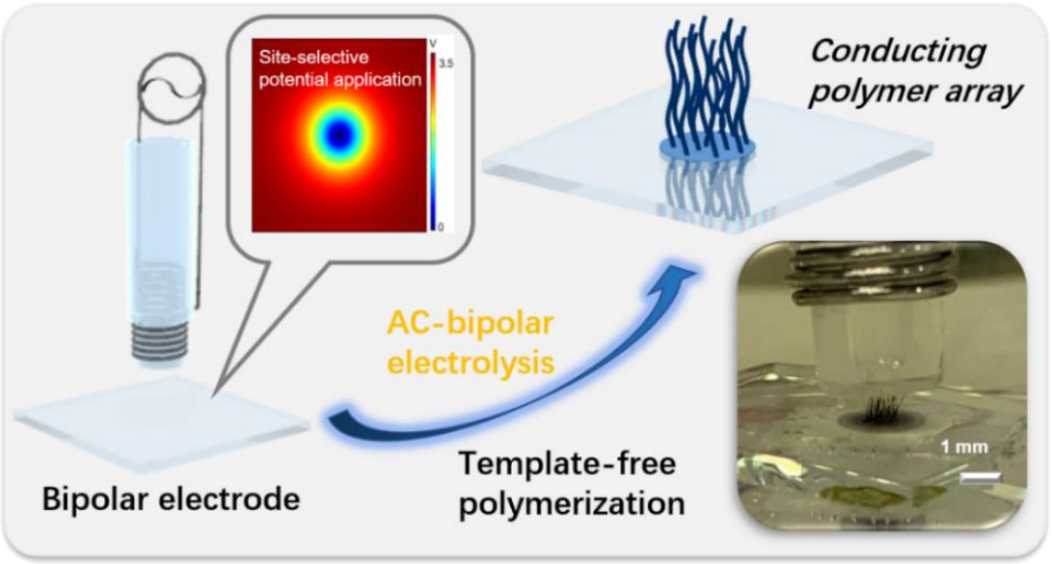

Figure 1. Template-free electropolymerization of PEDOT fiber arrays using a cylindrical electrolytic setup by AC-bipolar electrolysis.

In Chapter 3, the author demonstrated the templated fabrication of one-dimensional (1D) polymer nanowires by bipolar electropolymerization promoted by electrophoresis effect (Figure 2). Porous anodic aluminum oxide (AAO) membrane was used as a template modified on the BPE surface. Charged monomers used for the bipolar electropolymerization could migrate under an external electric field, undergoing the forced diffusion into the nanopores of an AAO template. Cationic monomer of ruthenium-polypyridine moved towards the BPE cathode, while anionic monomer of thiophene derivative migrated to the BPE anode. Both of ruthenium-polypyridine and thiophene-based polymer nanowires were successfully obtained by the cathodic reduction or the anodic oxidation on the BPE, respectively. The obtained polymer nanowires were robust enough to keep standing even after the removal of the templates due to the significant

improvement in the mechanical strength. The approach proposed a reliable strategy to fabricate polymer nanowires using charged monomers.

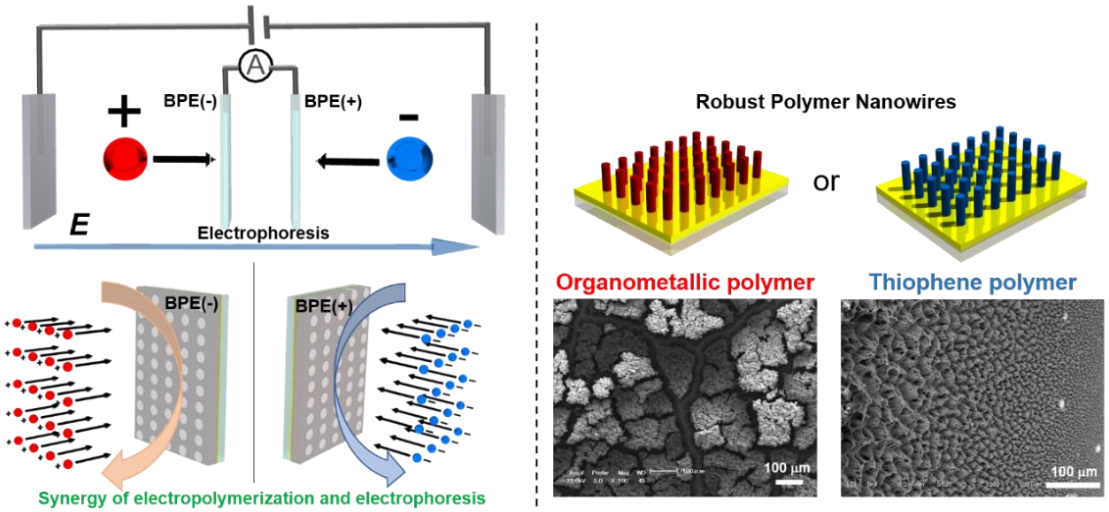

Figure 2. Schematic illustration of bipolar electrochemical setup for the templated bipolar electrolysis assisted with electrophoresis to prepare robust organometallic polymer and thiophene polymer nanowires.

In Chapter 4, the author established a bipolar electrolytic micelle disruption (BEMD) approach for the preparation of shaped organic thin films (Figure 3). Micelles composed of electroactive surfactants broken up when the surfactants were electrochemically oxidized on the BPE, thus incorporated organic molecules in the micelles were released and deposited on the BPE. A U-shaped bipolar electrolytic setup gave a sigmoidal potential gradient on the BPE, generating gradient thin films covering various interesting organic compounds, such as a polymerizable monomer, an organic pigment and aggregation induced emission molecules. Besides, corresponding patterned organic films were fabricated using a cylindrical bipolar electrolytic setup that enables site-selective potential distribution on the BPE. The method provided a general way for gradient and patterned organic film preparations.

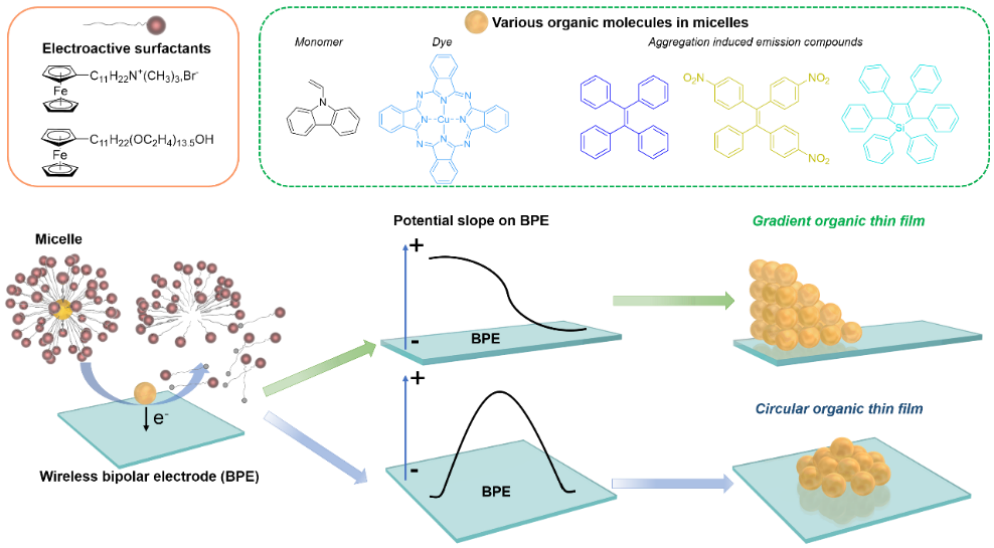

Figure 3. Schematic illustration of BEMD approach established by integrating bipolar electrochemistry with a redox-controlled micelle disruption process. Using the BEMD approach, gradient and patterned organic films with a wide range of a polymerizable monomer, an organic pigment and aggregation induced emission (AIE) molecules, were successfully fabricated.

In Chapter 5, conclusions were summarized aiming at the contents of this thesis.

In summary, electric field-driven electrosynthesis of conducting polymers and modification of electrode surfaces were achieved by bipolar electrochemistry. Based on the combination of the electrophoresis and electropolymerization in the bipolar electrochemical system, the author successfully prepared PEDOT microfiber arrays by AC-bipolar electrolysis and robust CP nanowires by reductive electropolymerization of cationic ruthenium complexes or oxidative electropolymerization of anionic thiophene derivative. In addition, with the help of sigmoidal and mountain-like potential distributions on the BPE, the author established a BEMD approach to achieve the preparation of gradient and patterned organic thin films in a general way. In a word, the application scope of bipolar electrochemistry on materials science was extended in this thesis. The author believes these works will open a long-term perspective with respect to fabricate one-dimensional CPs and various organic thin films. More importantly, these research achievements could inspire more researchers in various research branches.

List of publications

Chapter 2

"Template-free perpendicular growth of a poly(3,4-ethylenedioxythiophene) fiber array by bipolar electrolysis under an iterative potential application."

Y. Zhou, N. Shida, Y. Koizumi, T. Watanabe, H. Nishiyama, I. Tomita and S. Inagi. *Journal of Materials Chemistry C,* **2019,** *7,* 14745–14751.

Chapter 3

"Fabrication of one-dimensional polymer nanowires by templated bipolar electropolymerization promoted by electrophoretic effect."

Y. Zhou, N. Shida, Y. Koizumi, K. Endo, I. Tomita and S. Inagi. *Macromolecules,* **2020,** *53,* 8123–8130.

Chapter 4

"Fabrication of gradient and patterned organic thin films by bipolar electrolytic micelle disruption approach using redox-active surfactants."

News release on EurekAlert (18th May, 2021)

Research highlight on Tokyo Tech News (9th June, 2021)

Spotlight Research on Chem-Station (21st June, 2021)

News posted on NIKKEI BUSINESS DAILY (5th July, 2021)

Other publication

Bipolar electrochemistry: a powerful tool for electrifying functional material synthesis.

N. Shida, Y. Zhou and S. Inagi. *Accounts of Chemical Research,* **2019,** *52,* 2598–2608.

Acknowledgements

First and foremost, the author would like to express her gratitude to her supervisor,

Associate Professor Shinsuke Inagi. He helped her a lot both on academia and life in Japan. When she firstly arrived at Japan, he kindly arranged student members in his group to pick her up from Haneda airport to dormitory. It was an unforgettable start of the life in Japan. Under his supervision and guidance, her research headed the correct direction. Research topics, originalities and methods were all from the fruitful discussion with Prof. Inagi. Thanks for his constructive advice, she was into her research step by step, deeper and deeper. He encouraged her to join in the academic conferences held in Japan and overseas and offered her the chance to learn the skills how to introduce research to others in a comprehensive way and to enlarge her horizon. He also guidance her to detect and define a problem, and find a solution, which is essential of being a qualified researcher.

The author would like to deeply appreciate Professor Ikuyoshi Tomita for his insightful advice and valuable suggestions. She is grateful to Assistant Professor Naoki Shida. He inspired her a lot on research projects and taught her how to carry out scientific writing, which benefits to all her research life. More important things she learned from him are how to think logically and how to keep passion for work. She also would like to thank Assistant Professors Hiroki Nishiyama and Ryoyu Hifumi for their advice, and Professor Mahito Atobe for his generous sharing on the experimental equipment.

Thanks for Dr. Elena Villani, she built an electrochemiluminescence platform for group and broaden her knowledge. Dr. Yuki Koizumi gave a lot of help when she started her research. His kind talk let she know the new research field at a very short time.

Many thanks to all the members in Tomita-Inagi laboratory, who were very supportive and kept her going through Ph.D. journey. Thanks for Tomoyuki Kurioka, he often discusses chemical knowledges and experiment plans with each other. The time to study together in every morning will be the best memory. Thanks to Mariko Konishi, she always kindly share Japanese culture and food with her. It brought her a lot of pleasure.

Last, the author would like to express her appreciation to her dear family and life-long friends, especially for her parents, Mr. Shixiong Zhou and Mrs. Xi'e Zou for their unwavering support, assistant and encouragement, being a continuous source of

inspiration in every aspect of her life. She will be grateful forever for their love. Additionally, she owes thanks to her husband, Mr. Yingxue Hu, for his company on the road of learning from undergraduate to PhD. Because of his optimism, goodness and childish curiosity, the life is full of sunshine.

Yaqian Zhou

July 2021